RICE UNIVERSITY

Numerical Modeling, Determination, and Characterization of Electrical Properties of Nanocomposites

by

Matthew Wichmann, 2nd Lt USAF

A THESIS SUBMITTED
IN PARTIAL FULFILLMENT OF THE
REQUIREMENTS FOR THE DEGREE

Master of Science

APPROVED, THESIS COMMITTEE:

Dr. Pol D. Spanos, Chair
Lewis B. Ryon Professor in Engineering

Dr. John E. Akin
Professor of Mechanical Engineering &
Materials Science

Dr. Ilinca Stanciulescu
Assistant Professor of Civil Engineering

HOUSTON, TEXAS
APRIL 2011

The views expressed in this article are those of the author and do not reflect the official policy or position of the United States Air Force, Department of Defense, or the U.S. Government.

Abstract

Numerical Modeling, Determination, and Characterization of Electrical Properties of Nanocomposites

by

Matthew Wichmann

A numerical model is presented for the determination of the electrical properties of carbon nanotube-based composites. The model incorporates several experimentally-based statistical distributions to account for the stochastic nature of the problem. These distributions include parameters such as nanotube length and diameter in addition to contact resistance. Using a Monte Carlo-based simulation technique, a random nanotube geometry is generated, checked for a percolation spanning network and then converted into a pseudo-3D resistor network for which the effective electrical conductivity is found. Each data point is the ensemble average of 500 or more simulations, each with a unique set of realized parameter values thereby reducing statistical variations of the solution. Studies are conducted to investigate the importance of incorporating the stochastic parameters and to characterize the impact of nanotube waviness and alignment on the effective composite properties. Electron tunneling distance is also included as a variable model parameter.

Acknowledgements

I would like to sincerely thank the numerous individuals who made this thesis come to fruition. First and foremost, I am truly grateful for my advisor, Professor Pol D. Spanos, who granted me the opportunity to come and study at Rice University. His mentorship along with innovative vision has been a source of personal growth and enrichment.

I would further like to thank Brad Ward, as a colleague and a source of motivation, whose collaboration has made this thesis possible. Special thanks go to Professor John Akin and Dr. Ilinca Stanciulescu for not only serving on my thesis committee but for their support and guidance along the way. Their technical expertise helped overcome numerous obstacles encountered during the research process.

Additional gratitude is due to George Evaggelatos and John Kougioumtzoglou, whose insight and knowledge along with humor has made my graduate school experience not only fruitful but enjoyable as well.

Finally, I would like to thank my friends and family for their continuous and unwavering support. Their daily encouragement helped me overcome the many hurdles and slumps in motivation I experienced and for that I am truly grateful. I will truly miss my fellow Air Force friends here at Rice University, especially my roommates Wyatt Harris and Tim Phillips.

Contents

Abstract iii

Acknowledgements iv

List of Figures i

List of Tables v

1 Introduction 1

1.1 Motivation 1

1.2 Electrical Conduction in Composites 3

1.2.1 Percolation Theory 4

1.2.2 Microscale Overview and Nanoscale Effects 6

1.3 Critical Issues in Experimentation 8

1.4 Numerical Modeling 11

1.4.1 Thermal and Electrical Conduction Modeling Differences 11

1.4.2 Previously Published Models 12

1.4.3 Proposed Model 16

2 The Representative Volume Element 18

2.1 Geometry Generation 18

2.2 Accurate Microscale Representation 25

2.2.1 Periodic Geometry and CNT Dispersion 26

2.2.2 RVE dimensions 27

3 Spanning Network Identification 31

3.1 Algorithm Specifics 31

3.2 Algorithm Steps 35

4 The Resistor Network Model 39

4.1 Components of the Resistor Network 39

4.2 Model Steps 44

5 Numerical Results 48

5.1 Analysis Methods 48

5.2 Model Verification 52

5.2.1 Modeling Parameters 53

5.2.2 Computational Checks 55

5.2.1 Monte Carlo Convergence Analysis 58

5.3 Model Validation 61

5.3.1 Comparison to Numerical Models 61

5.3.2 Comparisons to Experimental Data 63

5.4 Case Study 1: Effect of Stochastic Parameters 65

5.5 Case Study 2: Effect of Nanotube Waviness 71

5.6 Case Study 3: Effect of Nanotube Alignment 77

6 Concluding Remarks 87

List of Figures

Figure 1. A microscale overview of the problem is presented. 6

Figure 2. A histogram of 1341 Weibull randomly generated nanotube lengths is presented. 20

Figure 3. The extraction of the nanotube diameter distribution is shown with (a) the experimental histogram by Ziegler et al. [48] and (b) the reproduced histogram with log-normal distribution fit. 21

Figure 4. A histogram of 1341 lognormal randomly generated effective nanotube diameters using the parameters by Ziegler et al. [48] are presented, including carbon-carbon spacing. 22

Figure 5. A histogram of 1341 nanotube aspect ratios resulting from the Weibull length distribution and lognormal diameter distribution is presented. 23

Figure 6. Two RVEs each with 1.0% volume fraction are depicted. The figures show the controllable morphology of the model with (a) having straight, partially aligned nanotubes while (b) has randomly-oriented, wavy nanotubes. The highlighted nanotubes in (b) simulate the physical phenomenon where longer nanotubes are wavier than shorter nanotubes. 25

Figure 7. An RVE highlighting the periodic nature of the generated geometry is presented. 26

Figure 8. The number of top and side nanotube boundary crossings along with both horizontal and vertical centerline crossings is presented. The lack of scatter within the data points indicates homogenous dispersion characteristics for generated periodic RVEs. 27

Figure 9. An idealized carbon nanotube-based composite is presented to depict the computational thickness, with (a) showing the multilayer composite, (b) representative layer, (c) separation between nanotubes, and (d) the overlap between nanotubes [41].... 30

Figure 10. Details of the bonding criterion are illustrated highlighting the VSR capability. 32

Figure 11. Details of the SNIA are illustrated by (a) a complete RVE along with (b) an enhanced view. 34

Figure 12. Details of the SNIA are illustrated by (a) an original fiber segment and (b) the same segment with the added split nodes. 35

Figure 13. Pseudocode of the spanning network identification scheme. 36

Figure 14. An illustrative model is presented depicting how the resistor network is formed. 40

Figure 15. The theoretical tunneling resistance as function of insulating film thickness as determined by Li et al. [41] along with a curve fit for the 2nm case is presented. 42

Figure 16. A histogram of 10,000 insulating film thickness values using estimated parameters from Li and Chou [18] is presented 43

Figure 17. A histogram of 10,000 contact resistance values resulting from the film thickness distribution in Figure 16 and lower bound of 100 kΩ based on the direct contact. 44

Figure 18. An RVE illustrating the (a) entire resistor network and the (b) estimated backbone with limited nodal voltages is presented 47

Figure 19. The percolation threshold determination process is presented, with (a) percolation probability vs volume fraction and (b) the same data as a histogram with a normal distribution fitting curve. 50

Figure 20. The fitting of the percolation probability curve by a cumulative distribution function is presented along with a vertical line indicating the estimated threshold. 50

Figure 21. The percolation power law process is presented, with (a) the electrical conductivity vs volume fraction and (b) the same data plotted against the percolation ratio with the critical exponent shown. 51

Figure 22. Electrical conductivity vs volume fraction simulation data along with a power fit curve using a mean σ_0 is presented 52

Figure 23. The effect of RVE size on (a) percolation threshold and (b) electrical conductivity is presented. RVE size within the ranges shown has a very weak on resulting values. Nanotubes of 300 nm length are used 54

Figure 24. Electrical conductivity vs contact resistance for 100% volume fraction is presented. As R_c is reduced, the effective conductivity approaches the nanotube conductivity of 10^7 S/m. 56

Figure 25. The effect of tunneling distance is presented. Note that electrical conductivity increases and percolation threshold decrease with increased tunneling distance. 57

Figure 26. A Monte Carlo convergence analysis with all variable parameters fixed is presented. 59

Figure 27. A Monte Carlo convergence analysis with all variable parameters is presented. 60

Figure 28. A percolation probability curve comparison between numerical modeling by Theodosiou and Saravanos [53] and the proposed model. 62

Figure 29. A comparison between the numerical model by Hu et al. [67] and the proposed model is presented for the electrical conductivity vs volume fraction. 63

Figure 30. A comparison between experimental data (Hu et al. [75], pt. #1 [81], #2 [52], and #3 [82]) and proposed model with all variable parameters presenting electrical conductivity vs volume fraction..... 64

Figure 31. A comparison between three experimental data sets (squares [83], circles [75], and triangles [84]) and proposed model presenting electrical conductivity vs volume fraction. 65

Figure 32. The effects of contact resistance on effective electrical conductivity are shown. With variable resistance (blue-diamond), conductivity continues to increase as opposed to leveling off when a fixed value is used. The inset shows percolation does not change with contact resistance. 67

Figure 33. Power law fitting along with critical exponents for the data in Figure 32 is presented. 68

Figure 34. Simple parallel circuit diagrams are presented illustrating the effect of variable resistance on the overall equivalent resistance. The equivalent resistance is reduced by 3 fold in (a) and in (b), a random placement of variable resistors shows that a potentially less resistive circuit is possible compared to when fixed values are used for the resistors. 69

Figure 35. The effect of nanotube waviness on electrical conductivity is shown. Conductivity decreases as nanotube waviness, controlled by θ_{max}, increases. The inset plot shows how the percolation probability decreases with waviness. 73

Figure 36. Utilized volume fraction, or the ratio of in-network fibers to the total number of RVE fibers, is presented vs volume fraction for varying degrees nanotube waviness. Straight nanotubes maintain a higher utilized volume fraction. 74

Figure 37. The number of network contacts vs volume fraction is presented for varying degrees of nanotube waviness. 75

Figure 38. The number of network contacts vs the number of fibers in the network, or bond density, is presented for varying degrees of nanotube waviness. The inset exemplifies the prominent behavior where bond density increases with nanotube waviness. 76

Figure 39. Electrical conductivity vs number of contacts is presented for varying degrees of waviness. Straight nanotubes yield higher conductive networks with the same number of contacts as wavy nanotubes, indicating the formation of straighter and/or more conduction paths. 76

Figure 40. The effect of alignment on electrical conductivity is shown, comparing the randomly distributed case (θ_a = 90°) to three levels of increasing alignment (θ_a = 75°, 45°, and 15°). Note how strong alignment decreases conductivity. 80

Figure 41. Four RVEs are shown, (a) through (d), at 0.008 vf for each level of alignment θ_a = 15°, 45°, 75°, and 90°, respectively. The current carrying fibers of the spanning cluster are in blue. 81

Figure 42. The details of the spanning cluster are shown for the randomly distributed case along with three levels of alignment and include (a) the utilized volume fraction vs volume fraction, (b) number of network contacts vs volume fraction, and (c) contact density. 82

Figure 43. Percolation threshold versus alignment angle for both straight and wavy CNTs is presented. The minimum threshold is reached at θ_a = 75° for both data sets. 84

Figure 44. Electrical conductivity vs alignment angle for both straight and wavy CNTs is presented. Maximum conductivity is achieved at θ_a = 45° for both data sets with wavy being slightly greater. 85

List of Tables

Table 1. Thermal and Electrical Conductivity Ratios..... 12

Table 2. Published Models for the Determination of Electrical Properties of Nanotube-Based Composites from Selected Literature..... 15

Table 3. RVE Dimensions from a Collection of Numerical Models..... 28

Table 4. Percentage Time Saved Compared to 1 Bin..... 54

Table 5. Total RVE Current Check for Top and Bottom Boundaries..... 56

Table 6. Monte Carlo Convergence Analysis: Case Study #1..... 70

Table 7. Monte Carlo Convergence Analysis: Case Study #2..... 77

Table 8. Monte Carlo Convergence Analysis: Case Study #3..... 86

1 Introduction

1.1 Motivation

By exploiting the properties of individual constituents, composite materials are able to achieve increased functionality and maximize specific performance properties of the composite as a whole. Thermally and electrically conductive polymer composites are produced by reinforcing the insulating matrix material with conductive filler particles. These types of composites are widely used in electronics, automotive and aerospace industries to dissipate heat and prevent the buildup of static charge [1]. However, the typical fillers of carbon black and copper wire require high loading levels, which often have a detrimental effect on the overall mechanical properties and manufacturability along with compromising weight [1,2]. Therefore, high aspect ratio and highly conductive materials such as carbon nanotubes (CNTs) are regarded as promising fillers because they can provide electrical conduction with extremely low filler content as a result of percolation [1,3].

Carbon nanotubes offer exceptional mechanical, thermal, and electrical properties based off their extremely high aspect ratios (10^3-10^4) and atomic structure. These properties include an elastic modulus on the order of 1 TPa, tensile strength of 200 GPa, and high fracture strain of 10-30%. Comparatively, the elastic modulus of CNTs is approximately three times larger than carbon fibers and five times that of steel at only one-sixth the weight [4,5]. Furthermore, carbon nanotubes exhibit extraordinary conduction properties. The theoretical thermal conductivity of single-walled carbon nanotubes

(SWCNTs) is over 6600 W/mK and experiments have shown conductivities greater than that of isotropic diamond in the range of 2000-3000 W/mK at room temperature [6,7]. Of particular interest to the present work, nanotubes also offer excellent electrical properties. Carbon nanotubes are ballistic conductors meaning no energy is dissipated along its length [8], and as such, they are capable of reliably carrying extremely high current densities of over 10^9 A/cm^2 [9]. Additionally, the electrical conductivity of these idealized one-dimensional conductors is on the order of 10^4-10^7 S/m [10-12], approximately 20 orders of magnitude higher than most polymers [13].

With such exceptional properties, carbon nanotube-based composites promise remarkably enhanced properties. The incorporation of CNTs into a polymer matrix has resulted in increases of 30% in elastic modulus and 18% in tensile strength [5] along with a 130% in thermal conductivity [14]. The effective electrical conductivity of a CNT-based composite can also be enhanced by over 10 orders of magnitude in comparison to the polymer matrix material [15]. Furthermore, the electrical conductivity of a composite can be tailored by varying the filler content for distinct electrical applications categorized by conductivity as electrostatic dissipation (10^{-6}~10^{-4} S/m), conductive (10^{-4}~10^{1} S/m), and highly conductive or shielding (>10^{1} S/m) [15].

Besides utilizing CNTs as passive reinforcement to tailor toughness, impact resistance, vibration damping, and electrical and thermal conductivity, significant research interest is focused on multifunctional applications of CNT-based composites [16]. These applications include electromechanical actuators and variety of sensing applications including mass, humidity, chemical, and strain sensors along with damage and structural health monitoring [16,17]. By structuring materials at the nanoscale, it is envisioned that

aircraft skins could provide not only structural support but electromagnetic interference protection, lightening strike shielding, and embedded sensing and actuation as well [18]. The significant promise of these novel composite materials has spurred the need to accurately predict their properties. As such, an accurate and versatile model for the determination of the electrical properties of carbon nanotube-based composites is sought.

1.2 Electrical Conduction in Composites

The electrical conduction of a composite consisting of conductive filler particles embedded in an insulating matrix is based on percolation theory. The composite behaves like an insulator until a certain filler volume fraction is reached at which point the conductivity jumps many orders of magnitude. Beyond this critical concentration of filler, known as the percolation threshold, the conductivity increases at a much slower rate [19]. Some explanations for the extremely low percolation thresholds for carbon nanotube-based composites focus on the formation of conductive pathways or networks through the medium [13,20,21]. However, experimental data has revealed percolation thresholds below estimated contact percolation thresholds, indicating nanoscale phenomena such as electron tunneling [3,13,19-23]. Therefore, both the formation of carbon nanotube networks and nanoscale effects are considered in the proposed model. This chapter further explains percolation theory, presenting a brief historical review, before providing a microscale overview and a look at known nanoscale effects on the conductivity of a CNT-based composite. Finally, a range of published models from literature are reviewed before the proposed model of this thesis is discussed.

1.2.1 Percolation Theory

In general, percolation theory is concerned with determining how a given set of sites, regularly or randomly positioned in space, is interconnected [24]. Mathematically speaking, the percolation threshold ϕ_c of a two part composite is defined as the volume fraction of filler at which an infinite spanning cluster forms in an infinite system [25]. As the volume fraction increases above ϕ_c, the infinite cluster grows rapidly, absorbing smaller clusters [26]. Percolation theory has found applications in a wide variety of fields. Besides applications in material science investigating polymers, concrete, composites, porous media, etc., percolation theory has been applied to geophysics, information technology, marketing, and medical or biological studies [27].

Regardless of the source of percolation behavior, the percolation power law fit is used to describe the quantity of interest following percolation [28]. In the current case, the effective composite conductivity σ_{eff} at volume fraction ϕ greater than the percolation threshold is described by the equation,

$$\sigma_{eff} = \sigma_o \left(\frac{\phi - \phi_c}{1 - \phi_c}\right)^t, \phi > \phi_c, \tag{1}$$

where σ_o is the conductivity coefficient and t is the critical exponent [29]. The exponent t generally reflects the dimensionality of the system with values typically around 1.3-2 for two and three dimensions [3]. However, for carbon nanotube-based composites, the exponent t shows a non-universal nature based off the interfacial phenomenon [29]. Note that Equation (1) does not capture changes in conductivity prior to percolation and cannot be used to distinguish the mechanisms leading to percolation, only describing the conductivity after percolation is reached [28].

Percolation thresholds were first formally studied by Broadbent and Hammersley [30], introducing lattice models for fluid flow through statistically random media. Kallmes and Corte [31] later investigated percolation in fibrous networks through analytical modeling. Using a semi-empirical approach, Kirkpatrick [27] identified percolation thresholds based on lattice and bond percolation for both 2D and 3D cases. Furthermore, pioneering work for the simulation of electrical properties of conductor-insulator mixtures was conducted through the use of resistor network models [26]. The classic work by Pike and Seager [24,32] used Monte Carlo simulations to solve random lattice percolation models in 2D and 3D. In addition, they concluded that percolation of hardcore particles in a continuous medium is too complex a problem for simple analytical methods, especially if a variety of shapes, size, and preparation techniques are included. As such, these types of problems are ideal for a Monte Carlo simulations approach.

It is important to distinguish the difference between geometrical percolation and physical percolation. As detailed by Hakobyan et al. [33], geometrical percolation corresponds to microstructural changes such as the creation of a direct contact spanning network through the sample while physical percolation is related to changes in the macroproperties of a specimen like the effective electrical conductivity. In the proposed numerical modeling, the generated element representing a composite is analyzed for the formation of a spanning network. However, carbon nanotubes need not be in direct contact for a network to form. Therefore, the proposed model reports percolation thresholds unique to carbon nanotube-based composites because of this incorporated tunneling effect.

1.2.2 Microscale Overview and Nanoscale Effects

A microscale overview of the problem is shown in Figure 1. The nanotube-based composite is idealized by a representative volume element (RVE). The sides are insulated and a potential difference is applied across the RVE. The RVE is considered percolated when a network of CNTs span the specimen from top to bottom. From here, the effective electrical conductivity is found. The effective conductivity is defined as the conductivity of an "equivalent" homogenous material that produces the same electric current under the same boundary conditions as the heterogeneous, or composite, specimen [33].

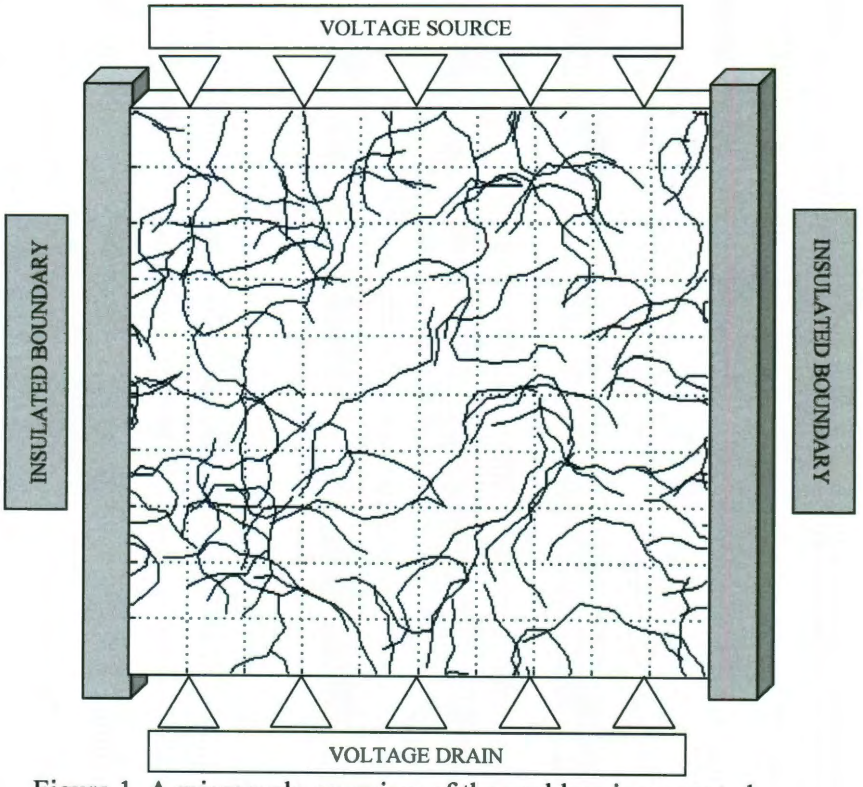

Figure 1. A microscale overview of the problem is presented.

The effective electrical conductivity of a composite is dependent on numerous nanoscale factors. Clearly, the conductivity is dependent on the filler content defined by the volume

fraction, *vf*, or the volume of the included nanotubes over the volume of the specimen. The conductivity of the filler sets the upper limit for the composite conductivity [34]. Furthermore, the size, geometric shape, and hardness of conductive fillers have a significant effect on the composite conductivity [35,36]. Many other factors, such as those mentioned in the following section, affect both percolation and conductivity. Also, aspect ratio plays an enormous role in governing the percolation threshold. Where carbon black with an aspect ratio of 1-2 requires loading levels as high as 50% *vf*, experiments have shown percolation thresholds of 0.1% *vf* for CNT-based composites [2]. Another factor is the type of carbon nanotube. Nanotubes can be single-, double-, or multi-walled. Single walled carbon nanotubes can be thought of as rolled up sheet of graphene and depending on the angle at which it is rolled, or chirality, SWCNTs can exhibit metallic or semiconducting properties [37,38].

Besides these considerations, the most important nanoscale effect for nanotube-based composites is electron tunneling. Electrons can tunnel or hop from one nanotube to another or intra-tube dependent on the separation distance between nanotubes, or parts of the same tube [39]. Therefore, nanotubes can remain fully encapsulated in the matrix and still form a conductive network [40]. Thus, this phenomenon helps elucidate why some experimental percolation thresholds (0.05-1.5 wt%) [3,13,19,21] are below estimated contact percolation thresholds (0.12-4.5 wt%) [20,22,23]. Theoretical calculations estimate the maximum tunneling distance between nanotubes to range between 1 and 2.5 nm depending on the insulating material [41,42]. With the maximum tunneling distance on the same order of magnitude as the diameter of SWCNTs, both the formation of

spanning networks and the electron tunneling play a significant role in the extremely low percolation thresholds [28].

1.3 Critical Issues in Experimentation

The electrical conduction of nanotube-based composites is no simple matter. Furthermore, major challenges exist in the research of nanocomposites, spanning across all length scales, from a lack of theoretical understanding of nanotubes to the characterization of reinforcing effects [43]. As discussed by Elsbernd [44], four critical issues exist in nanocomposite experimentation to include inadequate interfacial bonding, poor dispersion, waviness and alignment issues, and the accumulation of accurate experimental information.

The first critical issue in the development of CNT-based composites is inadequate interfacial bonding. Interfacial bonding describes the ability of the nanotubes to bond to the matrix material. Pristine nanotubes are essentially defect-free with an atomically smooth nonreactive surface. This inhibits the nanotubes ability to bond with the matrix thereby limiting the load transfer and the reinforcing capabilities. To aid in load transfer, the process of functionalization has been shown to be an effective solution. This process involves the attachment of various chemical functional groups to either nanotube end-caps or sidewalls through either covalent or noncovalent bonding [5]. A drastic increase in the interfacial bonding of nanotube-based composites can be achieved by specifically choosing functional groups based upon the selected composite matrix material [44]. Zhu et al. [5] reported a 30% increase in the elastic modulus of an epoxy composite with the addition of 1% weight fraction (wt) of functionalized SWCNTs. Furthermore,

functionalization is an excellent method because it allows nanotubes to be modified with specific functional groups based on the particular matrix material with only a slight degradation in the intrinsic properties of the nanotubes themselves [45].

Another challenge is dispersion. Due to the intrinsic van der Waals attraction between nanotubes, which is associated with their extremely high aspect ratio, nanotubes tend to agglomerate together forming ropes and bundles [5,13]. When embedded in a matrix material, nanotubes remain as entangled agglomerates reducing their effective aspect ratio and hindering dispersion. This inhibits the reinforcement of the matrix. Several methods have been proposed to overcome the various barriers for accomplishing dispersion: ultrasonication, high shear mixing, solution casting, surfactants, and several others [5,46]. The electrostatic charging of particles was also shown to aid in dispersion and hinder agglomeration [3]. Ramasubramaniam et al. [15] achieved homogenous dispersion through the use of non-damaging functionalization and reported achieving a 14-15 order of magnitude increase in electrical conductivity over the polymer with 7% wt SWCNT loading.

Waviness and alignment are additional challenges. As a result of their tremendous aspect ratio and very low bending rigidity, nanotubes possess a certain degree of curvature or waviness along their length [34]. The bending rigidity of carbon nanotubes is on the order of 10^{-25} Nm^2, due to their incredibly small diameters [47]. This waviness is preserved when the nanotubes are embedded into the matrix and can also be further induced by the manufacturing process [34]. In addition, current fabrication methods result in a large distribution of nanotube lengths and diameters [48,49], which in turn lead to a distribution of waviness exhibited by the nanotubes, increasing with nanotube length

[44]. Alignment is another consideration. The subject of alignment in conventional composites has been extensively studied and it is well known that unidirectional composites provide the highest strength and stiffness [18]. However, in relation to the impact on electrical conductivity of nanotube-based composites, conflicting experimental data has been reported [22,50-52]. Reported methods of alignment include mechanical stretching, melt spinning, extrusion or ejecting, magnetic field inducing, and shear flow [46]. As a prevailing feature of nanotube-based composites, waviness is incorporated into the proposed model. Also, to better understanding the effects of waviness and alignment, a case study is conducted to characterize their impact on the electrical behavior of CNT-based composites.

The final obstacle in nanocomposite experimentation is the accumulation of accurate knowledge about the effective properties. There are numerous potential composite permutations based on varying constituent material combinations, volume fractions, fiber morphologies, processing conditions, etc. Also, current fabrication methods may induce imperfections such as nanotube damage, filtration effects, agglomeration, and partial alignment [53]. Thus, challenges are present in the direct comparison of experimental data [40]. Consequently, inconsistencies are reported between results with varying interpretations [18]. These obstacles are relevant to all nanotube-based composites, while others are unique to the determination of electrical properties. As discussed earlier, percolation is probabilistic in nature: a percolating network in a finite-size specimen appears only with a certain probability. But in composite literature, the percolation threshold is usually taken as the volume fraction where specimens start to show percolation behavior, leading to surprisingly low thresholds being published [34]. Finally,

the accumulation of experimental data is not only difficult but also costly and time intensive. For polymer composites, nanotubes are usually functionalized before being dispersed into the epoxy matrix material and the resin cured. This process, as reported by Zhu et al [5], takes a minimum of 18 hours. Following this, samples are cut to size and prepped before being analyzed and tested. The complexity, expense, and time required for experimentation along with the variability in the composite itself are some of the driving motivators for numerical modeling.

1.4 Numerical Modeling

Because of the significant promise of these novel composite materials, the need to accurately predict their properties has developed. Furthermore, the sheer number of different material combinations limits experimental characterization. Numerical modeling provides the solution. Besides providing the ability to determine properties without resorting to testing, numerical modeling is a useful tool in understanding the link between the actual microstructure and the resultant electrical properties. With this knowledge, the optimization and specific tailoring of capabilities is possible. The motivation for the proposed model is derived from this context. The following sections discuss the differences in thermal and electrical conduction modeling, previous electrical conduction models, and the model proposed by this thesis.

1.4.1 Thermal and Electrical Conduction Modeling Differences

Although electrical and thermal conduction are described by continuum equations of the same form, these two transport processes cannot be solved in the exact same manner. For

thermal conduction, heat flux corresponds to electric current and temperature corresponds to electrical potential [54]. One major difference in solving these conduction problems is that finite element methods (FEM) may not be appropriate for electrical conduction [33]. Esteva [55] presented a finite element model for the determination of thermal conductivity of nanotube-based composite structure, accounting for the nanotube reinforcement in the polymer through the Embedded Fiber Method. This work was extended by Elsbernd [44], where non-linear thermal properties of nanotubes were incorporated. Despite the similarities of the continuum equations, these thermal models are not readily adaptable to electrical conduction. The reason can be traced back to the extremely large electrical conductivity ratio (10^{14}~10^{22}) between the nanotubes and the polymer. Table 1 illustrates this disparity between thermal and electrical conductivity ratios. This large electrical conductivity ratio leads to an ill-conditioned global stiffness matrix K in the FEM formulation leading to convergence difficulties [56]. Furthermore, carbon nanotube composites do not experience a thermal percolation effect due to the much lower thermal conductivity ratio and interfacial or Kapitza resistance [40,54].

Table 1. Thermal and Electrical Conductivity Ratios.

	Thermal (W/mK)	Electrical (S/m)	Ref.
Polymer Matrix	0.1 to 0.3	10^{-10} to 10^{-15}	[34,57]
CNTs	200 to 6600	10^{4} to 10^{7}	[7,10-12]
Conductivity Ratio	~10^{3} to 10^{5}	10^{14} to 10^{22}	

1.4.2 Previously Published Models

In seeking the accurate determination of electrical properties of nanotube-based composites, a variety of models are available in literature. These models include a diverse

range of parameters and simplifying assumptions. Table 2 presents a brief compendium of published models focused on the determination of the electrical properties of carbon nanotube-based composites. The table also illustrates key features included in the each model. One set of features are morphological features showing whether the model used a fixed value or distribution of values for length and diameter and if nanotube waviness is accounted for by the model. Another set of features are the sources of resistance accounted for in the determination of the effective conductivity to include both the intrinsic resistance of the nanotubes and the contacts between them. Table 2 also shows whether the models account for the effects of electron tunneling and gives the focus of each model's respective study.

With percolation being the fundamental concept behind electrical conduction in insulator-conductor composites, some models focus specifically on the determination of percolation thresholds [22,58]. Both models shown in Table 2 assume nanotubes are straight or "sticks." Beyond these percolation only models, numerous models are presented for the determination of the effective electrical conductivity. Using the straight stick assumption, Seidel and Lagoudas [28] present a micromechanical model using the composite cylinder approach as a nanoscale representative volume element and obtain the effective electrical properties for the composite using the Mori-Tanaka method. They also account for electron hopping and metallic/ semiconducting nature of nanotubes. Except for a few other micromechanical- and analytical-based models [59-61], the overriding majority of models in the determination of carbon-nanotube based composite electrical conductivity utilize the resistor network approach.

Among just resistor network models, there is great diversity. Modeling types vary between 2D, pseudo-3D, and 3-dimensional. In terms of resistor components, some models incorporate only the resistance of the nanotube while others use only the contact values between nanotubes. Other models use "effective resistance values," indirectly accounting for both. Nonetheless, many models directly account for both resistance components and due to the dominant effect of contact resistance on the overall conductivity [41], this is thought to be the more accurate approach. To account for the varying contact resistance between nanotubes, dependent on the varying thickness of insulating films surrounding each nanotube, two models incorporate distributions for contact resistance. The first model, presented by Li and Chou [18], included a distribution of contact resistances calculated using an assumed normal distribution for the thickness of insulating films. The model also included key parameters like electron tunneling, nanotube resistance, and nanotube waviness and was used to investigate alignment, waviness, and anisotropic effects on the effective composite conductivity. The second model to incorporate a distribution for contact resistance was the model presented by Jack et al. [62]. The model considered three separate contact types, e.g., metallic-metallic, metallic-semiconducting, and semiconducting-semiconducting, where the resistance of each type was described by a normal distribution. Additionally, distributions were used for both the length and diameter nanotube values. Studies were conducted to analyze the effect of the included stochastic parameters along with nanotube alignment and localized power concentration. Although distributions were used to account for the stochastic nature of the problem, the model neglects the resistance of nanotubes and does not account for electron tunneling or nanotube waviness.

Table 2. Published Models for the Determination of Electrical Properties of Nanotube-Based Composites from Selected Literature.

Type	Morphological Features			Resistor Components		Electron Tunneling	Focus	Authors	Ref.
	Length	Diameter	Wavy	Contact	CNT				
Resistor Network Models									
2D	fixed	fixed	no	yes	yes	no	AR, conductivity ratio, used "effective" mat prop's	Hansel et al	[63]
2D	fixed	fixed	no	no	yes	no	AR, alignment, compared to regular lattice	Cheng et al	[64]
Pseudo3D	fixed	fixed	yes	yes	yes	yes	AR, waviness	Li et al	[34]
Psuedo3D	fixed	fixed	yes	yes	yes	yes	calculated max tunnel distance, dominate effect of CR	Li et al	[41]
Psuedo3D	fixed	fixed	yes	dist.	yes	yes	waviness, alignment, anisotropic effects	Li and Chou	[18]
Psuedo3D	dist.	dist.	no	dist.	no	no	effect of including stochastic parameters, alignment, diameter, CNT prop's	Jack et al	[62]
3D	fixed	fixed	no	yes	yes	no	effect of alignment and measurement angle, CNT length, device length	Behnam et al.	[65]
3D	fixed	fixed	yes	yes	yes	no	AR, waviness, contact resistance	Dalmas et al	[66]
3D	fixed	fixed	yes	no	yes	no	AR, waviness, aggregation, CNT conductivity	Hu et al	[67]
3D	fixed	fixed	yes	yes	no	yes	AR, waviness, calculated max tunnel distance, CR	Sun and Song	[42]
3D	fixed	fixed	yes	yes	yes	yes	AR, waviness, van der Waals interactions and tunneling distance	Lu et al	[68]
3D	fixed	fixed	no	no	yes	yes	van der Waals interactions, agglomeration	Grujicic et al.	[2]
2D/3D	fixed	fixed	no	yes	yes	yes	piezoresistive nature, used "effective" mat prop's	Theodosiou & Saravanos	[53]
Other Model Types									
MM/ CC/ MT	fixed	fixed	no	no	yes	yes	AR, e^- tunneling, met/non-met CNTs, formation of conductive networks, CNT prop's	Seidel and Lagoudas	[28]
MM/ IDD	fixed	fixed	yes	yes	yes	no	AR, waviness, conductivity anisotropy, CR	Deng and Zheng	[59]
Num./ Anal.	fixed	fixed	yes	no	yes	yes	soft/hard core models, e^- tunneling, waviness	Berhan and Sastry	[60,61]
Percolation Only Models									
2D	fixed	fixed	no	N/A	N/A	yes	AR, alignment	Natsuki	[58]
2D	fixed	fixed	no	N/A	N/A	no	alignment	Du et al	[22]

Note: MM = micromechanical, CC = composite cylinder, MT = Mori-Tanaka, IDD = interaction direct derivation, Num. = Numerical, Anal. = Analytical, FEM = Finite Element Method, AR = aspect ratio, CR = contact resistance, dist. = distribution

1.4.3 Proposed Model

This thesis presents an accurate and versatile model to determine both the percolation threshold and effective electrical conductivity of a carbon nanotube-based composite. Through the incorporation of numerous statistical distributions along with key parameters, the model provides a realistic representation of both the geometry of the composites and physical behavior. Length and diameter distributions along with nanotube waviness are included in the generation of the geometry. Nanotube resistance and contact resistance, through the use of a distribution, are used in construction of the equivalent resistor network and the determination of the effective conductivity. Furthermore, electron tunneling is accounted for in the model. To the knowledge of the author, no other available model incorporates this set of features.

The model also incorporates Monte Carlo simulation (MCS) techniques which are a powerful tool in probabilistic studies [69]. Percolation type problems especially resistor network modeling where the effects of disorder and other stochastic parameters need to be accounted for are ideal for Monte Carlo simulations. Pike and Seager [24] along with Kirkpatrick [26] demonstrated its applicability to resistor networks in the early 1970s. The advantage of MCS techniques comes from the fact that the deterministic formulation of the problem remains unchanged. The problem is defined in terms of a set of random variables, which are quantified in terms of their statistical moments and probability density functions. In the proposed model, these variables represent the electrical properties of the composite and carbon nanotube morphological features. Next, values for the each random variable are numerically generated and used to solve the deterministic problem. This problem is solved many times each with a unique set of values for the

random variables. Finally, statistically processing of the generated ensemble of results allows viable information about the composite's electrical properties to be extracted. The accuracy of the results increases with the number of simulations or realizations. Nevertheless, by increasing the number of MCSs, computational time is also increased [69]. A convergence analysis is later conducted to determine the required number of simulations to yield statistically valuable data.

2 The Representative Volume Element

The approach presented in this paper is a Monte Carlo-based pseudo-three dimensional resistor network model. This chapter along with the Chapter 3 and Chapter 4 detail how the proposed model works. The model is broken down into three distinct steps which are the generation of the representative volume element, identification of the potential spanning network, and solving of the equivalent resistor network problem. First, to create the nanotube geometry of the RVE, nanotubes are randomly generated one at a time using the morphological parameter distributions until the desired volume fraction is reached. Second, through a specially developed algorithm, the RVE is checked for the formation of a spanning network. Finally, if a spanning network is identified within an RVE, an equivalent resistor network is constructed based off the given nanotube geometry and the effective electrical conductivity for that RVE is found. The current chapter focuses on the generation of the RVE, detailing the creation of the geometry at the nanoscale along with analyzing the accuracy of the representation at the microscale.

2.1 Geometry Generation

The first step in accurately modeling a composite material requires a realistic representation of the reinforcing constituents to include both geometry and properties [44]. The effective properties of the carbon nanotube-based composite as a whole are represented by the representative volume element. The RVE is the smallest material region characteristic on average of the entire material, as viewed from a continuum point

of view. For case of multiphase media such as composites, the RVE contains all phases in relative concentrations reflective of the overall composite and is therefore large enough to be representative of the overall morphology of the material structure [70]. Recently, statistical information on nanotube morphology such as length and diameter has been extracted from experimental images [48,49]. To achieve accurate geometrical representation within the RVE, these distributions along with nanotube waviness and orientation are integrated into the proposed model.

Although it has been experimentally shown that nanotube lengths can vary within a wide range of values from less than 100 nm to over many microns [48,49] depending on the method of fabrication, very few other numerical models have incorporated these types of distributions. The proposed model incorporates a Weibull distribution of lengths reported by Wang et al. [49]. This distribution was performed over a large number of nanotubes and is viewed as being statistically accurate. Wang et al. went on to report both the scale and shape parameters of the Weibull distribution of a = 5E6 and b = 2.4, respectively [49]. Using the inverse transformation method, which is a simple technique used to sample from an arbitrary distribution, the cumulative density function (CDF) for a Weibull distribution,

$$F(x) = 1 - e^{-\left(\frac{x}{\alpha}\right)^{\gamma}}, \tag{2}$$

is rearranged and x is isolated giving the equation

$$x = -\alpha[ln(1-u)]^{\frac{1}{\gamma}}, \tag{3}$$

where x is a random number from a Weibull distribution and u is a random number from a uniform distribution between 0 and 1. The constants α and γ above are related to the reported scale and shape parameters in the following manner:

$$\alpha = e^{-\frac{ln(a)}{b}}, \gamma = b. \tag{4}$$

Using Equation (3) along with the imposed minimum and maximum nanotube lengths of 20 nm and 800 nm, respectively, the length of each nanotube in the proposed model is randomly generated from the experimentally reported Weibull distribution using the inverse transformation method. This same technique is described and employed by Elsbernd [44] and Esteva [55]. Figure 2 shows a histogram of 1,341 random lengths generated in this fashion. The distribution of lengths has a mean of 140.9 nm and a median of 136.7 nm.

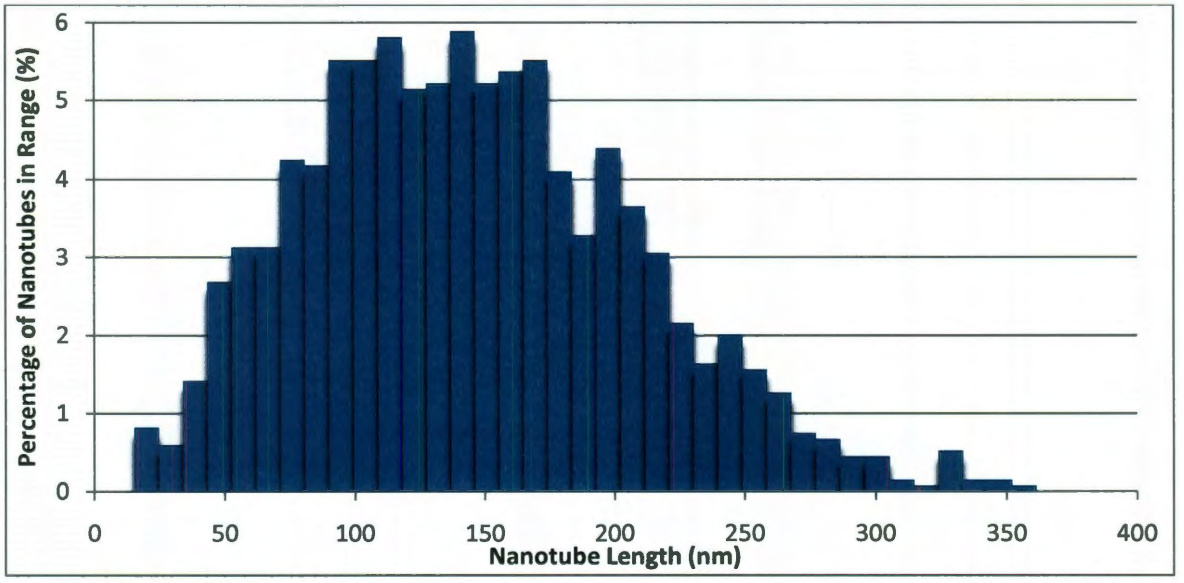

Figure 2. A histogram of 1341 Weibull randomly generated nanotube lengths is presented.

Just as lengths vary among nanotubes, diameters do as well. Although SWCNTs with diameters as large as 6 nm are reported, the average diameter tends to be between 1 to 2

nm [71,72]. On the other hand, nanotube bundles are reported with diameters having many tens of nanometers in width [62]. With advancements in processing, agglomeration such as this is ignored. Ziegler et al. [48] reported a histogram of individual nanotube diameters ranging between 0.5 nm and 2 nm as shown in Figure 3(a). Since no particular distribution is reported, the histogram is reproduced and a log-normal distribution fit is chosen to fit the data, shown in Figure 3(b). Using the MATLAB "dfittool" capability, the mean and standard deviation are calculated for this distribution as $\mu = 0.02847$ and $\sigma = 0.3363$, respectively.

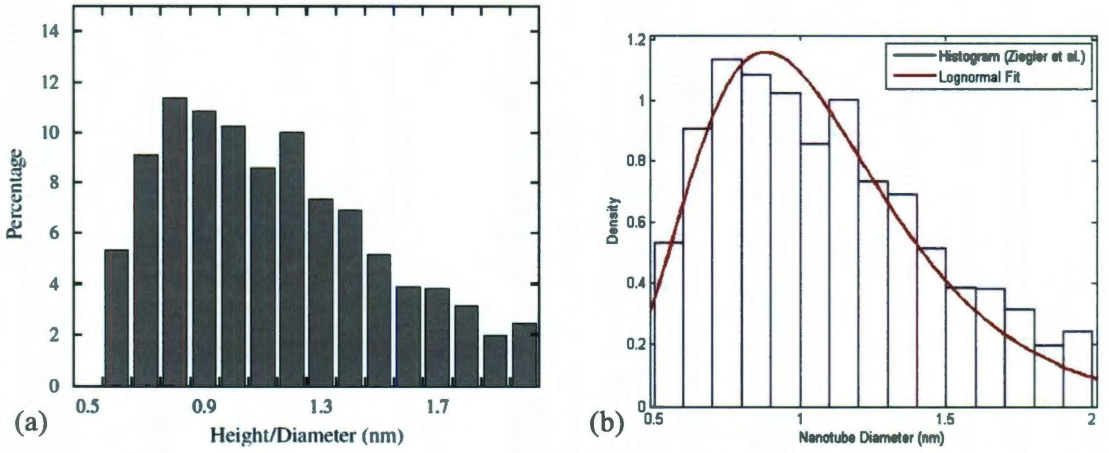

Figure 3. The extraction of the nanotube diameter distribution is shown with (a) the experimental histogram by Ziegler et al. [48] and (b) the reproduced histogram with log-normal distribution fit.

With these parameters determined, the same inverse transformation method as described above is applied. The CDF for a lognormal distribution is given by the equation,

$$F(x) = \frac{1}{2} + \frac{1}{2} erf\left[\frac{ln(x) - \mu}{\sigma\sqrt{2}}\right]. \tag{5}$$

Solving the CDF for x yields the equation

$$x = e^{(\sigma\sqrt{2} erfinv[2u-1]+\mu)}, \tag{6}$$

where x is a random number from a lognormal distribution and u is a random number from a uniform distribution. Using Equation (6) along with the calculated distribution parameters, the proposed model generates random nanotube diameters, with an imposed lower limit of 0.5 nm as experimentally found by Ziegler et al. [48] and supported by theoretically computations by Pipes et al. [73]. This diameter, however, is not the effective diameter of the CNTs once embedded within the matrix material. The equilibrium separation distance between a nanotube and polymer is equal to carbon-carbon bond spacing of 0.34 nm, thereby increasing the effective diameter of each nanotube by 0.68 nm. This effect is ignored for the nanotube lengths which are 2-3 orders of magnitude higher but cannot be neglected for the diameters [73]. A histogram of 1,341 random effective diameters is shown Figure 4 with a mean of 1.76 nm and median of 1.71 nm.

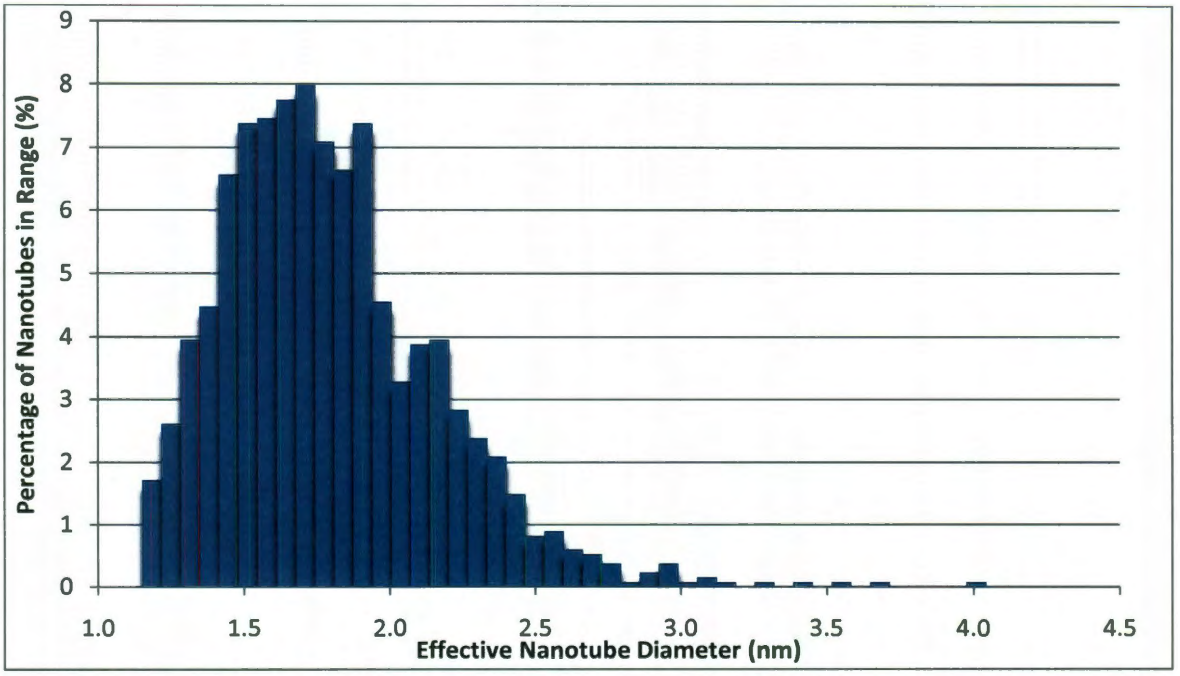

Figure 4. A histogram of 1341 lognormal randomly generated effective nanotube diameters using the parameters by Ziegler et al. [48] are presented, including carbon-carbon spacing.

As explained earlier, the percolation threshold of a composite is very sensitive to the aspect ratio of the filler. Figure 5 shows the resulting distribution of aspect ratio values resulting from the Weibull length distribution and lognormal diameter distribution.

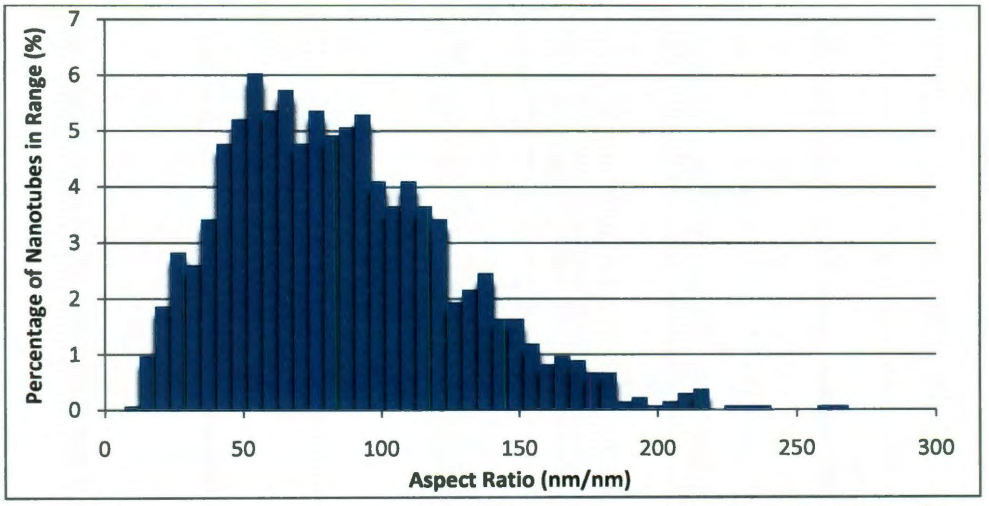

Figure 5. A histogram of 1341 nanotube aspect ratios resulting from the Weibull length distribution and lognormal diameter distribution is presented.

The final morphological parameters integrated into the geometry generation of the RVE are waviness and alignment. To account for the experimentally observed waviness, each nanotube is divided into ten segments. Each segment is assumed straight with neighboring segments having an angle of deviation between them. This angle of deviation follows a uniform distribution between $sin(-\theta_{max}/2)$ and $sin(\theta_{max}/2)$, where θ_{max} is some upper limit. Néda et al. [74] showed that this form of distribution results in complete isotropy of the generated segment orientation and is used by other numerical models, such as Dalmas et al. [66]. As mentioned in the Section 1.3 and explained by Elsbernd [44], the waviness of a nanotube can be considered a function of its length. Due to the lack of experimental data detailing this subject, a linear model of waviness is

assumed, where the maximum angle of deviation between neighboring nanotube segment is given by

$$\theta_{max} = \frac{180°}{upper\ length\ limit} \times actual\ nanotube\ length. \quad (7)$$

The overall alignment or orientation of the nanotube geometry is controlled through the generation of each individual nanotube. The first point of a nanotube is generated randomly within the RVE. The location of the second point is determined by the angle of alignment, θ_a, with respect to the y-axis. The angle of alignment is generated from a uniform distribution within the interval $-\theta_a < \theta < \theta_a$, where 90° yields the randomly oriented or isotropic case and 0° results in perfect alignment in the y-direction. The use of any angle less than 90° results in some form of alignment creating an anisotropic RVE. Both Du et al. [22] and Natsuki et al. [58] controlled alignment of the nanotube morphology in a similar fashion. Once the second point is created, the first segment is defined and the following 2^{nd} -10^{th} segments are generated based on the angle of deviation. With this generation of nanotube geometry, the alignment control is limited to straight or slightly-wavy nanotubes, where alignment control is lost for high levels of waviness. Except for the latter case study on alignment, the alignment angle is set to 90° yielding a completely random orientation of nanotubes.

With the specifics of the stochastic morphological parameters explained, the nanotube geometry of a RVE is produced. The positions and orientations are randomly generated for each nanotube. With a unique length and diameter realized from there respectively distributions, the volume of a nanotube with the assumed shape of a cylinder is determined. Nanotubes are added one by one until a user-defined volume fraction is

reached. A completely generated geometry is referred to as a microstructure [44]. Figure 6 shows two RVE microstructures with 1.0% volume fraction highlighting the capabilities of the model.

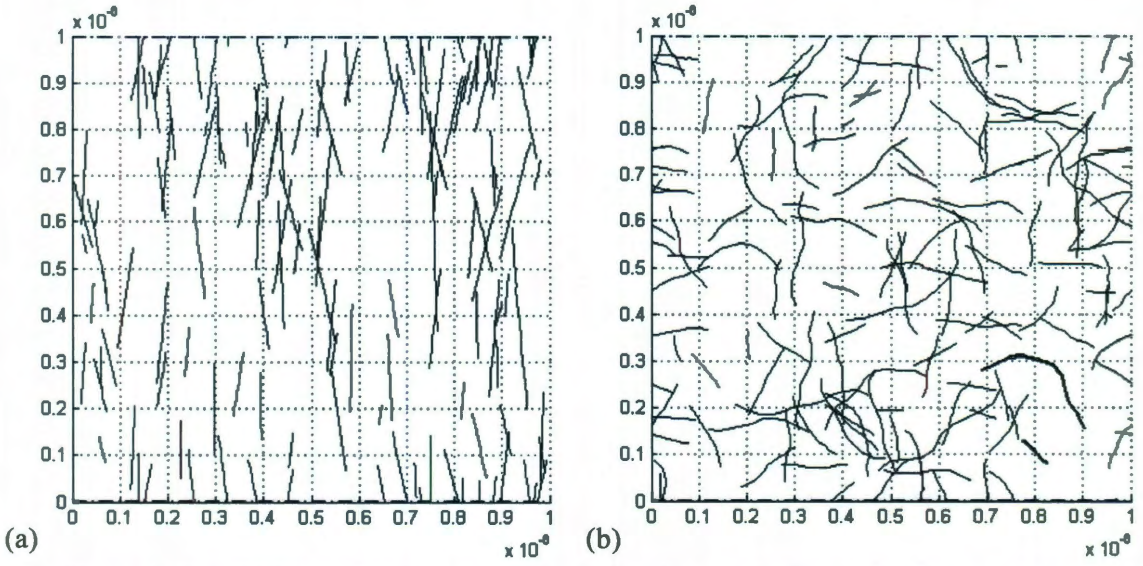

Figure 6. Two RVEs each with 1.0% volume fraction are depicted. The figures show the controllable morphology of the model with (a) having straight, partially aligned nanotubes while (b) has randomly-oriented, wavy nanotubes. The highlighted nanotubes in (b) simulate the physical phenomenon where longer nanotubes are wavier than shorter nanotubes.

2.2 Accurate Microscale Representation

Having incorporated various distributions into the generation of the nanotube geometry, the stochastic nature of CNT-based composites is captured. Nonetheless, to ensure a realistic microscale representation of the composite, the attributes of the RVE are checked. These attributes include a periodic geometry with random nanotube dispersion along with the dimensions of the RVE itself.

2.2.1 Periodic Geometry and CNT Dispersion

Again, the RVE is the smallest material region which is structurally typical of the entire solid [70] and can be thought of as an excised piece from a larger whole. To form an effective representative element, continuity is required by adjacent elements, thus requiring geometric continuity of adjacent sides of a single RVE [62]. This is accounted for by creating a periodic geometry as shown in Figure 7.

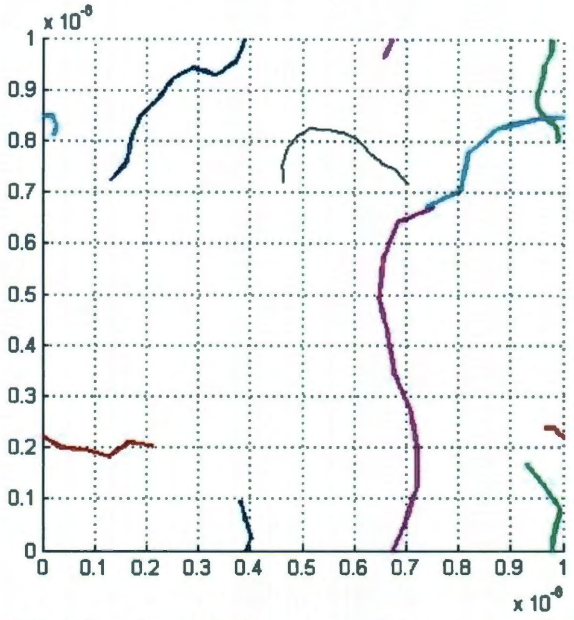

Figure 7. An RVE highlighting the periodic nature of the generated geometry is presented.

Figure 7 shows how a nanotube going through a RVE boundary is ended at the boundary, transposed to the opposing boundary, and continued. The colors indicate nanotubes being split across a RVE boundary. Few models note the inclusion of a periodic geometry. However, Jack et al. [62] states that the periodic continuity is one of two main considerations in accurate representation and subsequently includes the feature as does the proposed model.

Furthermore, with recent experimental advances in processing [46], the proposed model works under the assumption of homogenous nanotube dispersion throughout the RVE. Thus the placement of nanotubes within the RVE is completely random. Combined with a random nanotube orientation, the resulting RVE is isotropic in nature. Therefore any equal length measurement along the composite should yield the same number of crossings by the nanotubes. Figure 8 shows that this holds true and that excellent dispersion is achieved with the proposed model.

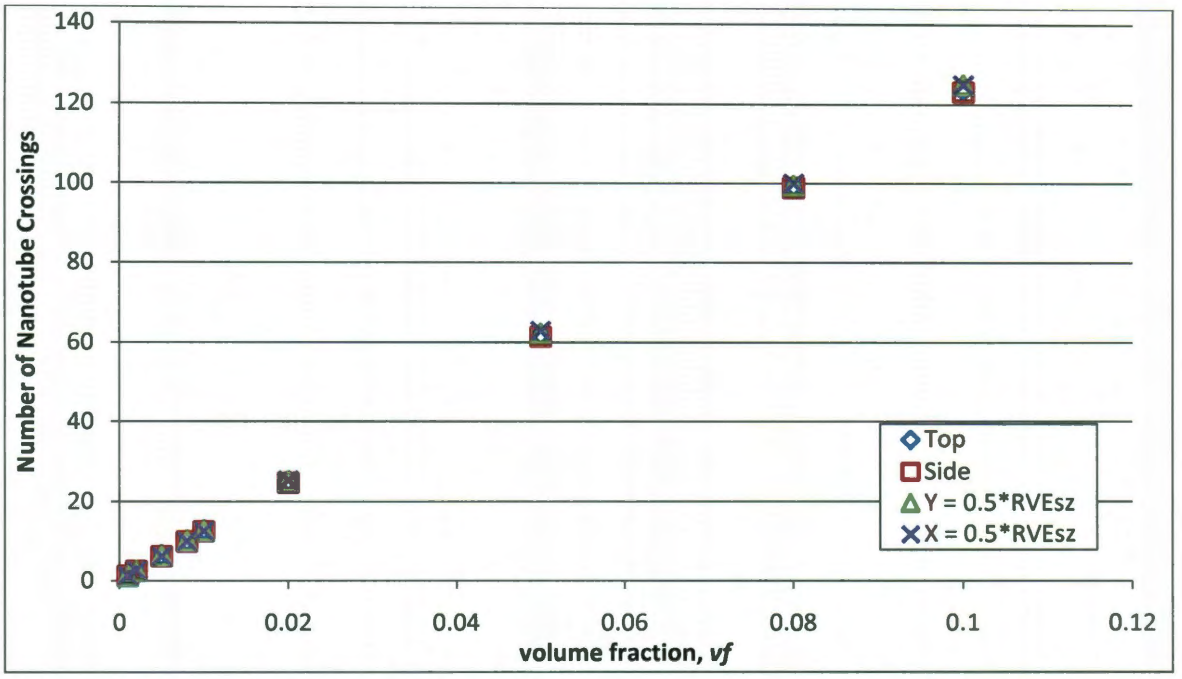

Figure 8. The number of top and side nanotube boundary crossings along with both horizontal and vertical centerline crossings is presented. The lack of scatter within the data points indicates homogenous dispersion characteristics for generated periodic RVEs.

2.2.2 RVE dimensions

The final consideration in the realistic representation of a carbon nanotube-based composite structure is the size of the RVE. As previously mentioned, the RVE from a statistical point of view is large enough to be representative of the overall morphology of

the material [70]. The dimensions of the RVE are the second main consideration defined by Jack et al. [62] necessary for effective representation. Jack et al. [62] continues by stating that the representative element must be sufficiently larger than the largest geometric feature, capturing the stochastic nature of the geometric effects.

Clearly, the selection of the RVE dimensions is paramount in effectively representing the microscale structure of the composite. With the proposed pseudo-3D modeling, a square RVE with specified thickness is used. This gives two dimensional parameters to consider, length and thickness. Table 3 reports a small collection of dimensions from published numerical models including the RVE length, nanotube length, and the resulting ratio between the two.

Table 3. RVE Dimensions from a Collection of Numerical Models.

Authors	Model Type	RVE Length	CNT Length	L_{RVE}/L_{CNT} Ratio	Ref.
Theodosiou and Saravanos	2D	1x1 μm	1 μm	1	[53]
Li et al.	Psuedo-3D	20 μm	2 μm	10	[34]
Li and Chou	Psuedo-3D	30 μm	1-1.5 μm	20-30	[18]
Jack et al	Psuedo-3D			10x mean L_{CNT}	[62]
Dalmas et al.	3D	1 (unit cube)	0.4	2.5	[66]
Grujicic et al.	3D	10, 15, 20, 15 μm	3 μm	~3.3, 5, ~6.6, ~8.3	[2]

Table 3 shows that length ratios ranging between 1 and 30 are used for numerical models investigating electrical properties of CNT-based composites. Note that the model by Jack et al. [62], which employs a distribution for nanotube lengths, uses a RVE length 10 times the mean nanotube length. Numerical modeling by Grujicic et al. [2] showed that the length ratio, varying between 3.3 and 8.3, has very weak effect on the computed percolation threshold. Although increasing the length ratio may potentially improve results, there is a tradeoff with computational time where a larger RVE means more

nanotubes to create, check for a spanning network, and solve as a resistor network. As such, a compromise is sought. The necessary ratio of nanotube length to RVE length for accurate modeling is one of the topics of investigation discussed later.

The RVE thickness is the final dimensional concern. In three dimensional modeling, where the RVE is a cubic shape, the thickness is the same as the length [2,42,66,68]. For pseudo-3D modeling, thickness is a greater concern. As the thickness is increased so is the volume, which acts to increase the density of nanotubes when the microstructure is viewed from two dimensions. To alleviate this issue, the methodology presented by Li et al. [41] for pseudo-3D modeling is used. The model composite is considered a multi-layer nanotube-based composite as shown in Figure 9(a), where due to uniformity in the thickness direction it is reasonable to consider only a representative layer, shown in Figure 9(b). This representative layer is pseudo-3D where nanotubes are distributed in two stacked layers separated by polymer, shown in Figure 9(c). This layer of polymer, or insulating film, could range from 0 to the maximum insulating film thickness allowing the tunneling of electrons. In conclusion, the resulting thickness of the pseudo-3D RVE is equal to twice the nanotube diameter plus the specified tunneling distance. Note that the average diameter value is used here. Figure 9(d) shows the contact area between overlapping nanotubes, which will become pertinent in the formation of the resistor network.

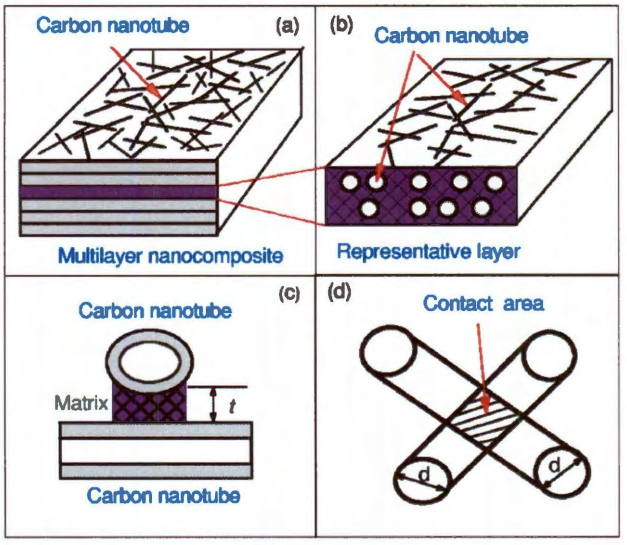

Figure 9. An idealized carbon nanotube-based composite is presented to depict the computational thickness, with (a) showing the multilayer composite, (b) representative layer, (c) separation between nanotubes, and (d) the overlap between nanotubes [41].

As depicted in Figure 9, the thickness of the RVE is dependent on the diameter of the embedded nanotubes and specified tunneling distance. Also note that nanotubes are considered 'hard-core' and do not penetrate each other, instead stack in layers. In 3D modeling, this distinction between 'hard-core' (impenetrable) and 'soft-core' (penetrable) nanotubes becomes applicable in the geometry generation. While many 3D models assume the less computationally expensive 'soft-core' approach [23,42,66,67,75], other models have used impenetrable nanotubes or a 'hard-core' approach with the overall conclusion that the difference in modeling techniques becomes negligible at higher aspect ratios (>300) especially at low volume fractions [2,61,68].

3 Spanning Network Identification

With the generation of the stochastic microstructure complete, the RVE is checked for the formation of a spanning network. A spanning network is considered a continuous chain of nanotubes in either direct contact or within the specified tunneling distance, reaching from the top of the RVE to the bottom. Before the spanning network identification algorithm (SNIA) is explained in full, the specifics of the algorithm to include the bonding criterion, fiber bin sorting, and fiber discretization are covered.

3.1 Algorithm Specifics

As described by Pike and Seager [24], the essence of percolation theory is determining how a given set of regularly or randomly positioned sites are interconnected. In the proposed model, these sites are the randomly positioned embedded fibers. Note that for the SNIA process nanotubes are referred to as fibers and the points which define the nanotubes are referred to as nodes. To determine if an unbroken sequence of fibers form a cluster or network spanning the RVE, bonding criterion is used to specify whether nodes of different fibers are connected. The bonding criterion is a function of the bonding parameters, which are considered deterministic in the proposed model because they are directly associated with the nodes [24].

The bonding parameters for two specified fibers include each fiber's respective radius along with the user-defined tunneling distance. Therefore, the bonding parameters vary not only between fibers but between which two fibers are being checked for contact. The

tunneling distance is a user defined parameter, where a value of zero yields a network with only direct contact between fibers and any value larger than zero simulates the ability of electrons to hop or tunnel a distance up to that defined value. Having the ability to vary this parameter is one of the major advantages of this model. Contact between fibers is checked by comparing the proximity of their nodes. Two nodes of different fibers are considered to be in contact or bonded when the distance between them is equal to or less than the summation of each fiber's respective radius and the specified tunneling distance. Therefore, the bonding criterion is met if the separation distance between nodes is less than or equal to the variable searching range (VSR), where the VSR is the summation of each fiber's radius and the tunneling distance (R_1+R_2+TD). Figure 10 provides a simplistic illustration of this concept.

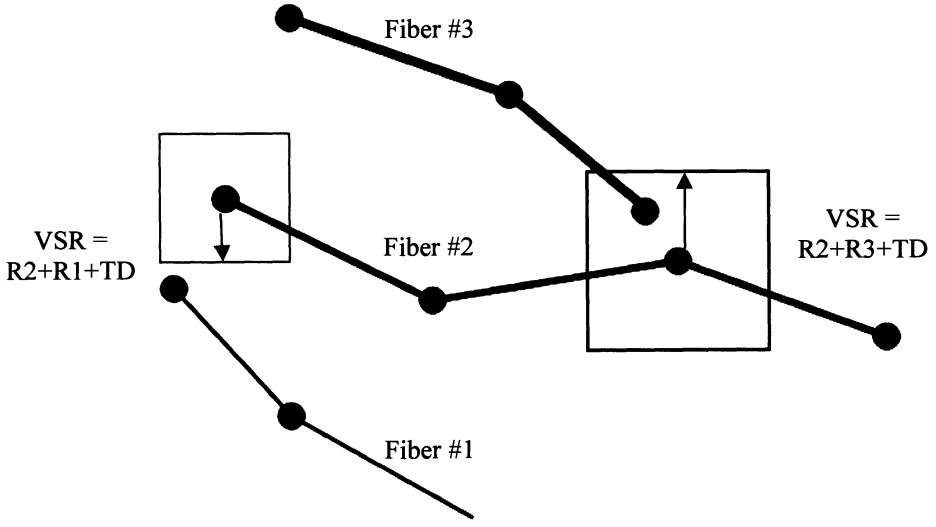

Figure 10. Details of the bonding criterion are illustrated highlighting the VSR capability.

The VSR concept is depicted by Figure 10. The dimensions of the searching box vary based on the current fiber's radius (R_1) and the radius of the fiber it is being checked against (either R_1 or R_3) along with the tunneling distance. The VSR concept therefore

accounts for the distribution of nanotube diameters. In Figure 10, the searching box from fiber #2 encompasses a node of fiber #3 and as such, the two fibers are connected. Also note that the actual dimensions of the searching box are twice the VSR. The bonding criterion of the proposed model is very similar to the 'inclusive figure' model defined by Pike and Seager [24], where two sites are connected if they lie within each other's searching area. Pike and Seager [24] went on to report a minimal difference in results between the use of squares and circles for the bonding criterion. Therefore, with computational time a consideration, squares are used in the proposed model.

With the bonding criterion explained, two important steps are completed before the RVE is checked for a network. These two steps are the sorting of the fibers into bins and the discretization of the fibers, both occurring once the RVE microstructure is generated. The first of these steps sorts the embedded fibers within the RVE into bins used for the searching of a network. Bins can be thought of as a regular grid mesh overlaid on the microstructure. Because the RVE is square shaped, the number of bins is equal to the square of the number of divisions, both vertical and horizontal. For example, one division yields only one bin, two divisions yield four bins, and so on. This concept is illustrated in Figure 11(a), where an RVE with 5 divisions or 25 bins is shown. The bin locations of the each fiber are recorded and later used in the SNIA. Note that a fiber can be located in multiple bins. For a given fiber and its defined bin or bins location, that fiber only needs to be checked against other fibers located in that same bin or bins, thereby eliminating the need to check that one fiber for connections with all other fibers in the RVE. As such, computational time is greatly reduced as shown later by the incorporation of bins.

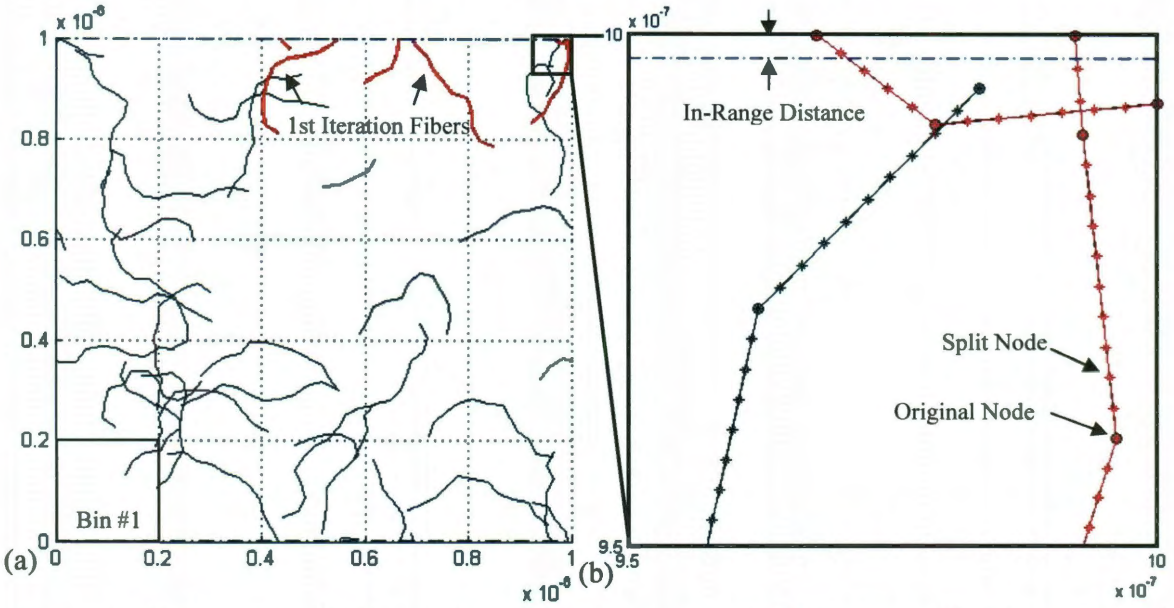

Figure 11. Details of the SNIA are illustrated by (a) a complete RVE along with (b) an enhanced view.

The final step before the RVE is checked for a spanning network is the discretization or "splitting" of the fiber segments. This subroutine is referred to as the "fiber splitter" for the sake of simplicity. As explained with the bonding criterion, the SNIA identifies contacts between fibers through proximity of their nodes. Since the VSR searching boxes are relative small in comparison to the length of the fiber segments, nodes are added along a fiber segment to ensure potential contact between neighboring fibers is not lost. To ensure adequate coverage of the searching boxes, the number of discrete nodes added, referred to as split nodes, along a fiber segment is dependent on not only its length but the morphology of the current RVE and the specified tunneling distance. The number of nodes to add along a segment is determined by the equation

$$\lceil number\ nodes\ to\ add \rceil = \frac{L_{seg}}{d_{min} + TD} - 2, \tag{8}$$

where the L_{seg} is the length of the original segment, d_{min} is the minimum diameter value in the current RVE, and TD is the specified tunneling distance. A value of less than one from Equation (8) means that no new nodes are required. Using d_{min} in determination of the number of split nodes ensures searching gaps are eliminate regardless of the fibers being checked against each other. Nonetheless, searching boxes along a fiber segment do overlap as shown in Figure 12.

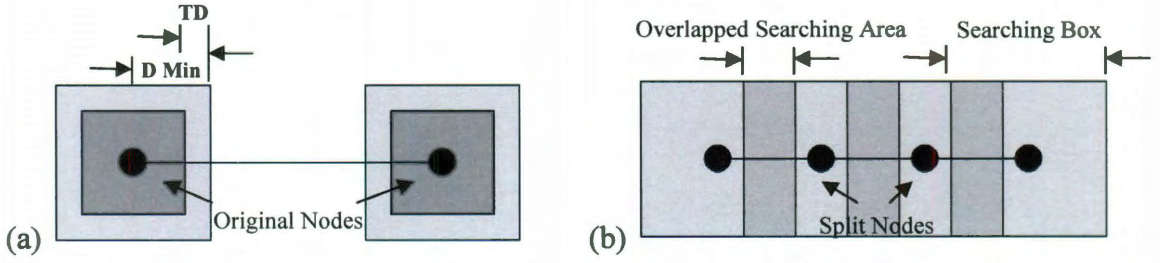

Figure 12. Details of the SNIA are illustrated by (a) an original fiber segment and (b) the same segment with the added split nodes.

The details of the fiber splitter are shown in Figure 12. The original segment is shown in Figure 12(a) with an illustrative searching box around the original nodes. Figure 12(b) shows the same segment with the additional split nodes along with the overlapped searching area. Note that the addition of the split nodes does not change the straight geometry of the original segment. Figure 11(b) also illustrates the split nodes concept, where the circles designate original nodes and asterisks designate split nodes.

3.2 Algorithm Steps

With these concepts in place, the actual spanning network identification algorithm is explained. A simplified version of the SNIA is presented in Figure 13.

```
(1) Geometry Generation
(2) Fiber Bin Sorting
(3) Fiber Splitter
(4) Spanning Network Identification
  (a) IF Potential Network exists - Fibers on top and bottom
    (b) WHILE Iteration Counter < I_MAX - (Iteration Loop)
      (c) DO loop over Fibers added in past Iteration (Checker Fiber Loop)
        (d) DO loop over Bins of Checker (Bin Loop)
          (e) DO loop over Nodes of Checker (Checker Nodes Loop)
            (f) DO loop over Fibers in Current Bin - (Checkee Fiber Loop)
              (g) DO loop over Nodes of Checkee - (Checkee Node Loop)
                (h) IF bonding criteria btwn Checker node and Checkee node met
                    Add Checkee Fiber to Network
                    Add contact
                END
      (i) IF no new fibers added in current Iteration – Iteration Counter = I_MAX
    END
    (j) IF Network formed – RVE bottom reached
        Eliminate contact duplicates
    END
  END
(5) Resistor Network
```

Figure 13. Pseudocode of the spanning network identification scheme.

Clearly, even in simplified form, the algorithm developed to identify spanning networks is quite complex. In an attempt to clarify the explanation, the steps of the algorithm are labeled in Figure 13. With the first three steps complete, the RVE microstructure is ready to be checked for a spanning network (step 4). In order for a spanning network to be possible, fibers need to be within range of both the top and bottom boundary (step a). Fibers need not cross these given boundaries but must be closer than the maximum in-range distance, equal to the minimum nanotube radius plus the specified tunneling distance. Figure 11 illustrates this concept with the blue-dashed line above and below the

bottom and top boundaries, respectively. If a network is not possible based off this criteria, the remaining SNIA is passed over.

Assuming a possible network, the SNIA is continued. The searching process works in iterations (step b), where the first iteration of fibers in the network is considered the fibers touching the top boundary. Figure 11(a) highlights these first iteration fibers in red. Fibers in the network are recorded based on the iteration number they are found. The code then loops over all the fibers in the current iteration (step c). Taking a fiber at a time, the current fiber, which is already in the potential network, is referred to as the "checker fiber" as it is the fiber that other fibers not in the network are "checked," meaning searched for contacts, against. With the current checker fiber determined, the SNIA then loops over the bin or bins that the specific fiber is located in (step d). Next, the nodes of the current checker fiber are looped over (step e). Taking one checker fiber node at a time, the fibers located in the current bin are looped over (step f). These fibers are ones that are not yet in the network and are being checked for potential contact, referred to as the "checkee fiber." With the current checkee fiber determined, the SNIA loops over the nodes of that fiber (step g). The bonding criterion is then used to determine if contact is made between checker and checkee fiber nodes, accounting for the radii of each fiber (step h). If the bonding criterion is met, the contact is added between the two nodes and the checkee fiber is added to the network designated by the current iteration number plus one. The looping is continued for the rest of the nodes of the checkee (step g), the rest of the checkee fibers (step f), nodes of the checker (step e), bin locations of the checker (step d), and checker fibers in the current iteration (step c).

Iterations of the SNIA are continued until there are no new fibers added and therefore no future iterations (step i). When this happens, the iteration loop is terminated (step b). The network is then checked to see if it spans the RVE (step j). This simple step is accomplished by seeing if the network contains any of the fibers already specially designated as touching the bottom of the RVE. If so, knowing that the network is started with fibers on the top, a spanning network across the entire RVE is formed. With the spanning network formed including the fiber segments and contacts, the resistor network is constructed and solved (step 5), as explained in the following chapter.

It is important to note again, that the SNIA process is simplified for basic comprehension. Consequently, there are a few notes of special interest. Fibers are only added once to the network but are allowed to make contacts with other fibers added in the same iteration. Just as experimentally found, multiple contacts can form between neighboring fibers. However, redundant contacts or contacts between the same two nodes are removed.

4 The Resistor Network Model

Following the identification of the spanning network, an equivalent resistor network is constructed and the effective electrical conductivity of the RVE is found. The resistor network approach constructs an equivalent circuit, an array of series and parallel resistors, based on the nanotube segments and contacts as defined by the spanning network. This approach is valid when the conductivity ratio is large between the constituents of the composite [63] and has been used for decades in the study of insulating material reinforced with conductive filler [24,26,32]. As reviewed earlier, there is a variety of carbon nanotube-based resistor models each distinguished from each other by the assumptions made in the modeling. The proposed model treats each nanotube as a 1D conductor embedded in an insulating material, where the system is an open circuit until a network is formed. Therefore the matrix has zero conductivity and an effective composite conductivity is only calculated for RVEs forming a network. This is a standard assumption among this type of modeling. Consequently, the only contributing components of the resistor network are the intrinsic resistance of the nanotubes along with the contact resistances between them. The following section details these components before explaining the steps of the resistor network model.

4.1 Components of the Resistor Network

The equivalent resistor network has only two sources of electrical resistance, which are the nanotubes themselves and the contact between them. Figure 14 illustrates how the

resistor network is formed based on the geometry of the spanning network. The red resistors in Figure 14 indicate the contact resistance between connected nodes of different nanotubes. The pseudo-3D nature of the model is also shown by the overlapping nanotubes on the right.

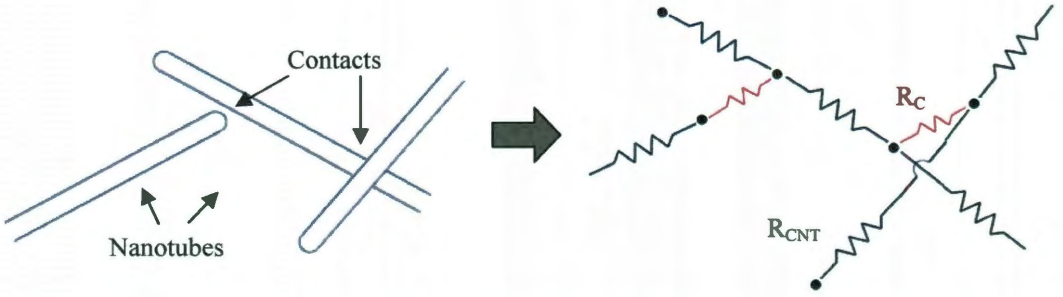

Figure 14. An illustrative model is presented depicting how the resistor network is formed.

It is important to note here that the resistor network is constructed with the original nanotube segments and not the split segments. This greatly reduces the number of nodes in the network. The number of nodes in the network is directly related to the size of the system of equations that need to be solved. By reducing the system of equations, computational time is saved. The split segments and associated split nodes are used only for the SNIA process. The contacts formed between these split nodes are translated to the original nodes of their respective fibers. Therefore, no contact information is lost and the nanotube resistance values which depend on length are fully accounted for in the network. Obviously, there is a slight disruption in the geometry of the resistor network but due to the stochastic nature of the geometry this effect is thought to be negligible.

Although not all experimental results are in agreement, the electrical conductivity of individual nanotubes ranges between 10^4 and 10^7 S/m [10-12]. Assuming all embedded nanotubes are metallic in nature, the proposed model uses a user-defined set value for the

electrical conductivity of the nanotubes, σ_{CNT}. With this parameter set, the electrical resistance of each nanotube segment R_{CNT} is calculated by the equation

$$R_{CNT} = \frac{4L_{seg}}{\sigma_{CNT}\pi d^2}, \tag{9}$$

where L_{seg} is the length and d is the diameter of the nanotube segment [41]. By using Equation (9), the stochastic nature of the nanotube length and diameter is reflected in the resistance value of each nanotube segment.

The second contributing source of resistance in creating the equivalent resistor network is the contact resistance between nanotubes. The contact resistance is assumed to be the sum of the resistance values from direct contact, nanotubes in contact without an insulating film present, and the resistance from the electric tunneling effect due to nanotubes being separated by a thin insulating film.

$$R_C = R_{direct\ contact} + R_{tunnel} \tag{10}$$

Measurements of direct contact between SWCNTs result in a resistance of 100 to 400 kΩ for metal/metal or semiconducting/semiconducting and 2 orders higher for metal/semiconducting junctions [37]. Theoretical calculations on the other hand predict a direct contact resistance varying between 100 kΩ to 3.4 MΩ [76].

For tunneling resistance, the value is dependent on the thickness and material of the insulating layer. Recently, Li et al. [41] studied the effect of electric tunneling resistance on CNT-based composites and determined that the upper limit of tunneling through an insulating polymer is 1.8 nm. The results of their study are reproduced in Figure 15. The figure also shows how nanotube diameter affects the resistance. However, due to the lack of reported parameters, the exact data as shown is not reproduced. Therefore to

incorporated the relationship between tunneling resistance and the thickness of an insulating film, a simple fit is applied to the data yielding the equation,

$$R_{tunnel} = e^{9.384x^3 - 28.974x^2 + 46.037x + 1.316}, \quad (11)$$

where x is the film thickness. The equation was found by applying a three coefficient exponential fit using MATLAB's "polyfit" tool. This fit is shown in Figure 15 by the orange dashed line for the 2 nm nanotube diameter, as it is closest to the mean diameter value from the current lognormal distribution.

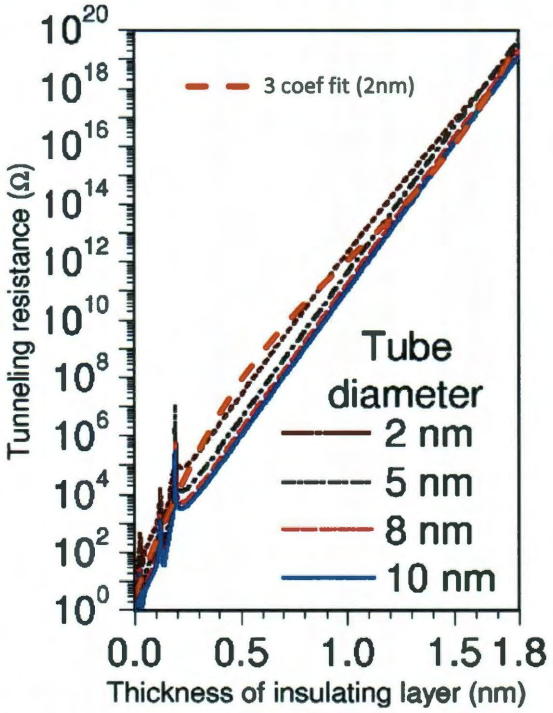

Figure 15. The theoretical tunneling resistance as function of insulating film thickness as determined by Li et al. [41] along with a curve fit for the 2nm case is presented.

With a decent curve fit achieved in Figure 15, the relationship between tunneling resistance and film thickness is defined. In order to determine the tunneling resistance values, a normal distribution is assumed for the thickness of the insulating film between 0 and 1.8 nm. Li and Chou [18] also made this assumption in their modeling, reporting the

histogram of the normal distribution of insulating film thickness they used. Since the parameters of the distribution are not reported, the histogram was reproduced and a normal distribution curve is fitted yielding a mean value of 0.8388 and a standard deviation of 0.02243. A histogram of 10,000 film thickness values is shown Figure 16 using these normal distribution parameters.

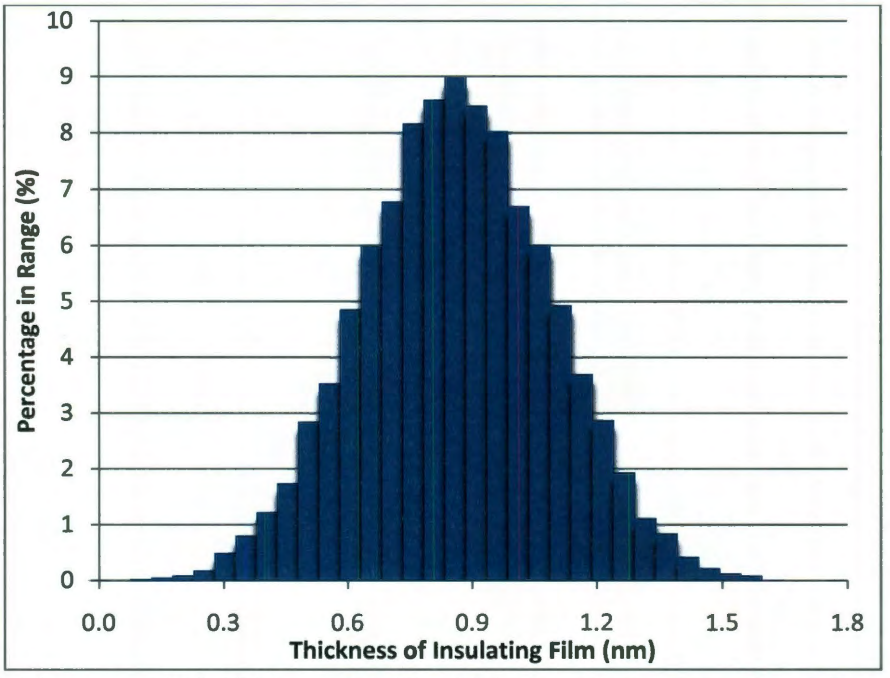

Figure 16. A histogram of 10,000 insulating film thickness values using estimated parameters from Li and Chou [18] is presented.

The distribution of tunneling resistances corresponding to the insulating film thicknesses of Figure 16 are calculated using Equation (11) and are shown in Figure 17. The lower bound of the values in Figure 17 is taken as 100 kΩ, which is the lowest contact resistance without an insulating film. Therefore, the values in Figure 17 represent the overall contact resistance, as the combination of direct contact and electron tunneling through a thin insulating film, and range between 10^5 and 10^{19} Ω. Li and Chou [18] also followed this same method in determining a distribution of contact resistance values.

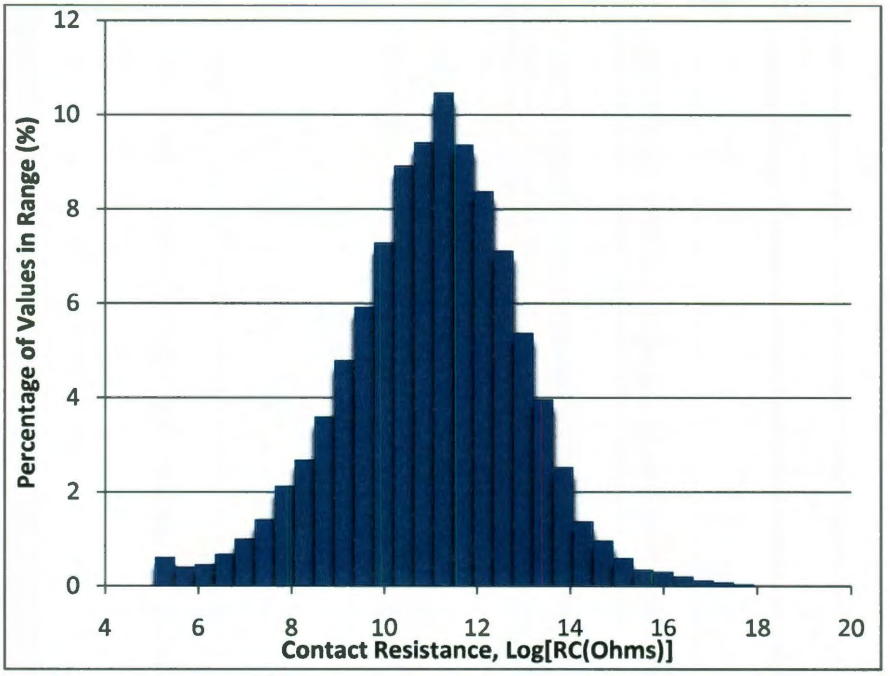

Figure 17. A histogram of 10,000 contact resistance values resulting from the film thickness distribution in Figure 16 and lower bound of 100 kΩ based on the direct contact.

4.2 Model Steps

As illustrated in Figure 14, the equivalent resistor network is constructed by replacing each nanotube segment along with contact between segments with resistors, where R_{CNT} is based on the length and diameter of the current segment and R_C is calculated based off a realized film thickness. These resistors are connected with the original nodes of the RVE. With these values in place and the applied boundary conditions shown in Figure 1, the electric potential distribution at each node of the resistor network is found by solving the a system of equations. This process is detailed by Li and Chou [27].

For a typical resistor element, defined by nodes *i* and *j*, the current *I* flowing through the element is related to the nodal voltages *V* by the equation, in matrix form,

$$\begin{Bmatrix} I_i^e \\ I_j^e \end{Bmatrix} = [K_{ij}^e] \begin{Bmatrix} V_i \\ V_j \end{Bmatrix} = \frac{1}{R^e} \begin{bmatrix} 1 & -1 \\ -1 & 1 \end{bmatrix} \begin{Bmatrix} V_i \\ V_j \end{Bmatrix}. \tag{12}$$

where R^e is the elemental resistance and K^e is the elemental conductance. According to Kirchhoff's current law, a system of algebraic equations is assembled for the entire network as

$$\boldsymbol{I} = \boldsymbol{KV}, \tag{13}$$

where $\boldsymbol{V}$ is the vector of nodal voltages and $\boldsymbol{I}$ is the vector of external input current at the nodes. Since there is no applied current, $\boldsymbol{I} = 0$. The term $\boldsymbol{K}$ is the global coefficient matrix defined by

$$\boldsymbol{K} = \sum_{e=1}^{m} [K_{ij}^e], \tag{14}$$

where m is the number of resistor elements in the network.

With the system of algebraic equations constructed, the voltage boundary conditions are applied to Equation (13) and the electric potential at each node of the network is then found. Note that the proposed model uses a potential difference of 100 V between the source and drain but that this chosen value does not affect the calculated effective conductivity value. With the nodal voltages determined, the current through each resistor is found by the equation

$$I^e = \frac{(V_i - V_j)}{R^e}. \tag{15}$$

Next, the total electric current I_{total} passing through the resistor network is determined by summing up the currents in the resistors directly connected either the top or bottom boundary. With I_{total}, the effective resistance R_{eff} of the entire network is calculated by

$$R_{eff} = \frac{(V_{top} - V_{bottom})}{I_{total}}, \tag{16}$$

where the effective conductance G_{eff} is the reciprocal of the effective resistance.

$$G_{eff} = 1/R_{eff} \tag{17}$$

Finally, the effective electrical conductivity of the composite is solved for by dividing the effective conductance with the thickness of the composite.

$$\sigma_{eff} = G_{eff}/t \tag{18}$$

Although the effective conductivity is the main value of interest, it is also possible to determine the effective backbone of the spanning network through the same process just described. The backbone as defined by Kirkpatrick [77] is the current-carrying part of the resistor network. Li and Chou [27] review numerous algorithms to find the backbone of a resistor network such as Tarjan's recursive depth-first-search algorithm, burning algorithm, dual lattice algorithm, and many more. The majority of these algorithms are recursive in nature, leading to potential stack overall when dealing with large systems. Li and Chou [27] go on to propose a new algorithm called the direct electrifying algorithm. The backbone is extracted from the complete resistor network based on the current-carrying definition. After the current in each resistor is calculated, all the resistors are scanned and ones with nonzero current are considered part of the backbone. This allows the extraneous nanotubes to be removed. Additionally, the effective backbone is further reduced by only including the components of the backbone carrying above a certain current value. Figure 18 illustrates this concept by showing the entire resistor network along with the reduced effective backbone. This particular reduced effective backbone shows only elements with a current value greater than one-third the max element current.

Select nodal voltages are also shown in Figure 18(b) decreasing from the top boundary value of 100 V to 0 V at the bottom.

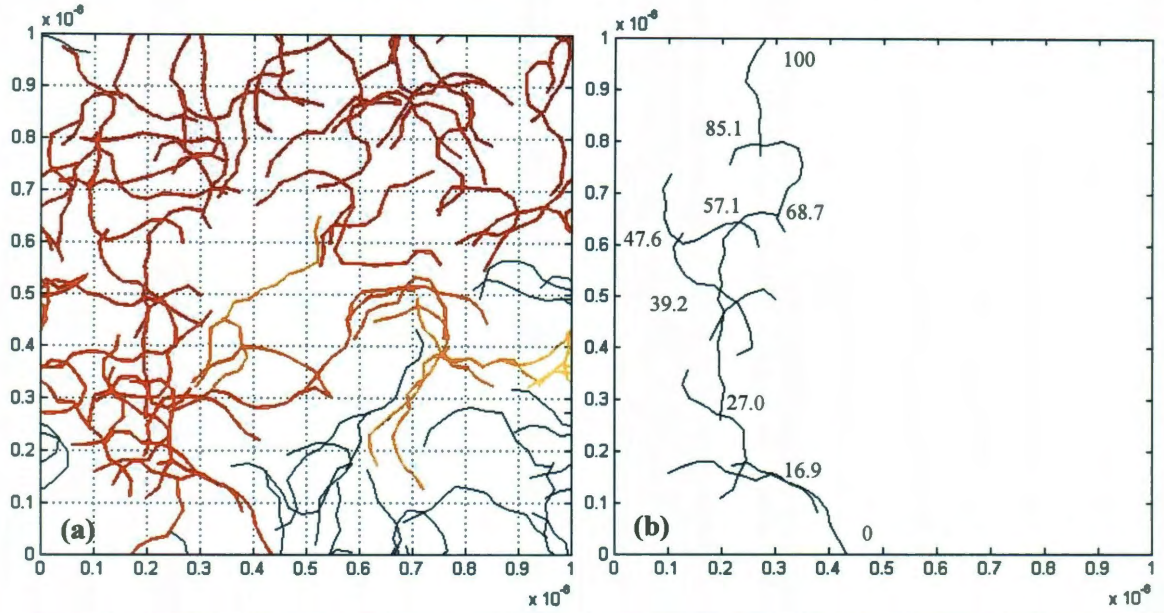

Figure 18. An RVE illustrating the (a) entire resistor network and the (b) estimated backbone with limited nodal voltages is presented.

5 Numerical Results

Having already discussed the theory of the problem along with the details and assumptions of the proposed model, the results are presented next. First, a few analysis methods are covered in order to provide insight into how certain results are achieved. Next, the functionality of the model is verified by examination of select modeling parameters, computational checks, and convergence analysis. The outputs of the model are then validated against other numerical models along with experimental data. Finally, case studies are conducted to show the versatility and applicability of the model.

5.1 Analysis Methods

This section discusses two analysis methods used in the processing of data. The first method is the determination of the percolation threshold, which is of particular importance when dealing with the finite-sized modeling of infinite systems like what is done here. The second part covers the percolation power law used to describe the electrical conductivity of nanocomposites after the percolation concentration is reached.

As discussed in Section 1.2.1, the percolation threshold ϕ_c of a two part composite is defined as the volume fraction of filler at which an infinite spanning network forms in an infinite system [25]. The probability of finding a spanning cluster at volume fractions greater than ϕ_c is 1 while the probability at volume fractions less than ϕ_c is 0. The percolation threshold for infinite systems is thus deterministic. However, experimental specimens and RVEs used numerically are finite-sized systems, where a spanning network forms only with a certain probability [34]. Yi and Sastry [78] explain that for

finite areas and volumes the percolation threshold is probabilistic and that realizations at the same volume fraction, with the same distributions in particle size, shape, location, and orientation, may or may not percolate. In order to calculate the strictly defined percolation threshold for a finite-size system, the threshold needs to be extrapolated to an infinite system based on finite-size scaling theory [25,34]. Several available techniques at accomplishing this scaling are reviewed by Yi and Sastry [78].

The current approach uses the fitting of a cumulative distribution function of data for the finite-size system to estimate the percolation threshold for the infinite system. First, percolation probability p is plotted as a function of volume fraction ϕ as shown in Figure 19(a). Percolation probability here is defined as the number of simulations for which a spanning network forms out of the total number of simulations. Next, the data from the p-ϕ plot is converted to a histogram and a normal distribution fit is applied using the "dfittool" capability in MATLAB. The histogram with the applied fit is shown in Figure 19(b). Finally, with the mean μ and standard deviation σ determined, the CDF fitting curve is generated with the equation,

$$p(\phi;\mu,\sigma) = \frac{1}{2}\left[1 + erf\left(\frac{\phi-\mu}{\sigma\sqrt{2}}\right)\right]. \tag{19}$$

This fit curve is shown with the original p-ϕ data in Figure 20, along with the estimated percolation threshold.

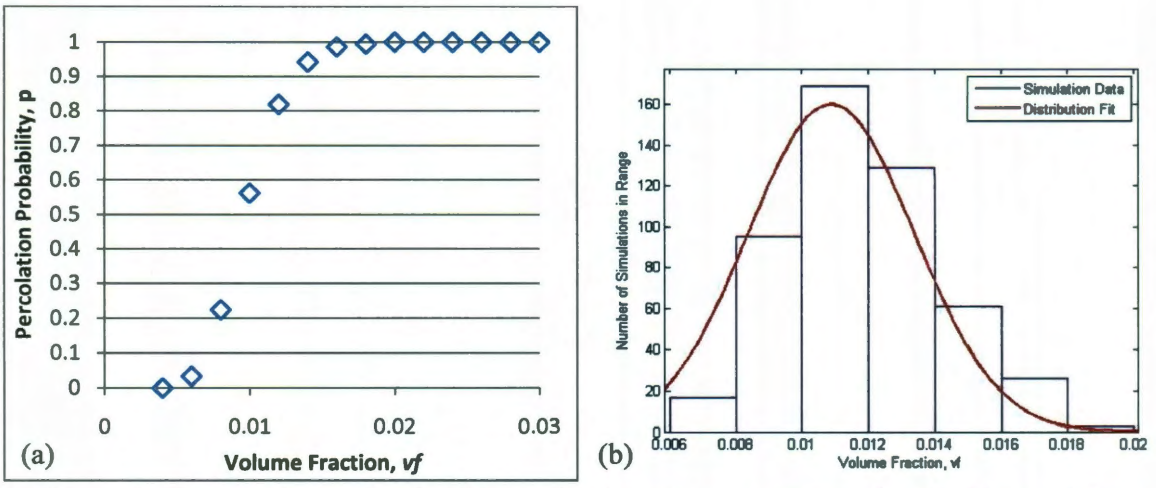

Figure 19. The percolation threshold determination process is presented, with (a) percolation probability vs volume fraction and (b) the same data as a histogram with a normal distribution fitting curve.

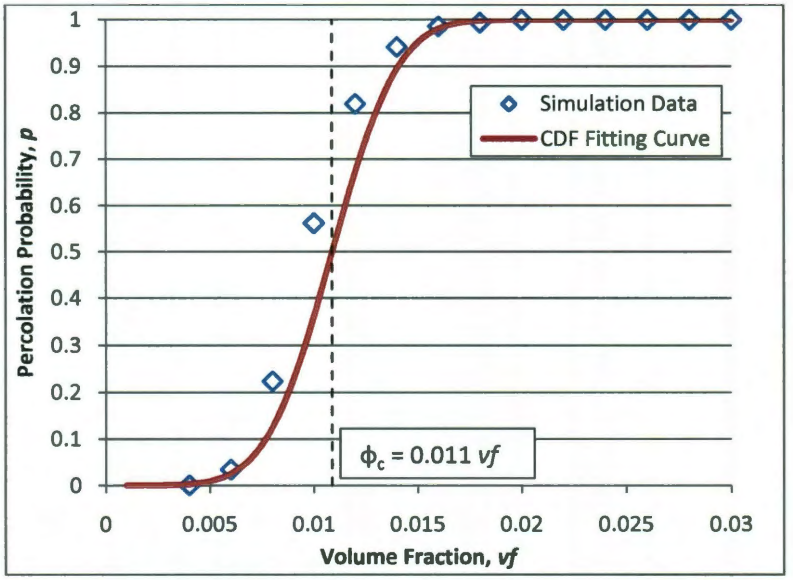

Figure 20. The fitting of the percolation probability curve by a cumulative distribution function is presented along with a vertical line indicating the estimated threshold.

This method of percolation threshold determination is very similar to the one presented by Li and Chou [79]. Li and Chou used the intersection of several finite-size CDF fitting curves as the infinite system's estimated percolation threshold. With the results of Section 6.2.2 showing negligible variation of percolation threshold with varying finite-

size systems, it is concluded that the use of only one finite-size system and thus one fitting curve is acceptable.

Once the percolation threshold is determined, the second analysis tool, the percolation power law fit, can be used. The electrical conductivity of a nanotube-based composite is divided into three regions being before, within, and after percolation [59]. As explained in Section 1.2.1, the power law fit describes the electrical conductivity of the composite at filler concentration levels greater than percolation. The fit is described by Equation (1), where the term $(\phi - \phi_c)/(1 - \phi_c)$ is referred to as the percolation ratio. Figure 21(b) shows the applied fit for the data in Figure 21(a), with the critical exponent $t = 1.56$. Note that the conductivity coefficient value σ_o is simply a scaling parameter and does not affect the calculation of t.

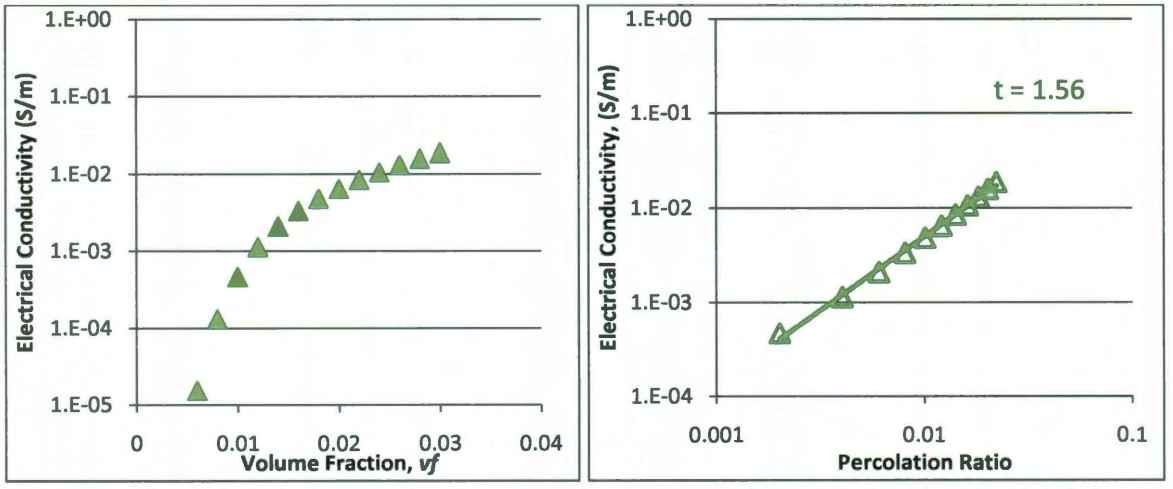

Figure 21. The percolation power law process is presented, with (a) the electrical conductivity vs volume fraction and (b) the same data plotted against the percolation ratio with the critical exponent shown.

With the power law fitting complete, it is possible to fit a curve to the data in Figure 21. This is accomplished by calculating the conductivity coefficient value σ_o for each data point. Then using the calculated average σ_o and the previously determined percolation

threshold, a power fit curve is generated using the same equation as Equation (1). This fit curve is shown in Figure 22 and is in excellent agreement with the numerical data points. This method allows the electrical conductivity to be estimated between actual numerical data points. Furthermore, this method can lead to the optimization of a composite's filler content when a specific level of conductivity is sought.

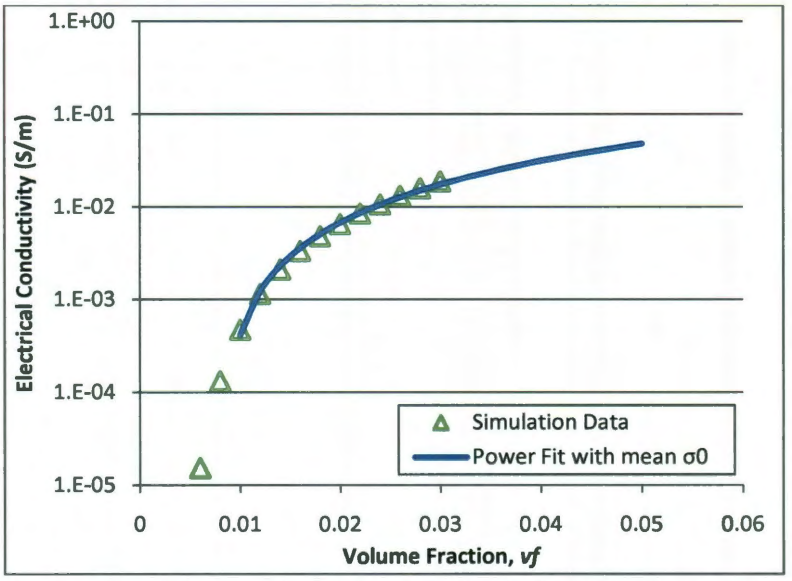

Figure 22. Electrical conductivity vs volume fraction simulation data along with a power fit curve using a mean σ_0 is presented.

5.2 Model Verification

Before studies are conducted with the model, verification of the model's functionality is ensured. The model verification is established in a variety of ways. First, the modeling parameters previously discussed are evaluated and selected. Numerous computational checks are then performed, confirming the model is operating as programmed. Finally, a Monte Carlo Convergence Analysis is conducted to ensure solution convergence and to determine the appropriate number of simulations.

5.2.1 Modeling Parameters

The accurate prediction of electrical properties of a carbon nanotube-based composite requires the realistic representation of the reinforcing constituent. The nanotube morphology parameters such as length, diameter, and waviness along with the dispersion of these nanotubes have already been verified. The distribution of contact resistances has also been confirmed. The final parameters required for accurate RVE depiction are the actual RVE dimensions.

Section 1.2.2 reviewed considerations for the RVE dimensions explaining how the thickness is determined. When the lognormal distribution is used for CNT diameter, the thickness is set at 5 nm. Otherwise, the thickness is stated for the particular study dependent on the chosen diameter and maximum tunneling distance. For RVE length, it was found that the ratio between this value and CNT length has a negligible effect on both the percolation threshold and the effective electrical conductivity within range of ratios tested (2-10). This is shown in Figure 23. As such, the RVE length is held constant for the remaining simulations at 1 μm. When the Weibull distribution is used for CNT length, the average value is 140.9 nm. For simulations where this distribution is not used, L_{CNT} = 300 nm is used. Both scenarios result in a L_{RVE}/L_{CNT} ratio within the range shown to have a negligible impact on the final solution.

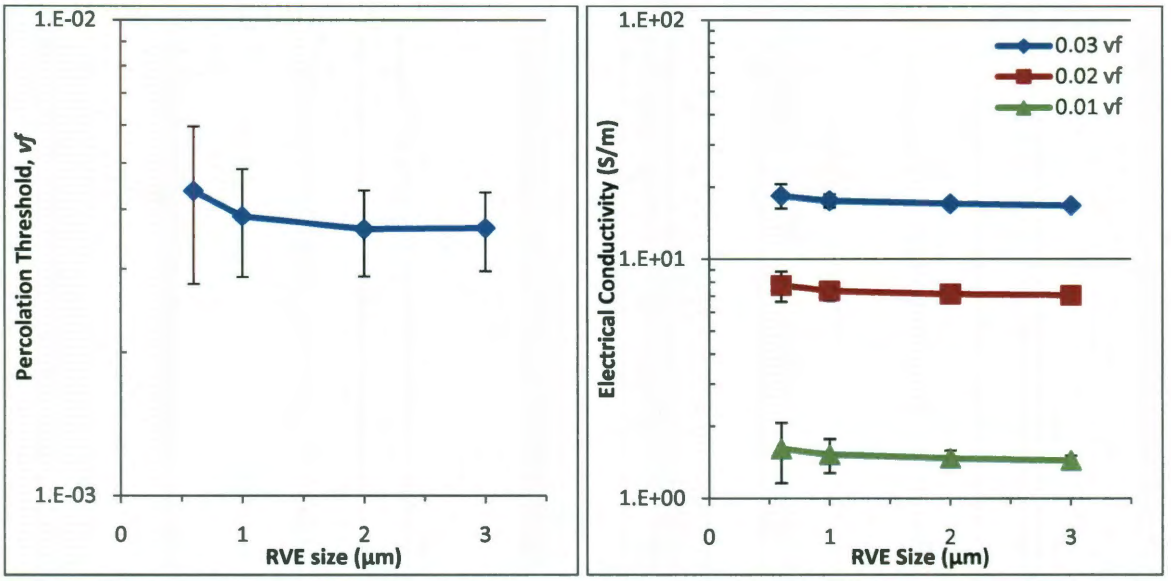

Figure 23. The effect of RVE size on (a) percolation threshold and (b) electrical conductivity is presented. RVE size within the ranges shown has a very weak on resulting values. Nanotubes of 300 nm length are used.

With the RVE parameters fully described and chosen, the last parameter for the model is the number of bins used in the spanning network searching algorithm. Bins are incorporated into this algorithm to reduce computational time by limiting the nanotubes needed to be checked for potential contact. Table 4 reports the computational time savings through the use of these bins.

Table 4. Percentage Time Saved Compared to 1 Bin.

		Volume Fraction		
# Div	# Bins	0.01	0.012	0.015
2	4	42.7%	37.4%	22.8%
5	25	61.1%	66.1%	30.9%
8	64	63.8%	66.8%	33.2%
10	100	64.1%	68.1%	33.6%
12	144	65.3%	68.1%	33.6%
15	225	66.1%	68.5%	33.9%
18	324	62.7%	69.3%	35.5%
20	400	57.3%	68.3%	35.6%

The values in Table 4 show the percentage of time saved by the use of two or more bins as compared to only one bin. Three different volume fractions are represented. Clearly, this time saving approach is effective yielding large reductions with only 2 bins and leveling off after 5 bins. There is however, the potential for data to be lost because the bins do not overlap in the searching algorithm. This loss is found to be minimal at 10 bins slightly increasing in severity by 20 bins. Thus, five bin divisions are chosen for simulations, presenting no recorded loss of data along with a significant reduction in computational time.

5.2.2 Computational Checks

With confidence in the chosen modeling parameters, the outputs of the model are verified to certify that the code is operating as programmed. This is accomplished through a series of checks on the conservation of flux, effective conductivity at 100% volume fraction, and the effect of tunneling distance.

The first computational check is the conservation of flux or the total current check. As depicted earlier, the top of RVE is the source while the bottom is the drain while the sides of the RVE are insulated. With these prescribed boundary conditions, there is no loss of flux or electric current out the sides. There are also no other inputs to the system. As such, the flux must be conserved meaning the electric current flowing into the top of the RVE must equal the electric current leaving the bottom [80]. Table 5 confirms this, showing the average current at the top and bottom of the RVE for a wide range of volume fractions. With the conservation of flux, the voltage decreases from the max value at the source to the minimum value at the drain, as shown prior.

Table 5. Total RVE Current Check for Top and Bottom Boundaries.

vf	Current Averages		Standard Deviation
	Top	Bottom	
0.01	5.400E-13	5.400E-13	3.101E-17
0.012	2.047E-11	2.097E-11	3.512E-13
0.015	3.993E-10	3.976E-10	1.163E-12
0.017	7.125E-10	7.133E-10	5.340E-13
0.02	3.136E-09	3.118E-09	1.291E-11
0.022	7.199E-09	7.184E-09	1.054E-11
0.025	1.677E-08	1.681E-08	2.895E-11
0.028	2.933E-08	2.927E-08	4.471E-11
0.03	5.542E-08	5.535E-08	5.337E-11

Knowing that the model conserves electric current, the next verification test is conducted to ensure accurate effective electrical conductivity calculations. Simulations are performed at 100% volume fraction as shown in Figure 24, where the conductivity is plotted as a function of contact resistance. By reducing the contact resistance below the intrinsic resistance of the nanotubes, thus negating the impact of the contact resistance, the conductivity of the composite approaches the conductivity of the nanotubes, 10^7 S/m.

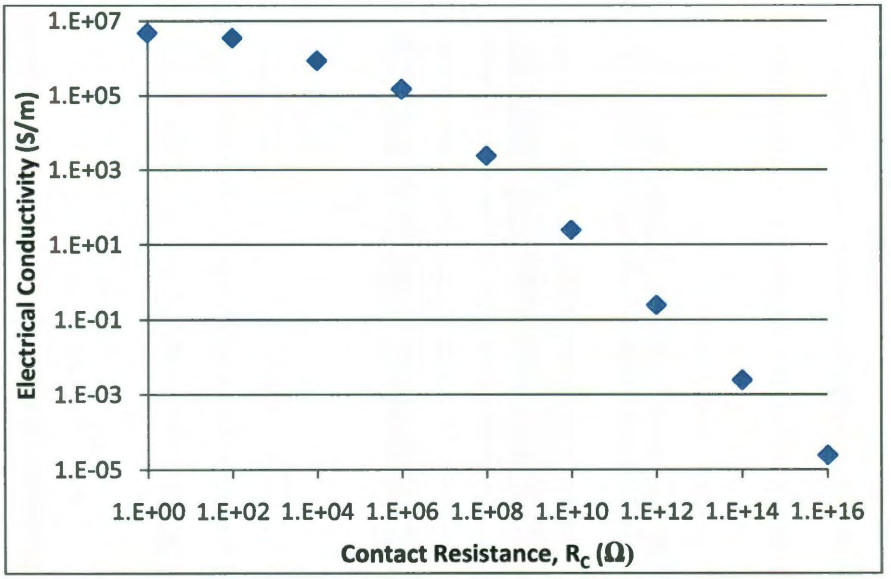

Figure 24. Electrical conductivity vs contact resistance for 100% volume fraction is presented. As R_c is reduced, the effective conductivity approaches the nanotube conductivity of 10^7 S/m.

At a contact resistance of 1 Ω, the effective conductivity equals 4.72 x 10^6 S/m, within half an order of magnitude the CNT conductivity thus indicating confidence in the model's ability for simulating electrical conductivities. A very similar model verification is performed by Li et al. [34]. The electrical conductivity of a composite without an insulating layer is extrapolated to 100% concentration, where the value falls within the same order of magnitude as the conductivity of the individual nanotubes.

The last computational check is on the effect of tunneling distance. As an added check to further ensure that the spanning network searching algorithm is functioning properly, the electrical conductivity curves are simulated using four levels of tunneling distance. Figure 25 presents the results. As expected, the percolation threshold decreases and the electrical conductivity increases with higher tunneling distances by allowing nanotubes not in physical contact to connect.

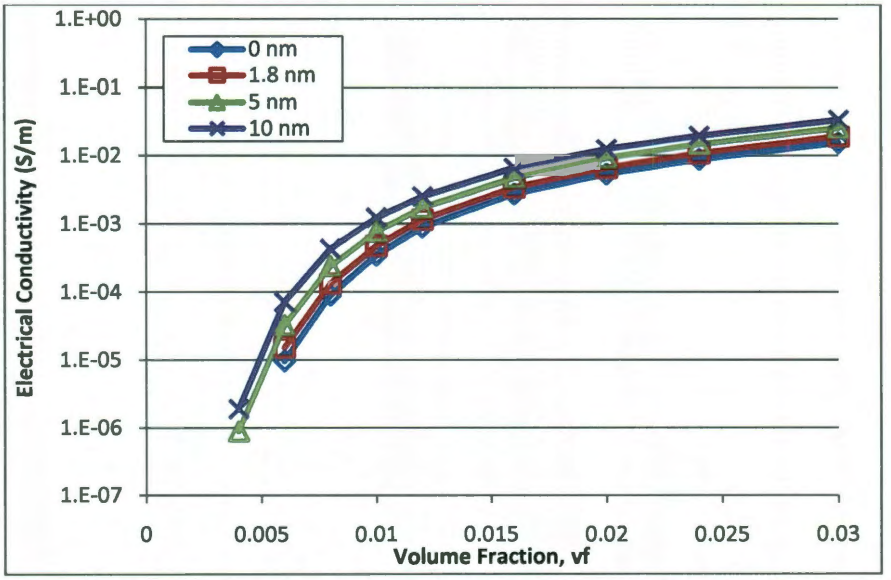

Figure 25. The effect of tunneling distance is presented. Note that electrical conductivity increases and percolation threshold decrease with increased tunneling distance.

5.2.1 Monte Carlo Convergence Analysis

The Monte Carlo Simulation technique is covered in Section 1.4.3. The statistical variance of the ensemble average can be reduced by increasing the number of simulations but at the cost of increased computational time. Monte Carlo convergence analyses (MCCA) are conducted with the proposed model to ensure solution convergence and allow the optimal number of simulations to be determined. For the first convergence analysis, all the stochastic parameters besides location and orientation of the nanotubes are held fixed. The second convergence analysis is performed with all variable parameters.

For the first convergence analysis, all the variable distribution parameters, i.e., diameter, length, and contact resistance, are held constant at 1 nm, 300 nm, and 10^9 Ω, respectively. The tunneling distance is 1.8 nm and σ_{CNT} is 1E6 S/m. The resulting nanotube geometry consists of randomly located and orientated ($\theta_a = 90°$) straight nanotubes ($\theta_{max} = 0°$). The results of the first convergence analysis are shown in Figure 26.

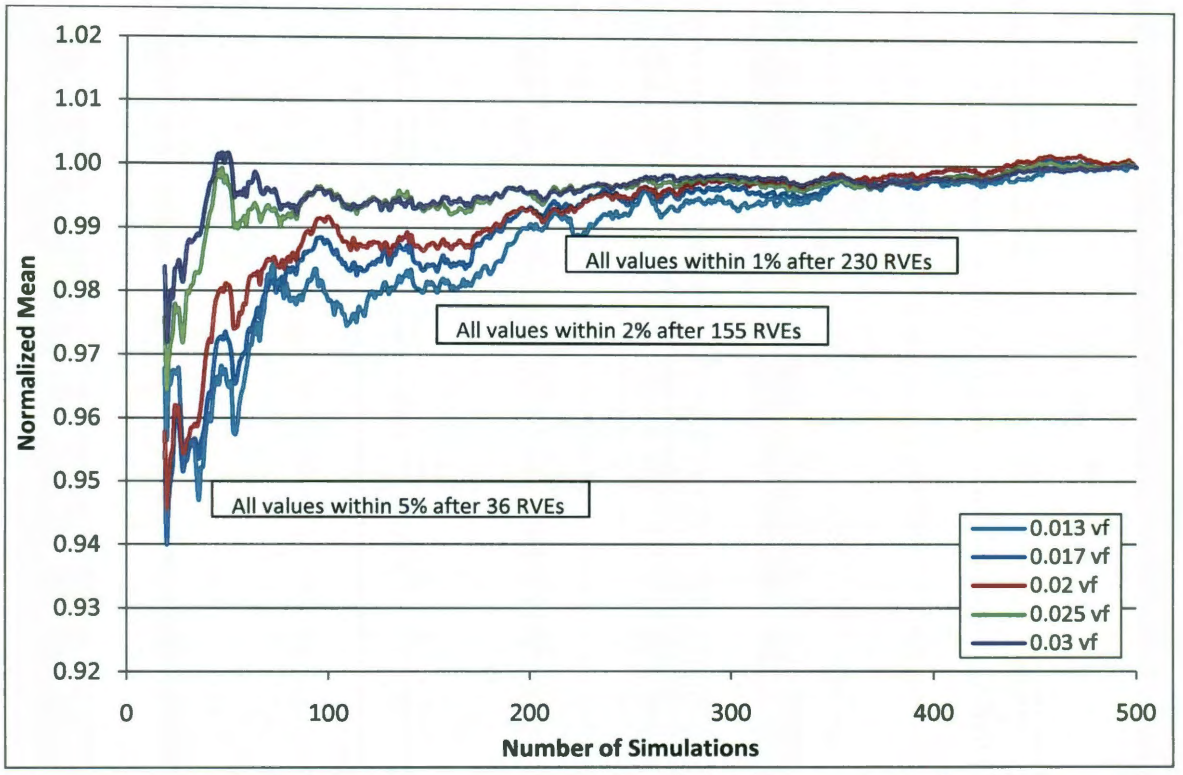

Figure 26. A Monte Carlo convergence analysis with all variable parameters fixed is presented.

The results in Figure 26 undoubtedly show that the underlying model converges. All the calculated values after 230 simulations are within 1% of the value at 500 simulations. It is also evident that the higher volume fractions tend to converge at a lower number of simulations. All the volume fractions shown in Figure 26 had 100% percolation.

Having shown the model converges with the exclusion of the distribution parameters, a second MCCA is conducted including these parameters. The previously defined length, diameter, and contact resistance distributions are used along with Equation (7) for varying waviness. The tunneling distance and σ_{CNT} are kept the same and the nanotubes are randomly located and orientated (θ_a = 90°). The results of the second convergence analysis are shown in Figure 27.

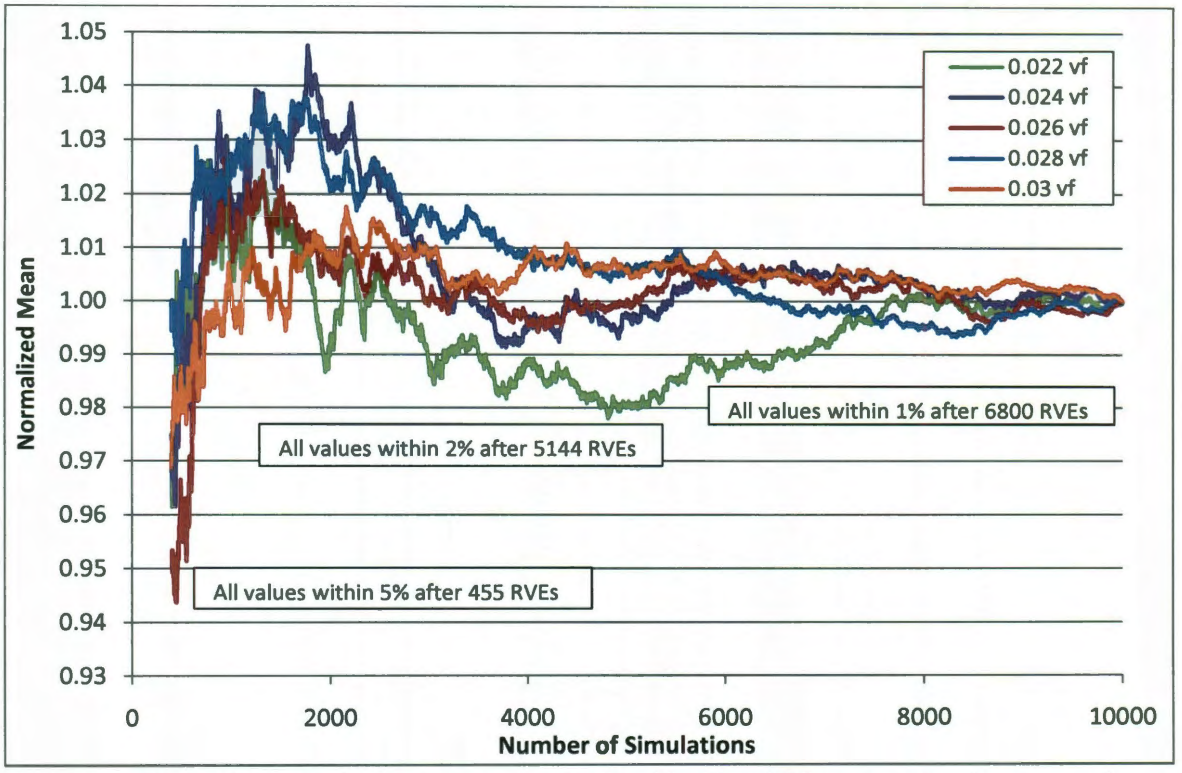

Figure 27. A Monte Carlo convergence analysis with all variable parameters is presented.

With the inclusion of all parameter distributions, the variability in the solution is increased requiring many more simulations to achieve similar levels of convergence. It requires 6800 realizations of the model to reach a level where all following values are within 1% of the value at 10,000 simulations. This is an extremely high number of simulations requiring exceptionally long computational times. Figure 27 also shows the same trend as Figure 26 where the higher volume fractions tend to converge with fewer simulations.

The integration of the numerous statistical distributions creates greater deviations in the solution as compared to using all fixed parameters. Further studies with the model are conducted to isolate the effects of specific parameters and therefore do not incorporate all the variable parameters. As such, 500 simulations are used and the convergence for each

study is checked and reported. The convergence is reported at the lowest volume fraction yielding 100% percolation where the greatest variability tends to occur.

5.3 Model Validation

Having made certain that proper modeling parameters are chosen and the numerical code performs as programmed, the subsequent step is validating the outputs of the model. With one of the goals of numerical modeling being the accurate prediction of effective composite properties, validation of the model is paramount to ensure outputs are useful. This validation is accomplished through comparison to published numerical models and experimental data.

5.3.1 Comparison to Numerical Models

The proposed model is first compared to other numerical models to make certain the outputs are within a reasonable range. The two outputs used for validation are the percolation probability and the electrical conductivity. Difficulty does arise in making direct comparisons to many numerical models because the results are typically reported without giving full insight into the parameters used to obtain the results. It will be shown later that the parameters chosen to describe nanotube morphology for example have a drastic impact on the obtained results. Furthermore, every model makes some assumptions in the model itself, taking into account factors other models might neglect. Finally, every model operates in a slightly different fashion.

Very few numerical models report percolation probability versus volume fraction [53,79,65]. Figure 28 shows a comparison between the proposed model and one reported data set by Theodosiou and Saravanos [53].

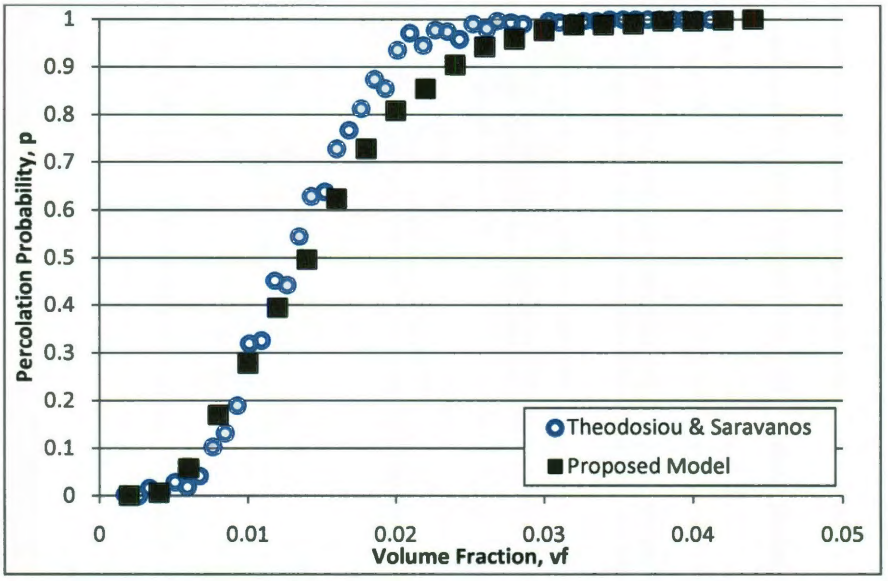

Figure 28. A percolation probability curve comparison between numerical modeling by Theodosiou and Saravanos [53] and the proposed model.

Theodosiou and Saravanos reporteed many of the parameters needed to replicate their data. The key parameter in percolation probability, aspect ratio, is given along with tunneling distance and Figure 28 shows that the proposed model is in very good agreement.

The electrical conductivity curve over a volume fraction range is used for the second numerical model comparison. Clearly, more modeling parameters are needed for the determination of conductivity then percolation. Also, there is greater variability in the assumptions made between numerical models. Figure 29 presents a comparison between the proposed model and 3D resistor network model by Hu et al. [67].

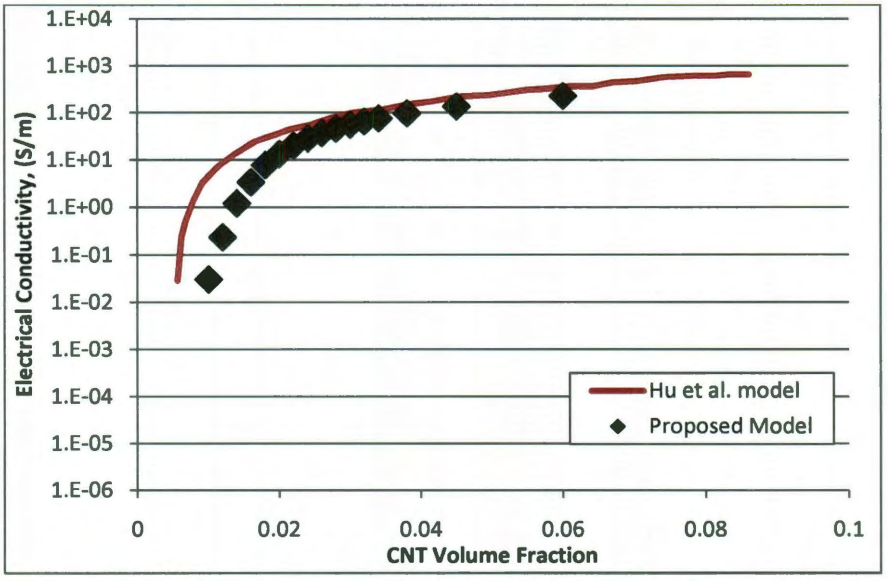

Figure 29. A comparison between the numerical model by Hu et al. [67] and the proposed model is presented for the electrical conductivity vs volume fraction.

The current model is in decent agreement with the model by Hu et al. and is within less than half an order of magnitude after 0.016 *vf.* Hu et al. report the majority of the modeling parameters required. But due to a modeling difference, Hu et al. did not use a strictly defined contact resistance and a value for the proposed model is chosen to provide a close match. Although Figure 29 validates the proposed model's ability to capture the behavior of other numerical models, it is believed that a closer match is easily possible with the adjustment of a few parameters.

5.3.2 Comparisons to Experimental Data

After validation of the proposed model against published numerical models, the proposed model is compared to experimental data. The accurate prediction of electrical properties of composites is a fundamental goal of numerical modeling. Similar to model comparisons, the comparisons between the proposed model and experimental data can be difficult because of the lack of morphological information along with other concerns as

discussed in Section 1.3. Figure 30 presents a comparison to experimental data with the proposed model using all the variable parameter distributions.

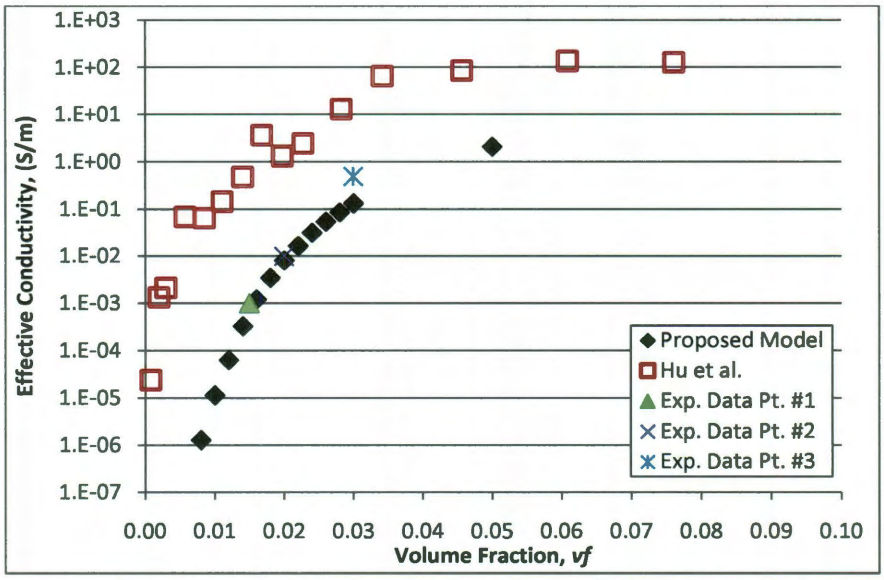

Figure 30. A comparison between experimental data (Hu et al. [75], pt. #1 [81], #2 [52], and #3 [82]) and proposed model with all variable parameters presenting electrical conductivity vs volume fraction.

The proposed model shows decent agreement with the experimental data shown in Figure 30. The numerical electrical conductivity data set (black diamonds) has the same shape as the full set of experimental data (red squares), but showing much better agreement with the individual data points. One possible explanation for the disagreement between the model and full data set is the use of the contact resistance distribution, whose wide range of values could be leading to the low effective conductivity predicted.

Another comparison to experimental data is conducted, this time using fixed values for the parameters based on those reported alongside the experimental data. This comparison is shown in Figure 31.

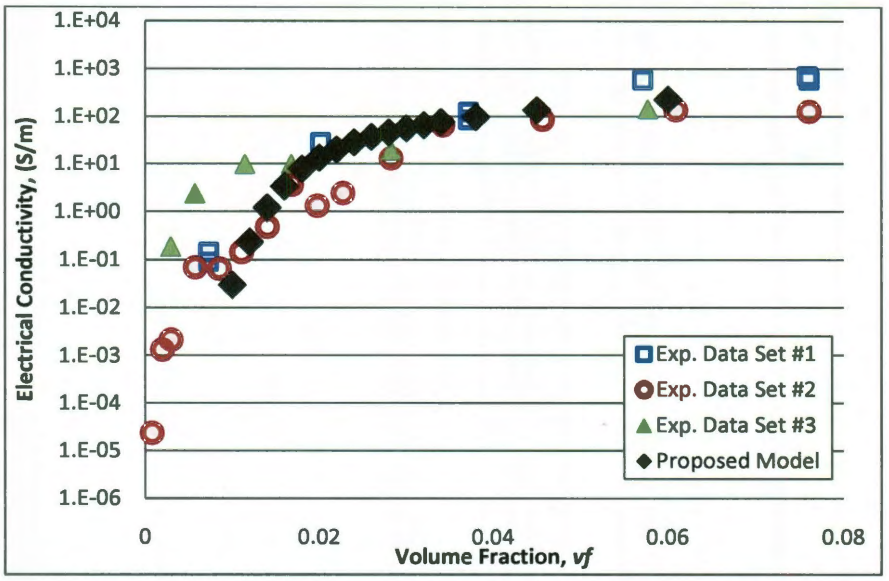

Figure 31. A comparison between three experimental data sets (squares [83], circles [75], and triangles [84]) and proposed model presenting electrical conductivity vs volume fraction.

Figure 31 shows great agreement between the model and experimental data. Clearly, the model is capable of matching real data especially when the parameters such as nanotube length and diameter are provided. In this case, 200 nm and 2 nm are used for the length and diameter, respectively. Tunneling distance is 0 nm, σ_{CNT} is 10^7 S/m, and the contact resistance is 10^5 Ω.

5.4 Case Study 1: Effect of Stochastic Parameters

The previous section shows that the proposed model is very capable of matching experimental data and therefore very capable of predicting the effective electrical properties of carbon nanotube based composites. The latter case studies investigate the effect of morphological parameters, providing insight into how composite properties can be controlled and optimized for the potential use in different applications. At any rate, the

current case study first looks at effective modeling, investigating the importance of incorporating the experimentally observed stochastic nature of the contact resistance distribution.

As previously discussed, the contact resistance R_c is the combination of resistance from direct contact between nanotubes and tunneling resistance based of the thickness of the insulating film between nanotubes. The proposed model and a few other numerical models [18,62] incorporate statistical distributions to account for this stochastic parameter. Using more parameter distributions require more simulations to reach convergence. Therefore, in an effort to seek faster convergence, the effect of this distribution is analyzed.

For the study, the diameter and length are held constant at 1 nm and 300 nm, respectively. The nanotubes are randomly oriented and wavy with $\theta_a = 90°$ and $\theta_{max} = 90°$. The tunneling distance is 1.8 nm and σ_{CNT} is 10^6 S/m. Simulations are completed with the R_c distribution and two fixed R_c values. The results are shown in Figure 32.

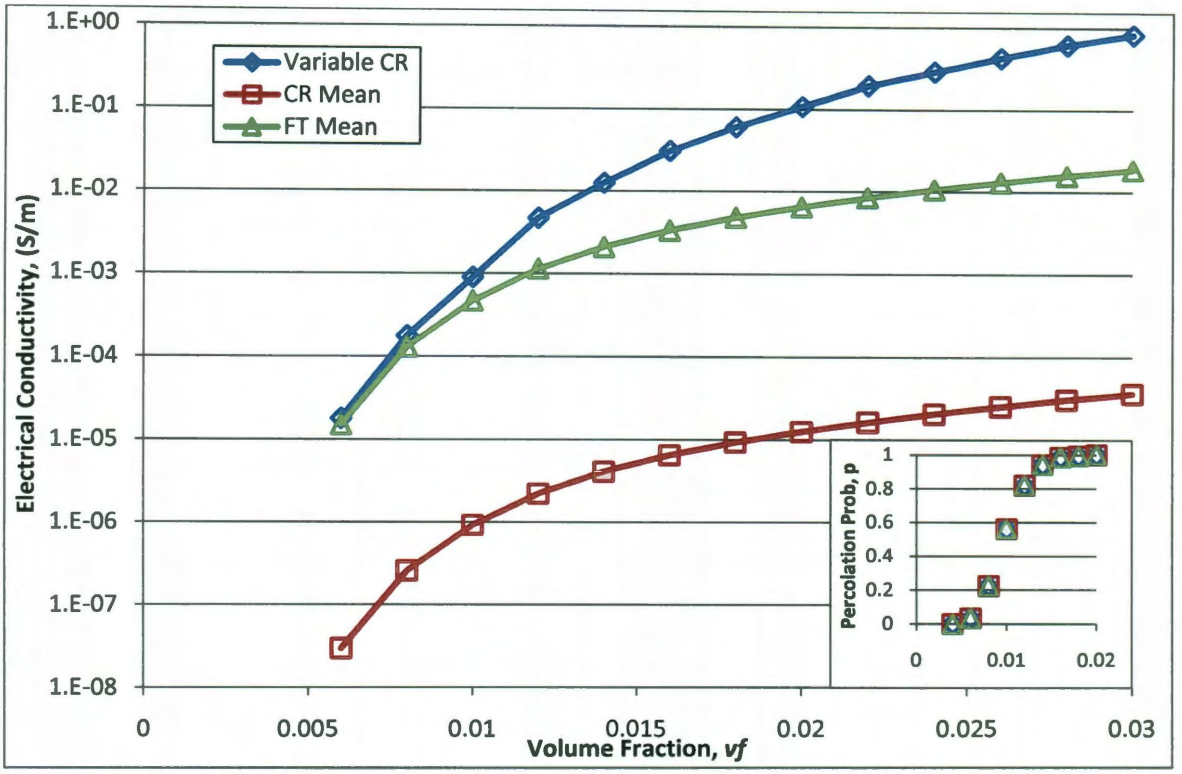

Figure 32. The effects of contact resistance on effective electrical conductivity are shown. With variable resistance (blue-diamond), conductivity continues to increase as opposed to leveling off when a fixed value is used. The inset shows percolation does not change with contact resistance.

The results in Figure 32 are very interesting. The first fixed R_c case (red-squares) corresponds to the mean contact resistance value from the distribution in Figure 17 with $R_c = 4.03 \times 10^{13}$ Ω. The second fixed case (green-triangles) corresponds to the mean and median insulating film thickness of 8.39 nm from the distribution in Figure 16. This film thickness results in $R_c = 7.83 \times 10^{10}$ Ω. The dependence of the effective electrical conductivity on R_c is first pointed out between these two fixed-value data sets, where the higher fixed R_c results in a much lower conductivity.

In comparing the fixed cases to the variable, it is evident in Figure 32 that the mean R_c value does not match the variable case. This is because the mean R_c value is skewed by the extremely high values in the distribution. Note that the R_c distribution is shown on a

log scale. Using the film thickness mean, the electrical conductivity is in very close agreement but only for the first few data points of the variable case. Past these data points the variable R_c curve continues to increase as opposed to the fixed cases where the conductivity tends to level off after complete percolation is reached. This behavior is illustrated better using the percolation power fit technique shown in Figure 33. Both the fixed cases result in the same critical exponent t = 1.56 which is within the range of so-called universal values of 1.33-2.0 [3]. The critical exponent for the variable case is almost twice as large at t = 2.92 indicating its greater increase with volume fraction. It is noted here that all three cases yield the same percolation probability as the inset of Figure 32 shows. This is in agreement with Sun and Song [42] where varying the contact resistance only influences the electrical conductivity and not the percolation threshold.

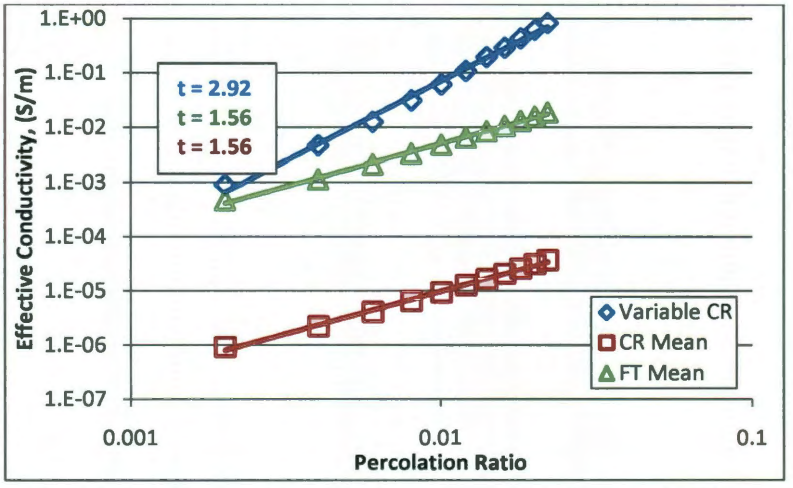

Figure 33. Power law fitting along with critical exponents for the data in Figure 32 is presented.

It is clear from both Figure 32 and Figure 33 that with variable contact resistance the conductivity curve does not flatten out as expected. This occurrence is understandable when the concept of parallelism in reference to electrical circuits is considered. Figure 34 presents two simple comparisons between circuit diagrams with fixed and variable

resistor values. Both the fixed and variable circuits have resistor values with the same average exponent value. For Figure 34(a), the fixed case has resistors of value 10^2 Ω, while the variable values are 10, 10^2, and 10^3 Ω. The total exponent value is 6 for an average of 2 per resistor. Note that this is very similar to the model in the current case study where the variable values come from a distribution on a log scale and the fixed value (FT mean) is the median value of this distribution. Figure 34(a) shows how a lower effective resistance results with variable value resistors as opposed to fixed. Figure 34(b) shows how this same occurrence is possible on a larger scale, where the locations of the variable resistors are chosen at random. Clearly, a lower effective resistance is possible with variable resistor values even though some of the values are an order of magnitude larger than the fixed values.

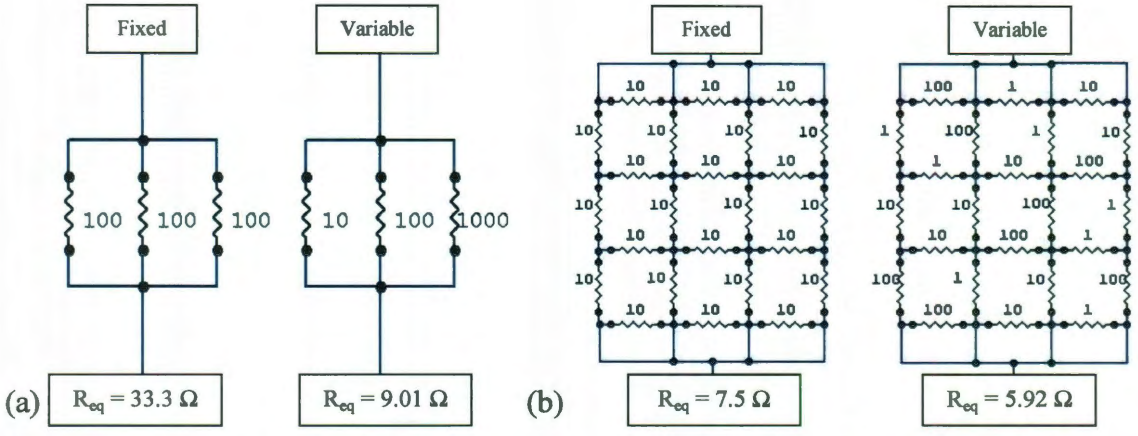

Figure 34. Simple parallel circuit diagrams are presented illustrating the effect of variable resistance on the overall equivalent resistance. The equivalent resistance is reduced by 3 fold in (a) and in (b), a random placement of variable resistors shows that a potentially less resistive circuit is possible compared to when fixed values are used for the resistors.

Due to parallelism, the random arrangement of variable resistors can result in a lower effective resistance or greater conductance. The simple circuit diagrams in Figure 34 help

elucidate why the electrical conductivity curve for the variable R_c case continues to increase when the fixed cases tend to level out. This also explains the higher critical exponent value for the variable R_c case. Although this value follows outside of the deemed universal range, carbon nanotube-based composite have been found to exhibit non-universality of the exponent t in the classical percolation equation [29]. Furthermore, the exponent value t = 2.92 falls well within the range of experimental values reported by Bauhofer and Kovacs [85].

To analyze the impact of the R_c as a stochastic parameter, a MCCA is conducted. Table 6 shows the results for a volume fraction of 0.02, which is the lowest filler content with all data sets reaching 100% percolation. Undoubtedly, the inclusion of the R_c distribution leads to greater variability in the solution and as such, the model requires more simulations to reach the same convergence level.

Table 6. Monte Carlo Convergence Analysis: Case Study #1.

Number of Simulations to Given Convergence Level			
Convergence Level	Variable CR	CR Mean	TD Mean
1%	486	373	373
5%	280	62	62

When debating if the contact resistance distribution should be retained, there are many considerations. The incorporation of a parameter distribution does increase the number of required simulations. The variable R_c also changes the shape of the electrical conductivity curve, where one fixed R_c value cannot match the curve. The remaining case studies are done to investigate the effect of specific morphological parameters and therefore use a set R_c value. For future CNT-based composite modeling, the incorporation of this parameter distribution is left to up to the design engineer and specific application of the model.

5.5 Case Study 2: Effect of Nanotube Waviness

With verification that the model is functioning appropriately and validation that it is providing reasonable solutions, the effect of CNT waviness is investigated. As previously mentioned, waviness is a prevailing feature of embedded carbon nanotubes in composites [34]. This non-straightness results from the combination of a very large aspect ratio and very low bending stiffness due to small tube diameters [18]. Intuitively, wavy nanotubes are able to make multiple contacts with a neighboring nanotube where straight tubes are only able to make one connection. Past numerical investigations [41,42] along with Case Study #1 indicate the overall resistance of the spanning network and therefore carbon nanotube-based composites are dominated by contact resistance. Thus waviness and the number of contact points within the spanning network are expected to play a significant role in the effective electrical conductivity.

The proposed model incorporates waviness into the morphology to provide a more realistic representation of a CNT-based composite. Many past percolation models [22,23,58] and computational simulations of electrical conductivity [2] have assumed "straight sticks". Other past studies have only investigated the effect of waviness on the percolation threshold [60,86] while others have used wavy nanotubes in electrical conductivity computations [42,68]. A few models such as Hu et al. [67], Dalmas et al. [66], and Li et al. [34] have quantified the effects of waviness on both percolation threshold and electrical conductivity with the general conclusion that increased waviness tends to increase the percolation threshold while decreasing the effective conductivity. The attributed cause of the decreased conductivity is the increased number of contacts. Beyond this simple observation no further investigation is given. The goal of the current

study is to systematically study the effects of nanotube morphology in the form of waviness on both the geometric percolation threshold and the effective electrical conductivity of the composite along with characterizing the impact on the spanning network's composition or attributes.

For the study, all the variable distribution parameters, i.e., diameter, length, and contact resistance, are held constant at 1 nm, 300 nm, and 10^9 Ω, respectively. The nanotubes are randomly dispersed and oriented. The tunneling distance is 1.8 nm and σ_{CNT} is 10^6 S/m. As described in the Section 2.1, the waviness of the nanotube is controlled by the parameter θ_{max}, varying between 0° (straight) to a max of 180°. Also, nanotube waviness can be described by the curl ratio λ, which is the actual nanotube length over the effective or end point to end point length.

With all the parameters fixed, the effects of waviness are isolated and shown in Figure 35. The three levels of waviness, θ_{max} = 0°, 120° and 180°, correspond to average curl ratios of λ = 1.0, 1.33, and 1.62, respectively. The values of θ_{max} were chosen to provide a wide range yet equal spacing between curl ratios. At a given volume fraction, electrical conductivity clearly decreases with increased nanotube waviness. This is as expected and reported by [34,66,67]. It is also noted that the effect of waviness decreases with volume fraction. Percolation probability also decreases with increased waviness as shown by the inset plot of Figure 35. This is consistent with the findings of [60,66,86].

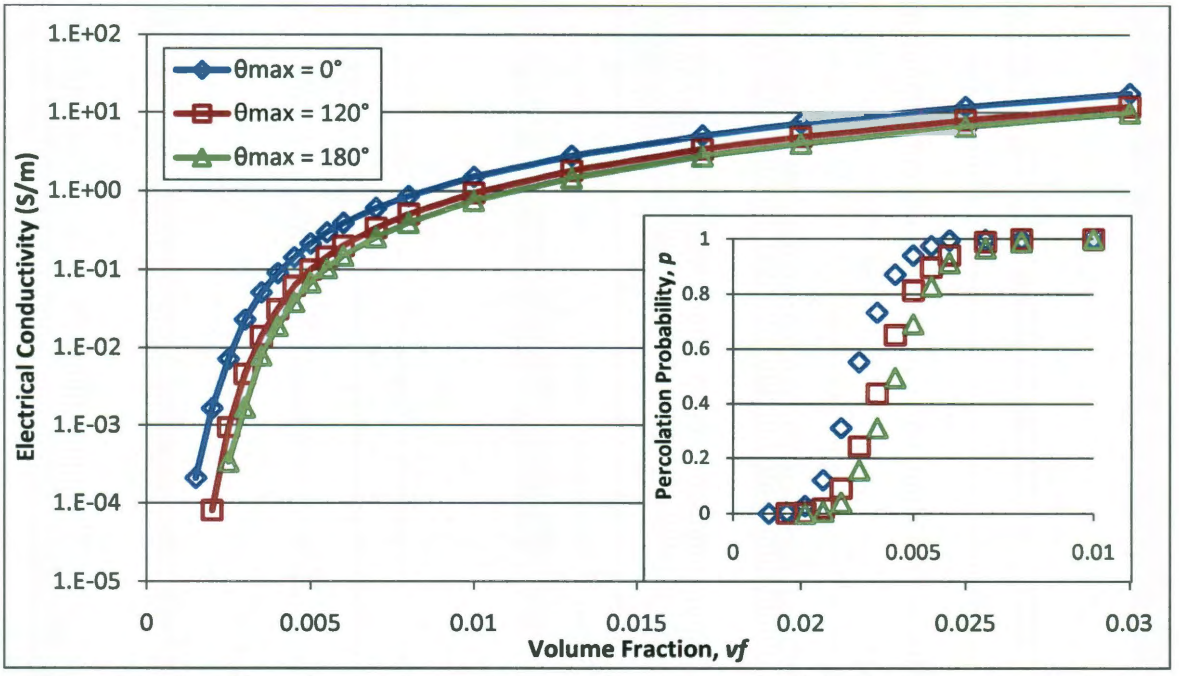

Figure 35. The effect of nanotube waviness on electrical conductivity is shown. Conductivity decreases as nanotube waviness, controlled by θ_{max}, increases. The inset plot shows how the percolation probability decreases with waviness.

With confidence in the results of Figure 35, the attributes of the spanning network are analyzed in order to characterize and quantify the effects of waviness. The utilized volume fraction, defined here as the number of nanotubes in the spanning network over the total number of nanotubes in the RVE, is plotted against volume fraction in Figure 36. This ratio is thought to give insight into the composite's morphology and its efficiency at employing the embedded nanotubes towards electrical conduction. Straight nanotubes led to a higher utilized volume fraction especially at lower volume fractions. The straight nanotubes have a greater effective length and are therefore able to span farther distances increasingly the likelihood of contacting another nanotube that would otherwise not be included in the network. This phenomenon does not explain the earlier percolation of straight fibers but yields the same conclusion. It does, however, help explain the higher

conductivity. By having more fibers in the network, there is a greater possibility of forming multiple conduction paths and thus by parallelism of resistors, a lower effective resistance.

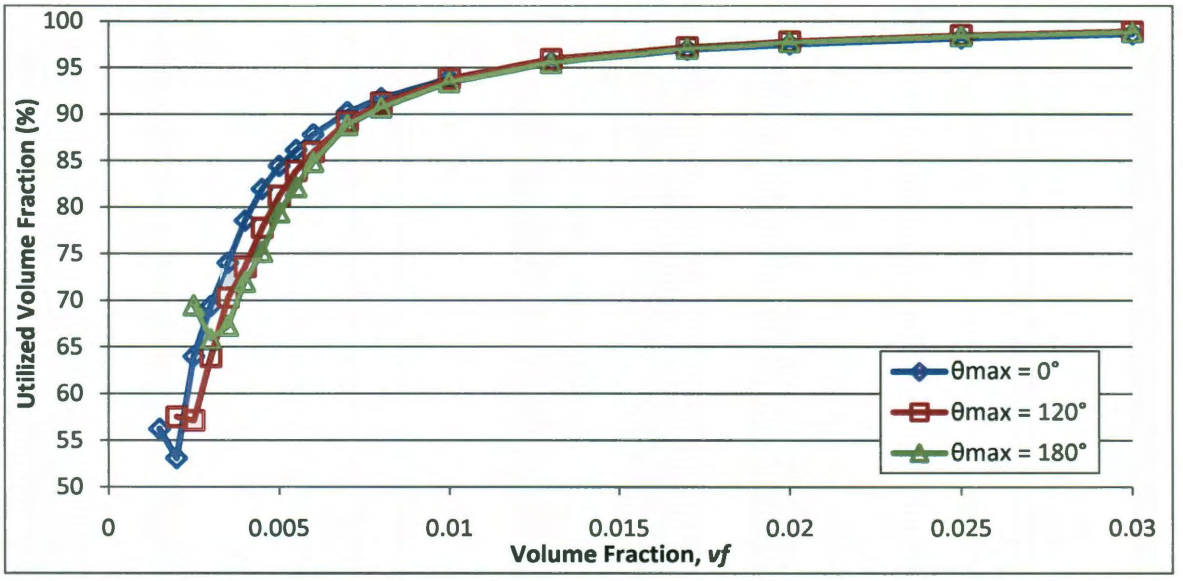

Figure 36. Utilized volume fraction, or the ratio of in-network fibers to the total number of RVE fibers, is presented vs volume fraction for varying degrees nanotube waviness. Straight nanotubes maintain a higher utilized volume fraction.

As previously mentioned, the effective conductivity of the spanning network depends on the unique formation of series and parallel resistors. In general, conductivity is increased and resistivity is decreased by the greater the number of conduction paths, the shorter the path length, and the lower the number of contacts along a path. These specific parameters cannot be directly determined by the model, only implied from the resulting spanning network attributes. A straight nanotube morphology results in a greater number of nanotubes in the network (Figure 36) and a greater number of contacts (Figure 37). With the combination of more nanotubes and contacts, straight fibers yield a more conductive network potentially through the formation of multiple conduction paths, whose individual paths are more direct.

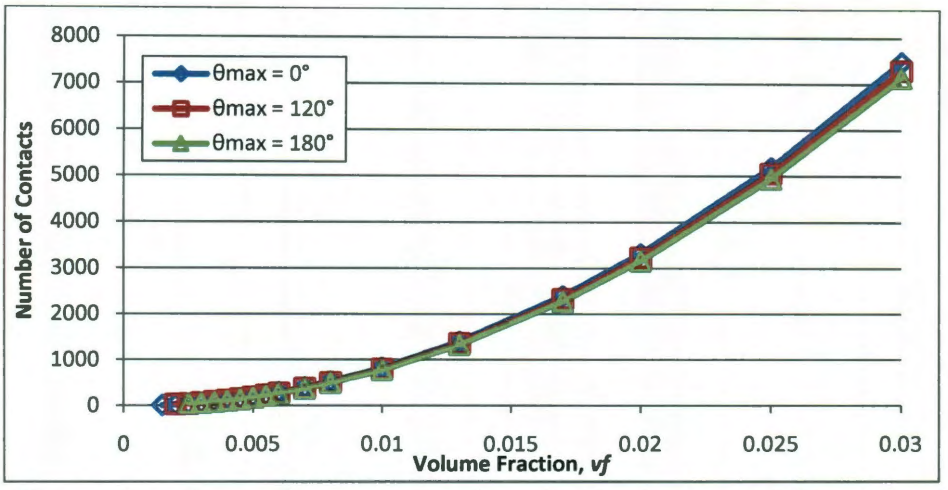

Figure 37. The number of network contacts vs volume fraction is presented for varying degrees of nanotube waviness.

Although the data in Figure 37 seems to go against intuition and the rationale of Li et al. [34], when the number of network contacts is plotted against the number of fibers in the network as shown in Figure 38, it is clear that wavy nanotubes result in more contacts per fiber than straight tubes. This is as expected, highlighted by the inset plot of Figure 38. The number of contacts formed per fiber is called contact or bond density.

The simulations show that wavy nanotubes result in higher bond densities. This however, does not directly lead to the decreased electrical conductivity. As Figure 39 illustrates, straight nanotubes yield greater electrical conductivities for the same number of contacts. It is concluded that increased nanotube waviness, or increased curl ratio, results in decreased percolation probability and electrical conductivity. The reduced conductivity is thought to be a combination of less conduction paths and less direct paths between the source and drain.

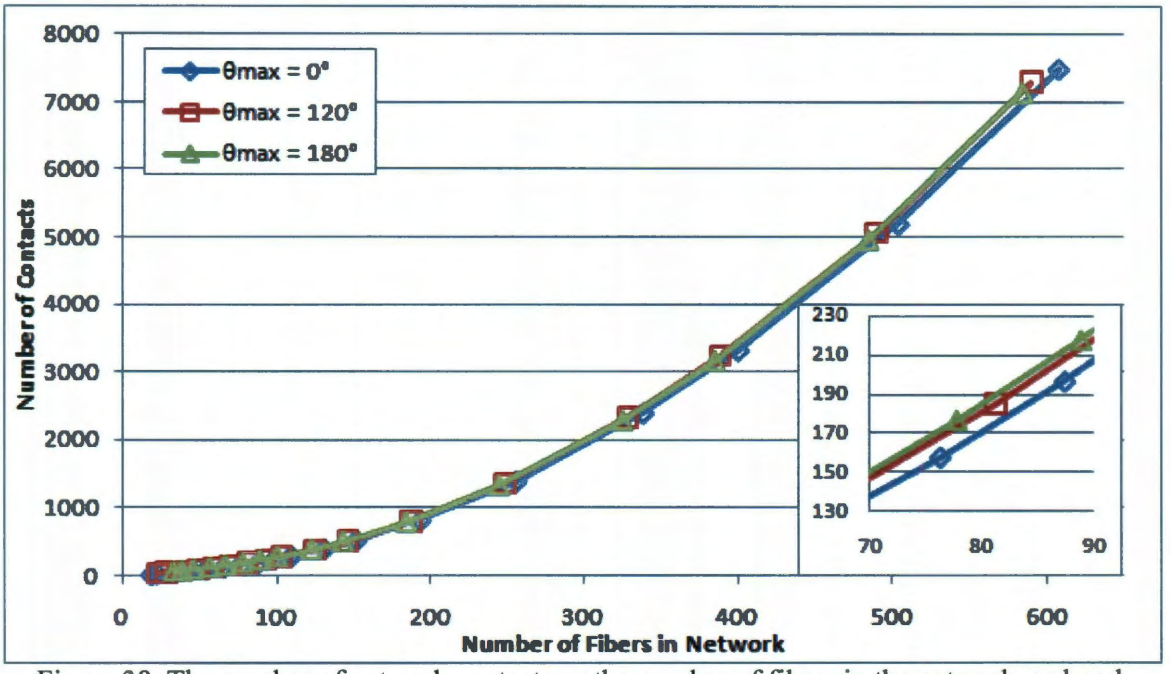

Figure 38. The number of network contacts vs the number of fibers in the network, or bond density, is presented for varying degrees of nanotube waviness. The inset exemplifies the prominent behavior where bond density increases with nanotube waviness.

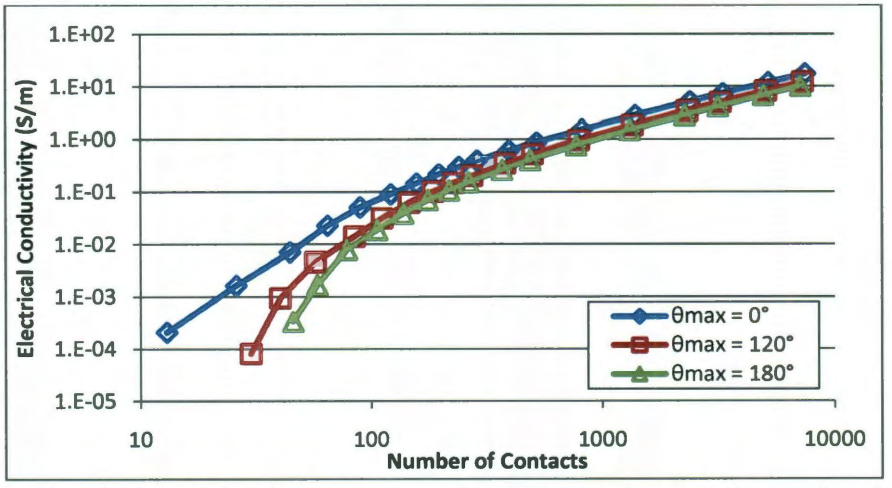

Figure 39. Electrical conductivity vs number of contacts is presented for varying degrees of waviness. Straight nanotubes yield higher conductive networks with the same number of contacts as wavy nanotubes, indicating the formation of straighter and/or more conduction paths.

In order to show convergence of the model with the incorporation of nanotube waviness, Table 7 reports the MCCA results. The analysis is conducted at a volume fraction of 0.01,

which was the lowest filler content with all data reaching 100% percolation. Note that there is no clear trend in the convergence with nanotube waviness.

Table 7. Monte Carlo Convergence Analysis: Case Study #2.

Number of Simulations to Given Convergence Level			
Convergence Level	$\Theta_{max} = 0°$	$\Theta_{max} = 120°$	$\Theta_{max} = 180°$
1%	207	295	133
2%	182	120	65

5.6 Case Study 3: Effect of Nanotube Alignment

Despite the extraordinary properties of carbon nanotubes, it is difficult to ascertain the full potential of these materials when embedded into a matrix [18] due to many issues such as but not limited to dispersion, interface bonding, agglomeration, and alignment [46]. As demonstrated in the previous section, the morphology of the embedded nanotubes can affect not only the electrical conductivity but also the onset of percolation in composites. Alignment is another morphology parameter and challenge in the processing of carbon nanotube based composites. Wang et al. [46] lists various techniques researchers have used to gain orientation control of carbon nanotubes within a matrix material, such as mechanical stretching, melt spinning extrusion or ejecting, shear flow, and electric and magnetic field induced alignment.

Recently, there has been a great deal of research interest in the aligning of CNTs in both thin films and composites [22,87]. However, there have been some inconsistent results regarding the effect of alignment on electrical conductivity. This topic is well covered in the review article by Li et al. [88]. Both Haggenmueller et al. [51] and Choi et al. [50] reported alignment leading to enhanced electrical properties of CNT-based composites,

owing this enhancement to the more creation of more efficient percolation paths and/or the decrease of disorder by aligning the nanotubes. Initial studies by Du et al. [52], however, showed a decrease in conductivity for aligned composites as compared to unaligned at the same volume fraction. It was further concluded by Du et al. [22] that slightly anisotropic, therefore showing some degree of alignment, and not the randomly isotropic case resulted in the highest conductivity. Consequently, both an increase and decrease in conductivity is expected based on the degree of nanotube alignment.

The topic of alignment has also been the focus of numerical studies. Du et al. [22] and Natsuki et al. [58] investigated the effect of alignment on percolation using straight stick models. With the emphasis of these studies on the percolation threshold, few studies have been focused on electrical conductivity. Behnam et al. [65] studied the effects of nanotube alignment and measurement direction on SWCNT films using straight sticks, concluding that minimum resistivity occurs for a partially aligned rather than a perfectly aligned nanotube film. More recently, Li and Chou [18] studied the effect of nanotube alignment on electrical conductivity for CNT-based composites using both straight and wavy nanotubes. Results show that both an increase and decrease in conductivity are possible dependent on the degree of alignment, yielding a maximum conductivity with slightly aligned nanotubes. With these thorough results known, the goal of the current study is to systematically study the effects of alignment in conjunction with fiber waviness on the both the percolation threshold and effective electrical conductivity of the composite along with characterizing and quantifying the effects on the spanning network's attributes.

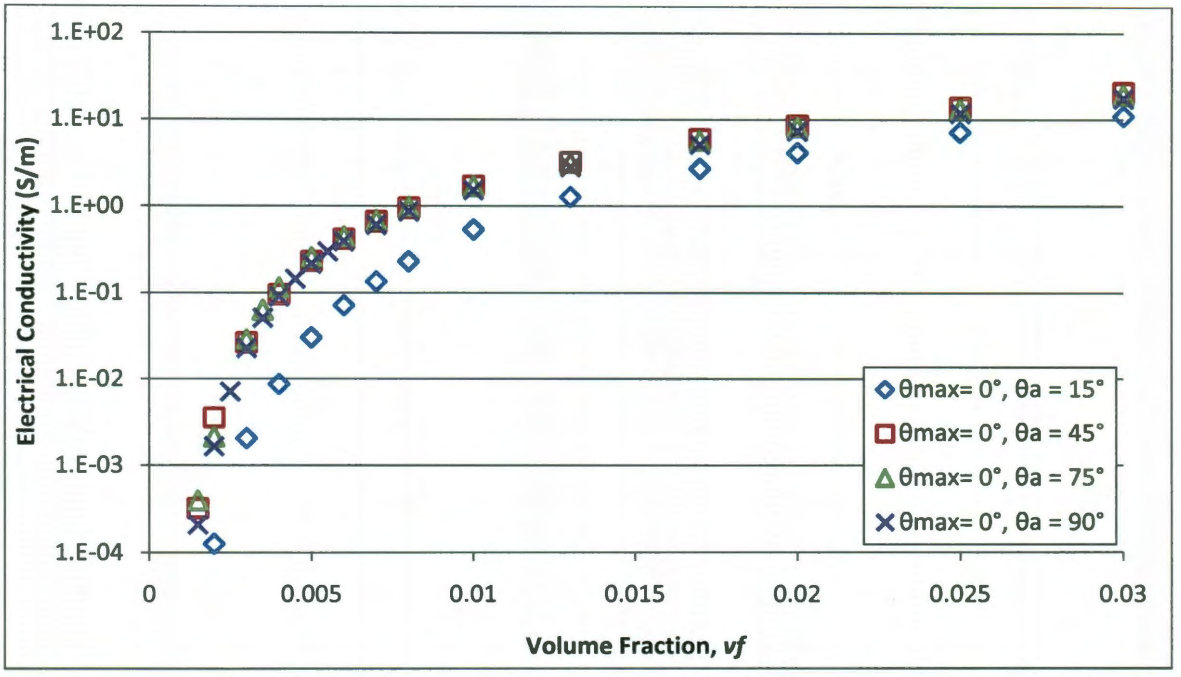

Figure 40. The effect of alignment on electrical conductivity is shown, comparing the randomly distributed case ($\theta_a = 90°$) to three levels of increasing alignment ($\theta_a = 75°$, 45°, and 15°). Note how strong alignment decreases conductivity.

Behnam et al. [65] concluded that the initial increase in conductivity with alignment from the isotropic case is due to nanotubes forming conduction paths with fewer junctions and shorter lengths between the source and drain. Further alignment significantly reduces the number of conduction paths and thus reduces conductivity. To verify this theoretical explanation, the visualizations of the spanning network, Figure 41, are qualitatively analyzed in conjunction with the attributes of the networks displayed in Figure 42.

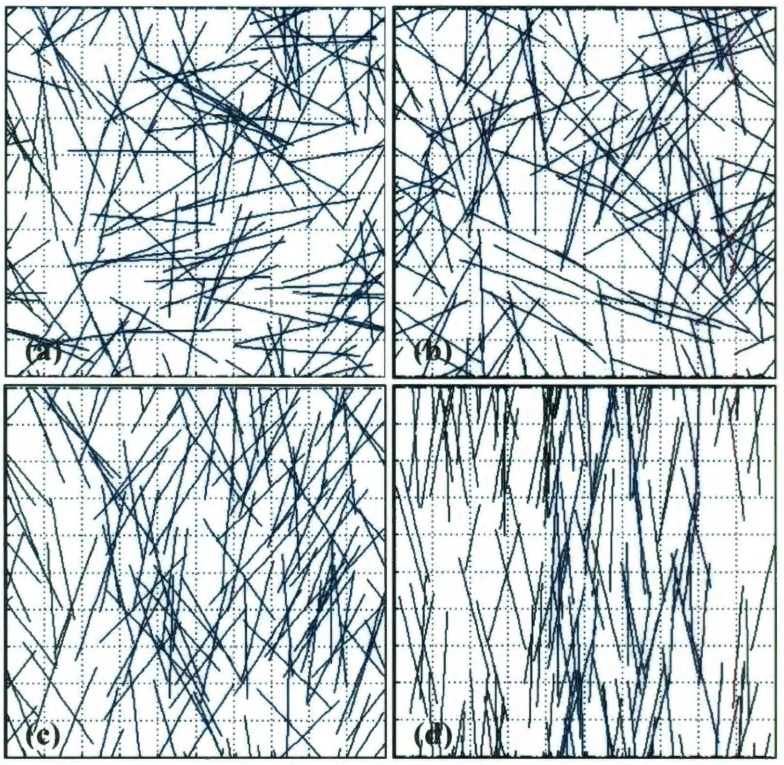

Figure 41. Four RVEs are shown, (a) through (d), at 0.008 vf for each level of alignment θ_a = 15°, 45°, 75°, and 90°, respectively. The current carrying fibers of the spanning cluster are in blue.

The effect of nanotube alignment within a composite on the resulting spanning cluster is evident in Figure 41. A cursory glance over the four visualizations reveals that alignment reduces the number of nanotubes included in the spanning cluster, refer to the reduction of blue fibers in relation to black fibers in (a) though (d). Figure 42(a) supports this observation showing a clear trend of decreasing utilized volume fraction with increased alignment. The randomly isotropic case (θ_a = 90°), with fibers running perpendicular to the alignment (and measurement) direction, are able to contact a higher percentage of RVE fibers in the network as opposed to the highly aligned case (θ_a = 15°), where fibers are more likely to run parallel to each other.

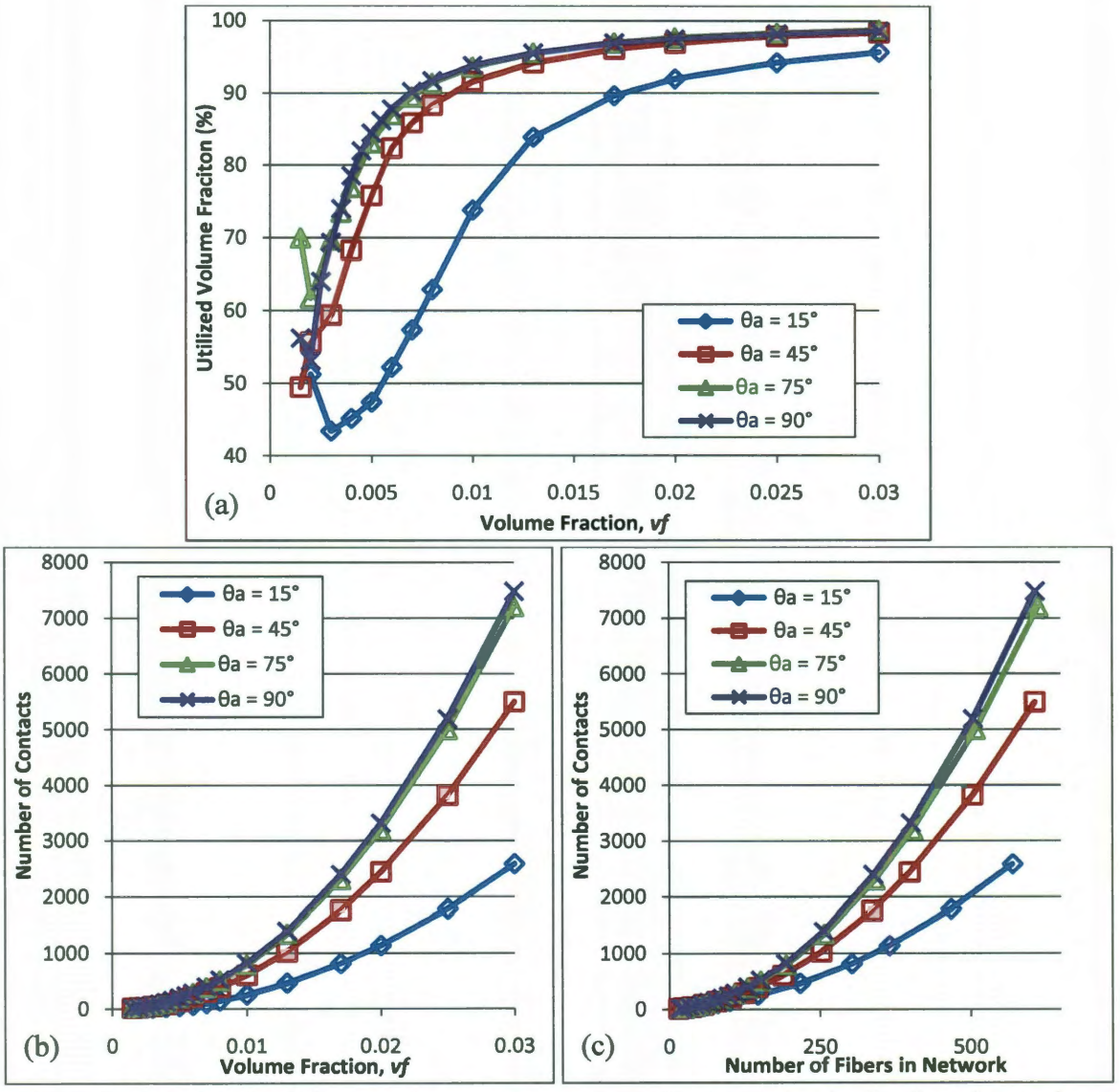

Figure 42. The details of the spanning cluster are shown for the randomly distributed case along with three levels of alignment and include (a) the utilized volume fraction vs volume fraction, (b) number of network contacts vs volume fraction, and (c) contact density.

The difference in utilized volume fraction is slight for very lower levels of alignment and becoming negligible at higher volume fractions. As such, the number of network fibers for the isotropic and slightly aligned cases is comparable at higher volume fractions. This observation matches recorded data which is not shown here for conciseness. Figure 42(b) and Figure 42(c) report the number of network contacts versus volume fraction and

For the study, the same parameters as those in Case Study #2 are used. Except now with a focus on alignment, θ_a is varied between 90° (randomly isotropic) to 15° (highly aligned) while waviness is kept constant at both θ_{max} = 0° (straight) and θ_{max} = 30° (slightly curved, λ = 1.02). As described in the Section 2.1, the alignment angle θ_a is defined as a uniform distribution within the interval $-\theta_a \leq \theta \leq \theta_a$ with respect to the y-axis.

Processing techniques such as extrusion used to gain alignment control over a composite's reinforcing constituents also have the effect of straightening the filler [18]. For the first set of simulations shown in Figure 40, the nanotubes are idealized as being perfectly straight, allowing the overall trends of alignment to be identified. As expected, both an increase and decrease in electrical conductivity is experienced dependent on the level of alignment. The two moderate levels of alignment θ_a = 45° and 75° show a slight increase in conductivity in comparison to the isotropic case. Beyond these levels of alignment, conductivity decreases significantly, reference the blue diamonds corresponding to θ_a = 15°. These results are consistent with the numerical studies by Du et al. [22] and Behnam et al. [65] along with final conclusion of Li and Chou [18]. They also match the experimental data of Du et al. [22]. It is worth noting that Behnam et al., using straight sticks found that the minimum resistivity (maximum conductivity) occurred at an alignment angle of 45° with respect to the direction of conductivity measurement. The proposed model is an excellent agreement with these results.

versus the number of network fibers, respectively. Both of these plots show a decrease in the number of contacts with alignment. Orienting the reinforcement fibers limits their ability to contact neighboring fibers, decreasing their contact density.

Through the visual (Figure 41) and quantitative (Figure 42) analysis of the spanning networks integrated with the given conductivity trends of Figure 40, the same conclusion as Behnam et al. [65] on the effects of alignment for CNT-based composite conductivity is reached. Despite a reduction of network contacts and slight decrease of network fibers, partial levels of alignment tend to straighten conduction paths and generate a greater number of and/or more efficient conduction paths resulting in the lowest resistivity and highest electrical conductivity.

The effects of alignment on the percolation threshold are also studied. Figure 43 reports these results. For case of straight nanotubes (blue diamonds), there is a minute decrease in percolation threshold with initial alignment before increasing with the strongly aligned case. These results are in agreement with previous studies using straight sticks on the dependence of percolation threshold on alignment [22,58].

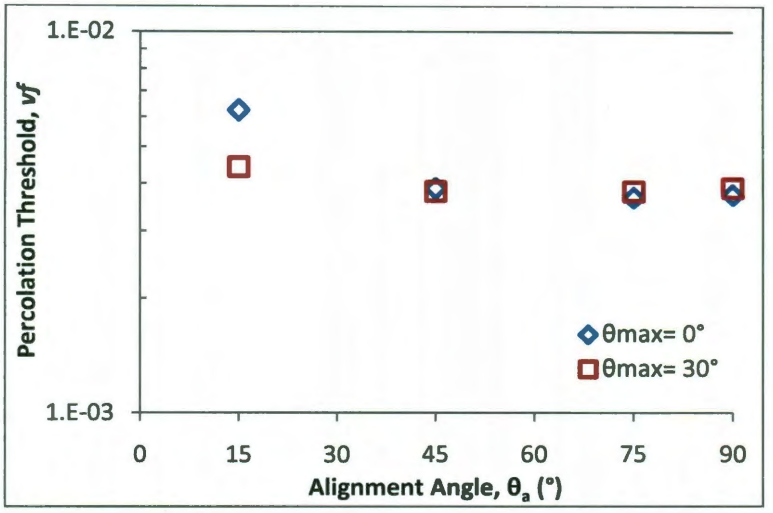

Figure 43. Percolation threshold versus alignment angle for both straight and wavy CNTs is presented. The minimum threshold is reached at $\theta_a = 75°$ for both data sets.

The simulations already discussed were under the idealization of nanotubes as straight fibers. In reality, nanotubes possess a degree of waviness even with advanced processing techniques [18]. Case Study #2 concluded the delay of percolation and reduction of electrical conductivity for the case of wavy nanotubes as compared to straight for the same volume fraction. With the ultimate goal of the model to achieve accurate representation of actual composites, waviness is included as a parameter. Knowing that alignment processing tends to limit waviness, θ_{max} is set low at 30°, yielding a 1.02 curl ratio.

It is clear from Figure 43 that wavy nanotubes follow the same trend in alignment effect as the straight case. The minimum percolation threshold is reached at $\theta_a = 75°$ while further alignment increases the threshold. The waviness does, however, reduce the deviation between the percolation threshold values. This lessening of the alignment effect is also evident in electrical conductivity as seen in Figure 44.

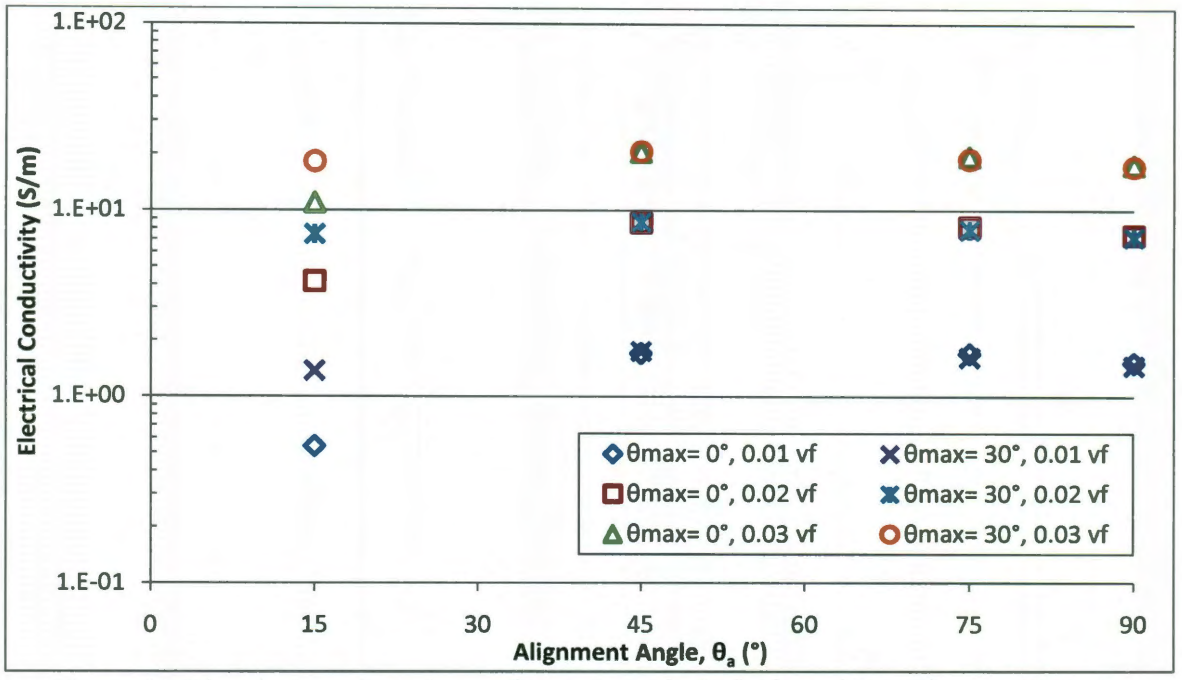

Figure 44. Electrical conductivity vs alignment angle for both straight and wavy CNTs is presented. Maximum conductivity is achieved at $\theta_a = 45°$ for both data sets with wavy being slightly greater.

Figure 44 reports electrical conductivity against alignment angle for set volume fractions. Incorporating nanotube waviness has the effect of limiting the change in electrical conductivity across the range of alignment angles. The same data on the spanning network's attributes reported for the straight case in Figure 42 was recorded, showing the same trends only with less deviation between alignment cases. Due to the similarities, the data is not reproduced here. Nevertheless, it is interesting to note a few points made with the data. In comparing the data between the wavy and straight cases at the same alignment level, the wavy nanotubes result in more network contacts especially at $\theta_a = 15°$ with the difference lessening as the isotropic case is reached. The waviness allows the highly aligned nanotubes to make more connections. Looking solely at the wavy data, the utilized volume fraction decreases with alignment as expected. Yet, when the

wavy data is compared to the straight at a set alignment level, there is no consistent trend. The cumulative effects of by alignment and waviness on a composite's electrical properties differ from the separate effects of each. For example, the maximum conductivity is reach in Figure 44 is achieved with $\theta_a = 45°$ and $\theta_{max} = 30°$. Using a modified normal distribution for the nanotube alignment and a higher curl ratio, Li and Chou [18] found a maximum conductivity with an alignment angle between 70°~80°. Considering the proposed model's much lower curl ratio, it is reasonable that the maximum conductivity was achieved at a low alignment angle.

The proposed model is in good agreement with both experimental results and past numerical simulations. Both an increase and decrease in effective electrical conductivity of can be achieved with carbon nanotube-based composites depending on the achieved level of alignment. Qualitative and quantitative data supports the theoretical explanation of this occurrence.

In order to show convergence of the model with varying alignment and the incorporation of nanotube waviness, Table 8 reports the MCCA results. The analysis is conducted at a volume fraction of 0.01, which is the lowest filler content with all data reaching 100% percolation. All data sets converge to less than 1% after 352 simulations. There are no distinct trends between convergence and alignment for either the straight or wavy case.

Table 8. Monte Carlo Convergence Analysis: Case Study #3.

Number of Simulations to Given Convergence Level								
	$\theta_{max}= 0°$				$\theta_{max}= 30°$			
Convergence Level	$\theta_a = 15°$	$\theta_a = 45°$	$\theta_a = 75°$	$\theta_a = 90°$	$\theta_a = 15°$	$\theta_a = 45°$	$\theta_a = 75°$	$\theta_a = 90°$
1%	341	245	276	207	170	212	352	279
5%	47	14	29	39	13	16	4	4

6 Concluding Remarks

Advances in nanotechnology enable the structuring of new materials at the nanoscale presenting the opportunity to develop novel carbon nanotube-based composite systems with multifunctional capabilities. However, the complexity, expense, and time required for experimentation along with the sheer number of different material combinations limits experimental characterization. In seeking the accurate determination of the electrical properties, a versatile pseudo-three dimensional Monte Carlo-based resistor network model has been proposed to address this need.

The proposed model provides a realistic representation of the composite's microstructure through the incorporation of experimentally-based length and diameter distributions along with nanotube waviness and homogeneous dispersion. Furthermore, the physical behavior of electrical conduction is considered through the inclusion of CNT resistance, contact resistance through a distribution, and the electron tunneling effect. Although numerous theoretical models have been proposed, including a diverse range of parameters and simplifying assumptions, no other available model, to the knowledge of the author, incorporates this set of features thought to best describe the stochastic nature of the problem.

The four major features of the proposed model have been exemplified in the results presented in this thesis. First, the capacity of the model to calculate both the percolation threshold and electrical conductivity has been demonstrated. This allows the electrical properties of a composite to be predicted without resorting to experimentation. Second, the importance of including the stochastic parameter of contact resistance has been

analyzed. The concept of resistor parallelism has helped elucidate how and why the incorporation of the parameter distribution alters the shape of the conductivity curve. Also, in agreement with both experimental and numerical findings, the dominant effect of contact resistance on the effective conductivity has been observed. The last two accomplishments deal with the determination and characterization of the effect of morphological parameters on the overall composite conductivity to include waviness and alignment. Nanotube waviness tends to increase the percolation threshold and decrease the electrical conductivity through a combination of a reduction in the number of conduction paths along with less direct paths. Finally, nanotube alignment can either lead to an increase or decrease in both percolation threshold and electrical conductivity. Qualitative and quantitative analyze shows that partial levels of alignment tend to straighten conduction paths along with generate a greater number of and/or more efficient conduction paths resulting in enhanced conductivity over the isotropic case. Further alignment shortens the conduction path but ultimately reduces conductivity by decreasing the number of conduction paths. These results are all in excellent agreement with published theoretical and experimental findings.

The new technique given herein was developed when the Embedded Fiber approach described by Spanos et al. [89] for structural and thermal applications failed when extended to electrical CNT applications. Clearly, the numerical ill conditioning found in that prior approach was due to the extreme ratios of the electrical conductivities between the binding matrix material and the CNT combined with the lack of a percolation path. That percolation path shortcoming was due to the lack of a priori representation of contact and tunneling electrical connections between the CNT. Obviously, extending the

Embedded Fiber approach to also include a tunneling element, and the new algorithm for the identification of their connection points, would cause that approach to duplicate the results presented herein. However, the contribution of the matrix vis-à-vis the contribution of the CNT, while being non-negligible for the case of the effective mechanical/thermal properties, would be minimal for the case of the effective electrical conductivity problem considered in this thesis.

Furthermore, the model is a useful tool for understanding the link between the actual microstructure and the resultant electrical properties. Methods have also been presented to interpolate both the percolation probability and electrical conductivity between data points. With this knowledge, the optimization and specific tailoring of capabilities of CNT-based composites are possible. Optimization allows the least amount of filler material to be used thereby minimizing cost along with degradation of key matrix properties like flexibility and reducing manufacturing difficulties.

Finally, the primary feature of the model its flexibility for use in a variety of applications. The model provides a timely and accurate calculation of both the percolation threshold and electrical conductivity, which can be applied to any number of new composite materials. Future work in the direction of this thesis may include utilizing the model to determine experimental parameters of actual composites along with the extension of the model to three spatial dimensions.

References

[1] A. Moisala, Q. Li, I. A. Kinloch, and A. H. Windle, "Thermal and electrical conductivity of single- and multi-walled carbon nanotube-epoxy composites," *Composites Science and Technology*, vol. 66, no. 10, pp. 1285-1288, Aug. 2006.

[2] M. Grujicic, G. Cao, and W. N. Roy, "A computational analysis of the percolation threshold and the electrical conductivity of carbon nanotubes filled polymeric materials," *Journal of Materials Science*, vol. 39, no. 14, pp. 4441-4449, Jul. 2004.

[3] J. K. W. Sandler, J. E. Kirk, I. A. Kinloch, M. S. P. Shaffer, and A. H. Windle, "Ultra-low electrical percolation threshold in carbon-nanotube-epoxy composites," *Polymer*, vol. 44, no. 19, pp. 5893-5899, Sep. 2003.

[4] A. V. Desai and M. A. Haque, "Mechanics of the interface for carbon nanotube-polymer composites," *Thin-Walled Structures*, vol. 43, no. 11, pp. 1787-1803, Nov. 2005.

[5] J. Zhu, J. Kim, H. Peng, J. L. Margrave, V. N. Khabashesku, and E. V. Barrera, "Improving the Dispersion and Integration of Single-Walled Carbon Nanotubes in Epoxy Composites through Functionalization," *Nano Letters*, vol. 3, no. 8, pp. 1107-1113, Aug. 2003.

[6] M. Grujicic, G. Cao, and B. Gersten, "Atomic-scale computations of the lattice contribution to thermal conductivity of single-walled carbon nanotubes," *Materials Science and Engineering B*, vol. 107, no. 2, pp. 204-216, Mar. 2004.

[7] S. Berber, Y.-K. Kwon, and D. Tománek, "Unusually High Thermal Conductivity of Carbon Nanotubes," *Physical Review Letters*, vol. 84, no. 20, p. 4613, May. 2000.

[8] Frank, Poncharal, Wang, and Heer, "Carbon nanotube quantum resistors," *Science (New York, N.Y.)*, vol. 280, no. 5370, pp. 1744-1746, Jun. 1998.

[9] B. Q. Wei, R. Vajtai, and P. M. Ajayan, "Reliability and current carrying capacity of carbon nanotubes," *Applied Physics Letters*, vol. 79, no. 8, p. 1172, 2001.

[10] W. A. deHeer et al., "Aligned Carbon Nanotube Films: Production and Optical and Electronic Properties," *Science*, vol. 268, no. 5212, pp. 845 -847, May. 1995.

[11] J. E. Fischer et al., "Metallic resistivity in crystalline ropes of single-wall carbon nanotubes," *Physical Review B*, vol. 55, no. 8, p. R4921, Feb. 1997.

[12] T. W. Ebbesen, H. J. Lezec, H. Hiura, J. W. Bennett, H. F. Ghaemi, and T. Thio, "Electrical conductivity of individual carbon nanotubes," *Nature*, vol. 382, no. 6586, pp. 54-56, Jul. 1996.

[13] Z. Ounaies, C. Park, K. E. Wise, E. J. Siochi, and J. S. Harrison, "Electrical properties of single wall carbon nanotube reinforced polyimide composites," *Composites Science and Technology*, vol. 63, no. 11, pp. 1637-1646, Aug. 2003.

[14] F. Du, C. Guthy, T. Kashiwagi, J. E. Fischer, and K. I. Winey, "An infiltration method for preparing single-wall nanotube/epoxy composites with improved thermal conductivity," *Journal of Polymer Science Part B: Polymer Physics*, vol. 44, no. 10, pp. 1513-1519, May. 2006.

[15] R. Ramasubramaniam, J. Chen, and H. Liu, "Homogeneous carbon nanotube/polymer composites for electrical applications," *Applied Physics Letters*, vol. 83, no. 14, p. 2928, 2003.

[16] C. Li and T.-W. Chou, "Modeling of damage sensing in fiber composites using carbon nanotube networks," *Composites Science and Technology*, vol. In Press, Accepted Manuscript.

[17] E. T. Thostenson and T.-W. Chou, "Carbon Nanotube Networks: Sensing of Distributed Strain and Damage for Life Prediction and Self Healing," *Advanced Materials*, vol. 18, no. 21, pp. 2837-2841, 2006.

[18] C. Li and T.-W. Chou, "Electrical Conductivities of Composites with Aligned Carbon Nanotubes," *Journal of Nanoscience and Nanotechnology*, vol. 9, pp. 2518-2524, Apr. 2009.

[19] C. A. Martin et al., "Formation of percolating networks in multi-wall carbon-nanotube-epoxy composites," *Composites Science and Technology*, vol. 64, no. 15, pp. 2309-2316, Nov. 2004.

[20] F. H. Gojny et al., "Evaluation and identification of electrical and thermal conduction mechanisms in carbon nanotube/epoxy composites," *Polymer*, vol. 47, no. 6, pp. 2036-2045, Mar. 2006.

[21] J. Sandler, M. S. P. Shaffer, T. Prasse, W. Bauhofer, K. Schulte, and A. H. Windle, "Development of a dispersion process for carbon nanotubes in an epoxy matrix and the resulting electrical properties," *Polymer*, vol. 40, no. 21, pp. 5967-5971, Oct. 1999.

[22] F. Du, J. E. Fischer, and K. I. Winey, "Effect of nanotube alignment on percolation conductivity in carbon nanotube/polymer composites," *Physical Review B*, vol. 72, no. 12, p. 121404, 2005.

[23] M. Foygel, R. D. Morris, D. Anez, S. French, and V. L. Sobolev, "Theoretical and computational studies of carbon nanotube composites and suspensions: Electrical and thermal conductivity," *Physical Review B*, vol. 71, no. 10, p. 104201, Mar. 2005.

[24] G. E. Pike and C. H. Seager, "Percolation and conductivity: A computer study. I," *Physical Review B*, vol. 10, no. 4, p. 1421, 1974.

[25] D. Stauffer and A. Aharony, *Introduction to percolation theory*. CRC Press, 1994.

[26] S. Kirkpatrick, "Percolation and Conduction," *Reviews of Modern Physics*, vol. 45, no. 4, p. 574, Oct. 1973.

[27] C. Li and T.-W. Chou, "A direct electrifying algorithm for backbone identification," *JOURNAL OF PHYSICS A: MATHEMATICAL AND THEORETICAL*, vol. 2007, no. 40, p. 14679–14686.

[28] G. D. Seidel and D. C. Lagoudas, "A Micromechanics Model for the Electrical Conductivity of Nanotube-Polymer Nanocomposites," *Journal of Composite Materials*, vol. 43, no. 9, pp. 917-941, May. 2009.

[29] W.-Z. Cai, S.-T. Tu, and J.-M. Gong, "A Physically Based Percolation Model of the Effective Electrical Conductivity of Particle Filled Composites," *Journal of Composite Materials*, vol. 40, no. 23, pp. 2131 -2142, Dec. 2006.

[30] S. Broadbent and J. Hammersley, "Percolation Processes I. Crystals and Mazes," *Proc. Cambridge Philos. Soc.*, vol. 53, pp. 629-641, 1957.

[31] O. Kallmes and H. Corte, "The Structure of Paper I. The Statistical Geometry of an Ideal Two Dimensional Fiber Network," *Tappi J.*, vol. 43, no. 9, pp. 737-752, 1960.

[32] C. H. Seager and G. E. Pike, "Percolation and conductivity: A computer study. II," *Physical Review B*, vol. 10, no. 4, p. 1435, 1974.

[33] Y. Hakobyan, K. D. Papoulia, and M. D. Grigoriu, "Physical and geometrical percolations of effective conductivity on a lattice," *Physical Review B*, vol. 76, no. 14, p. 144205, Oct. 2007.

[34] C. Li, E. T. Thostenson, and T.-W. Chou, "Effect of nanotube waviness on the electrical conductivity of carbon nanotube-based composites," *Composites Science and Technology*, vol. 68, no. 6, pp. 1445-1452, May. 2008.

[35] T. Ota et al., "Control of percolation curve by filler particle shape in Cu-SBR composites," *Journal of Materials Science Letters*, vol. 16, no. 14, pp. 1182-1183, Jul. 1997.

[36] R. Strumpler and J. Glatz-Reichenbach, "Conducting Polymer Composites," *Journal of Electroceramics*, vol. 3, no. 4, pp. 329-346, Oct. 1999.

[37] M. S. Fuhrer et al., "Crossed Nanotube Junctions," *Science*, vol. 288, no. 5465, pp. 494-497, Apr. 2000.

[38] N. Mureau, P. C. P. Watts, Y. Tison, and S. R. P. Silva, "Bulk electrical properties of single-walled carbon nanotubes immobilized by dielectrophoresis: evidence of metallic or semiconductor behavior," *Electrophoresis*, vol. 29, no. 11, pp. 2266-2271, Jun. 2008.

[39] R. C. Smith, J. D. Carey, R. J. Murphy, W. J. Blau, J. N. Coleman, and S. R. P. Silva, "Charge transport effects in field emission from carbon nanotube-polymer composites," *Applied Physics Letters*, vol. 87, no. 26, p. 263105, 2005.

[40] G. D. Seidel, Y. Bisrat, and D. C. Lagoudas, "Electrical and Thermal Conductivities of Carbon Nanotube-Epoxy Composites: Modeling and Characterization," *2007 ASME International Mechanical Engineering Congress adn Exposition*, pp. 245-253.

[41] C. Li, E. T. Thostenson, and T.-W. Chou, "Dominant role of tunneling resistance in the electrical conductivity of carbon nanotube–based composites," *Applied Physics Letters*, vol. 91, no. 22, p. 223114, 2007.

[42] M. Song and X. Sun, "Highly Conductive Carbon Nanotube/Polymer Nanocomposites Achievable?," *Macromolecular Theory and Simulations*, vol. 18, no. 3, pp. 155-161.

[43] E. T. Thostenson, C. Li, and T.-W. Chou, "Nanocomposites in context," *Composites Science and Technology*, vol. 65, no. 3-4, pp. 491-516, Mar. 2005.

[44] P. Elsbernd, "A Non-Linear Finite Element Model for the Elastic and Thermal Properties of Polymer Composites Reinforced with Carbon Nanotubes using the Embedded Fiber Method," Master of Science, Rice University, 2009.

[45] A. Garg and S. B. Sinnott, "Effect of chemical functionalization on the mechanical properties of carbon nanotubes," *Chemical Physics Letters*, vol. 295, no. 4, pp. 273-278, Oct. 1998.

[46] Q. Wang, J. Dai, W. Li, Z. Wei, and J. Jiang, "The effects of CNT alignment on electrical conductivity and mechanical properties of SWNT/epoxy nanocomposites," *Composites Science and Technology*, vol. 68, no. 7-8, pp. 1644-1648, Jun. 2008.

[47] C. D. Reddy, C. Lu, S. Rajendran, and K. M. Liew, "Free vibration analysis of fluid-conveying single-walled carbon nanotubes," *Applied Physics Letters*, vol. 90, no. 13, pp. 133122-3, Mar. 2007.

[48] K. J. Ziegler et al., "Statistically accurate length measurements of single-walled carbon nanotubes," *Journal of Nanoscience and Nanotechnology*, vol. 7, no. 8, pp. 2917-2921, Aug. 2007.

[49] S. Wang, Z. Liang, B. Wang, and C. Zhang, "Statistical characterization of single-wall carbon nanotube length distribution," *Nanotechnology*, vol. 17, no. 3, pp. 634-639, 2006.

[50] E. S. Choi et al., "Enhancement of thermal and electrical properties of carbon nanotube polymer composites by magnetic field processing," *Journal of Applied Physics*, vol. 94, no. 9, p. 6034, 2003.

[51] R. Haggenmueller, H. H. Gommans, A. G. Rinzler, J. E. Fischer, and K. I. Winey, "Aligned single-wall carbon nanotubes in composites by melt processing methods," *Chemical Physics Letters*, vol. 330, no. 3-4, pp. 219-225, Nov. 2000.

[52] F. Du, J. E. Fischer, and K. I. Winey, "Coagulation method for preparing single-walled carbon nanotube/poly(methyl methacrylate) composites and their modulus, electrical conductivity, and thermal stability," *Journal of Polymer Science Part B: Polymer Physics*, vol. 41, no. 24, pp. 3333-3338, Dec. 2003.

[53] T. C. Theodosiou and D. A. Saravanos, "Numerical investigation of mechanisms affecting the piezoresistive properties of CNT-doped polymers using multi-scale models," *Composites Science and Technology*, vol. 70, no. 9, pp. 1312-1320, Sep. 2010.

[54] N. Shenogina, S. Shenogin, L. Xue, and P. Keblinski, "On the lack of thermal percolation in carbon nanotube composites," *Applied Physics Letters*, 2005.

[55] M. Esteva, "Hybrid Finite Elements Nanocomposite Characterization by Stochastic Microstructuring," Doctor of Philosophy, Rice University, 2008.

[56] S. A. Vavasis, "Stable Finite Elements for Problems with Wild Coefficients," *SIAM Journal on Numerical Analysis*, vol. 33, no. 3, pp. 890-916, Jun. 1996.

[57] T. C. Clancy and T. S. Gates, "Modeling of interfacial modification effects on thermal conductivity of carbon nanotube composites," *Polymer*, vol. 47, no. 16, pp. 5990-5996, Jul. 2006.

[58] T. Natsuki, M. Endo, and T. Takahashi, "Percolation study of orientated short-fiber composites by a continuum model," *Physica A: Statistical Mechanics and its Applications*, vol. 352, no. 2-4, pp. 498-508, Jul. 2005.

[59] F. Deng and Q. Zheng, "Interaction models for effective thermal and electric conductivities of carbon nanotube composites," *Acta Mechanica Solida Sinica*, vol. 22, no. 1, pp. 1-17, Feb. 2009.

[60] L. Berhan and A. M. Sastry, "Modeling percolation in high-aspect-ratio fiber systems. II. The effect of waviness on the percolation onset," *Physical Review E*, vol. 75, no. 4, p. 041121, Apr. 2007.

[61] L. Berhan and A. M. Sastry, "Modeling percolation in high-aspect-ratio fiber systems. I. Soft-core versus hard-core models," *Physical Review. E, Statistical, Nonlinear, and Soft Matter Physics*, vol. 75, no. 4 Pt 1, p. 041120, Apr. 2007.

[62] D. A. Jack, C.-S. Yeh, Z. Liang, S. Li, J. G. Park, and J. C. Fielding, "Electrical conductivity modeling and experimental study of densely packed SWCNT networks," *Nanotechnology*, vol. 21, no. 19, p. 195703, May. 2010.

[63] R. A. Hansel, J. Rozen, and D. G. Walker, "Transport involving conducting fibers in a non-conducting matrix," *International Journal of Thermal Sciences*, vol. 49, no. 9, pp. 1561-1566, Sep. 2010.

[64] X. Cheng, A. M. Sastry, and B. E. Layton, "Transport in Stochastic Fibrous Networks," *Journal of Engineering Materials and Technology*, vol. 123, no. 1, pp. 12-19, Jan. 2001.

[65] A. Behnam, J. Guo, and A. Ural, "Effects of nanotube alignment and measurement direction on percolation resistivity in single-walled carbon nanotube films," *Journal of Applied Physics*, vol. 102, no. 4, p. 044313, 2007.

[66] F. Dalmas, R. Dendievel, L. Chazeau, J.-Y. Cavaillé, and C. Gauthier, "Carbon nanotube-filled polymer composites. Numerical simulation of electrical conductivity in three-dimensional entangled fibrous networks," *Acta Materialia*, vol. 54, no. 11, pp. 2923-2931, Jun. 2006.

[67] N. Hu, Z. Masuda, Y. Cheng, G. Yamamoto, H. Fukunaga, and Toshiyuki Hashida, "The electrical properties of polymernanocomposites with carbon nanotubefillers," *Nanotechnology*, vol. 2008, no. 19, pp. 1-10.

[68] W. Lu, T.-W. Chou, and E. T. Thostenson, "A three-dimensional model of electrical percolation thresholds in carbon nanotube-based composites," *Applied Physics Letters*, vol. 96, no. 22, p. 223106, 2010.

[69] P. D. Spanos and A. Kontsos, "A multiscale Monte Carlo finite element method for determining mechanical properties of polymer nanocomposites," *Probabilistic Engineering Mechanics*, vol. 23, no. 4, pp. 456-470, Oct. 2008.

[70] R. Hill, "Elastic properties of reinforced solids: Some theoretical principles," *Journal of the Mechanics and Physics of Solids*, vol. 11, no. 5, pp. 357-372, Sep. 1963.

[71] H. Takikawa et al., "Fabrication of single-walled carbon nanotubes and nanohorns by means of a torch arc in open air," *Physica B: Condensed Matter*, vol. 323, no. 1-4, pp. 277-279, Oct. 2002.

[72] M. Hiramatsu, T. Deguchi, H. Nagao, and M. Hori, "Area-selective growth of aligned single-walled carbon nanotube films using microwave plasma-enhanced CVD," *Diamond and Related Materials*, vol. 16, no. 4-7, pp. 1126-1130, April.

[73] R. B. Pipes, S. J. V. Frankland, P. Hubert, and E. Saether, "Self-consistent properties of carbon nanotubes and hexagonal arrays as composite reinforcements," *Composites Science and Technology*, vol. 63, no. 10, pp. 1349-1358, Aug. 2003.

[74] Z. Néda, R. Florian, and Y. Brechet, "Reconsideration of continuum percolation of isotropically oriented sticks in three dimensions," *Physical Review E*, vol. 59, no. 3, p. 3717, Mar. 1999.

[75] N. Hu, Y. Karube, C. Yan, Z. Masuda, and H. Fukunaga, "Tunneling effect in a polymer/carbon nanotube nanocomposite strain sensor," *Acta Materialia*, vol. 56, no. 13, pp. 2929-2936, Aug. 2008.

[76] A. Buldum and J. P. Lu, "Contact resistance between carbon nanotubes," *Physical Review B*, vol. 63, no. 16, p. 161403, Apr. 2001.

[77] S. Kirkpatrick, *Electrical Transport and Optical Properties of Inhomogeneous Media*. New York: ed Garland J. C. and Tanner D. B., 1978.

[78] Y.-B. Yi and A. M. Sastry, "Analytical approximation of the percolation threshold for overlapping ellipsoids of revolution," *Proceedings of the Royal Society of London. Series A: Mathematical, Physical and Engineering Sciences*, vol. 460, no. 2048, pp. 2353 -2380, 2004.

[79] C. Li and T.-W. Chou, "Continuum percolation of nanocomposites with fillers of arbitrary shapes," *Applied Physics Letters*, vol. 90, no. 17, p. 174108, 2007.

[80] G. Buchanan, *Schaum's Outline of Finite Element Analysis*, 1st ed. McGraw-Hill, 1994.

[81] J. B. Bai and A. Allaoui, "Effect of the length and the aggregate size of MWNTs on the improvement efficiency of the mechanical and electrical properties of nanocomposites--experimental investigation," *Composites Part A: Applied Science and Manufacturing*, vol. 34, no. 8, pp. 689-694, Aug. 2003.

[82] J. Dai, Q. Wang, W. Li, Z. Wei, and G. Xu, "Properties of well aligned SWNT modified poly (methyl methacrylate) nanocomposites," *Materials Letters*, vol. 61, no. 1, pp. 27-29, Jan. 2007.

[83] U. Ono, T. Aoki, and T. Ogasawara, presented at the 48th Conference on Structures Strength, Japan, 2006.

[84] Horikawamachi, Saiwai-ku, Kawasaki-shi, and Kanazawa, Nano Carbon Technologies Co., Ltd, 2004.

[85] W. Bauhofer and J. Z. Kovacs, "A review and analysis of electrical percolation in carbon nanotube polymer composites," *Composites Science and Technology*, vol. 69, no. 10, pp. 1486-1498, Aug. 2009.

[86] Y. B. Yi, L. Berhan, and A. M. Sastry, "Statistical geometry of random fibrous networks, revisited: Waviness, dimensionality, and percolation," *Journal of Applied Physics*, vol. 96, no. 3, p. 1318, 2004.

[87] S. J. Kang et al., "High-performance electronics using dense, perfectly aligned arrays of single-walled carbon nanotubes," *Nat Nano*, vol. 2, no. 4, pp. 230-236, Apr. 2007.

[88] C. Li, E. T. Thostenson, and T.-W. Chou, "Sensors and actuators based on carbon nanotubes and their composites: A review," *Composites Science and Technology*, vol. 68, no. 6, pp. 1227-1249, May. 2008.

[89] P. D. Spanos, M. Esteva, and J. E. Akin, "Determination of Elastic and Thermal Properties of Nanocomposites by Fiber Embedment in Finite Elements," presented at the NSTI Nanotechnology Conf., Houston, TX, 2009.